

Metamorphism of Graphitic Schists from Syros, Greece

Roxanne Renedo

Submitted to the Department of Geology
of Smith College
in partial fulfillment
of the requirements for the degree of
Bachelor of Arts

John B. Brady, Honors Project Advisor

May 11, 2009

*This thesis is dedicated in loving memory to
Wallace Buckland*

Table of Contents

List of Figures	ii
List of Tables	iii
Abstract	iv
Acknowledgements	vi
Chapter 1: Introduction	1
Geologic Evolution of the Aegean Sea and Syros	
Lithologies	
Previous work on the Aegean Sea and Syros	
Purpose of Study	
Chapter 2: Field Observations and Methods	13
Field Methods	
Lithology – Graphitic Schists	
Methods	
Chapter 3: Petrography	19
Textures	
Chapter 4: Chemical Analysis	26
Methods	
Mineral Description and Chemical Compositions	
Chapter 5: Microprobe Analysis	31
Previously Proposed Reactions	
Microprobe Images	
Discussion	
Chapter 6: ACFN and ACF Diagramming	57
Chapter 7: Geothermobarometry	64
Chapter 8: Summary	66
References	70
Appendices	72

List of Figures

1-1: Mediterranean Sea and Aegean Sea map	2
1-2: Slab subduction through time	2
1-3: Events Slide	4
1-4: Map of the Aegean with large-scale active and fossil faults	6
1-5: Cycladic map with major geologic units	6
1-6: Geologic map showing distribution of the three main units	7
2-1: Geologic map of Syros with sample locations	14
2-2: Field photo of graphitic schist with mineral clumps weathering in relief	17
3-1: Angle between mica foliations, mica bends around the pseudomorph	21
3-2: Mica running into a pseudomorph	22
3-3: Skeleton garnet	23
3-4: Size and pervasiveness of sphene	24
3-5: Mineralogic zoning in a pseudomorph	25
5-1: Proposed reaction mechanism	32
5-2: Set of electron microprobe images from thin section JBB00-33A.	34
5-3: Set of electron microprobe images from thin section JBB00-33A.	36
5-4: Set of electron microprobe images from thin section SYR99.25C.	38
5-5: Set of electron microprobe images from thin section JBB00-33C.	40
5-6: Set of electron microprobe images from thin section JBB00-33C.	42
5-7: Set of electron microprobe images from thin section SYR141F.	44
5-8: Set of electron microprobe images from thin section JBB99-33B.	46
5-9: Set of electron microprobe images from thin section LFL02.	49
5-10: Pie charts showing the overall distribution of modes inside and outside of the pseudomorphs.	51
6-1: ACFN diagram	58
6-2: ACFN diagram	58
6-3: ACFN diagram	59
6-4: ACFN diagram	59
6-5: ACF diagram	62
6-6: ACF diagram	62
6-7: ACF diagram	63
7-1: Geothermobarometry graph showing temperatures generated from the program GTB 65	

List of Tables and Appendices

Table 2-1: Hand sample descriptions	15
Table 5-1: Mass balance calculations for the percentage of original lawsonite	53
Table 5-2: Calculations for the percentage of original lawsonite based on a zoned pseudomorph	54
Table 7-1: Geothermometry points	64
Appendix 3-1: Petrography table with minerals, modes and textures	72
Appendix 4-1: Table of SEM compositions	77

Abstract

Graphitic schists found on the northern end of the island of Syros, in the Cyclades, underwent high pressure/low temperature metamorphism as evidenced by the presence of glaucophane-bearing mineral assemblages. Many samples contain clusters of minerals that weather in relief and appear to be pseudomorphs after one or more protocrusts. Most of the pseudomorphs are believed to be after lawsonite because of their shape and the presence of rare, remnant lawsonite found in metabasalts on Syros (Brady et al., 2001), though pseudomorphs after other minerals are possible. The pseudomorphs range in size (from 2mm to 2 cm) and abundance, but are present in most samples.

The typical matrix assemblage for the graphitic schists is phengite + quartz + calcite + sphene + graphite ± paragonite ± albite ± garnet ± clinozoisite ± glaucophane ± chlorite ± opaques. The pseudomorphs contain assemblages of phengite + quartz ± paragonite ± albite ± garnet ± clinozoisite ± chlorite ± sphene. The mineralogic composition within the boundaries of the pseudomorphs is inconsistent with the composition of lawsonite as the micas are K-rich and lawsonite is a Ca-Al silicate; this study attempts to reconcile the composition of the pseudomorph with the composition of lawsonite (or another protocrust) and the reactions that it could have undergone.

It is hypothesized here that there are two types of protocrusts to the pseudomorphs in the graphitic schists, one not yet identified and the second after lawsonite. SEM analyses and microprobe element mapping provided chemical compositions and detailed images of the minerals within the pseudomorphs. Through mapping, two types of pseudomorphs were revealed, a Ca-rich (clinozoisite-rich) pseudomorph and a Ca-poor pseudomorph. The Ca and Al are believed to have remained largely immobile throughout the reactions, thus the original

amounts of Ca and Al are still present within the boundaries of the pseudomorphs. Mass balance equations yielded 20 to 50% of the area of the pseudomorph as original lawsonite. This indicates that the lawsonite protocrust overgrew a number of inclusions, which is evidenced by the presence of a pervasive fabric preserved in many of the pseudomorphs that is at an angle to the fabric in the matrix.

Plotting the bulk compositions of the rocks on ACFN and ACF diagrams shows that the rocks fall into two distinct areas, the more Ca-rich bulk composition corresponds to the rocks that have Ca-poor pseudomorphs and the Ca-rich (clinozoisite-rich) pseudomorphs correspond to the more aluminous bulk compositions. This distribution supports the assertion that there are two different protocrusts because the bulk compositions of the rocks vary. Geothermobarometry was attempted using a garnet-phengite thermometer last calibrated by Hynes and Forest (1988), the results were low, but in a similar range as to what would be expected; the values ranged from 340 to 410 °C.

Acknowledgements

First off, I would like to thank my advisor, John Brady, for getting me started on this project and keeping me going all along the way. He showed me the tools while always encouraging me to come up with my own ideas, questions, tests and solutions. Throughout my years at Smith, and especially this year, he taught me how to explore, grow and learn without simply being taught.

Also, to Peter Crowley and Jack Cheney for coming through with an SEM and making sure that I was able to gather some sound data on which to base my thesis.

To the rest of the Smith College Geology Department, faculty and staff: Mark Brandriss, Bob Burger, Amy Rhodes, Bob Newton, Larry Meinert, Bosiljka Glumac, Sara Pruss, Al Curran, Tony Caldanaro and last but not least, Kathy Richardson. Thanks for all of your encouragement and support throughout my years at Smith that got me to where I am now.

Thanks to all of the other seniors writing theses who kept it all in perspective – Maya, Rachel especially Dani with all of our research obstacles – I don't know if I would have made it through without you being there!! And of course all of the other geology majors who let me be a little crazy all year long...

To all of my friends in Jordan House, for doing your best to keep me sane all the way through, not letting me sleep at lab too often, and keeping me open to the rest of the world... *Especially* Emily, who on top of everything else stuck by my side all the way - you're the best!

WE MADE IT!!

Chapter 1: Introduction

The Cycladic island of Syros is part of the Attic Cycladic Crystalline Belt (ACCB), which is located in the Aegean Sea. This region underwent blueschist grade metamorphism during the Alpine Orogeny, a Tertiary episode of high-pressure/low-temperature metamorphism (Okrusch and Bröcker, 1990). The whole ACCB experienced the blueschist metamorphism that is seen on Syros, but very few islands have well-preserved exposures due to a later greenschist overprint (Schmädicke and Will, 2003). The focus of this research is the blueschist grade graphitic schist found on Syros, specifically, the mineral clumps that weather in relief to the matrix. These replacement minerals have been previously interpreted as pseudomorphs after lawsonite because of their association with high pressure/low temperature metamorphism and the presence of rare, remnant lawsonite found in metabasalts on Syros (Brady et al., 2001). The pseudomorphs have not been widely studied but could lead to information about the protolith as well as further constrain the metamorphism that the rocks on Syros experienced.

This study attempts to better constrain the P/T path of the graphitic schists and understand the present state of the pseudomorphs and the reactions that the rock experienced. This is accomplished through detailed studies of thin sections, Scanning Electron Microscope (SEM) analysis, microprobe mapping and mass balance equations. Knowing the mineral compositions and modes of the pseudomorphs and matrix makes it possible to determine the relationship between the two as well as to calculate the chemical changes that the pseudomorphs have experienced.

Geologic Evolution of the Aegean Sea and Syros

The Mediterranean Sea, just south of the Aegean Sea (Figure 1-1), has undergone dramatic changes in the past 360 Ma that had a large impact on the geology that is seen on Syros.

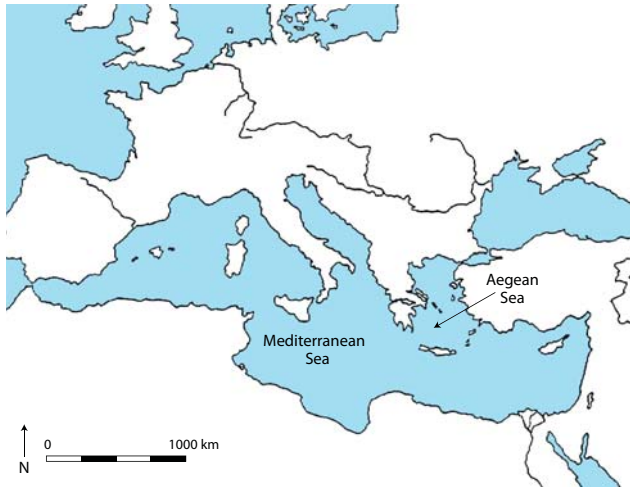
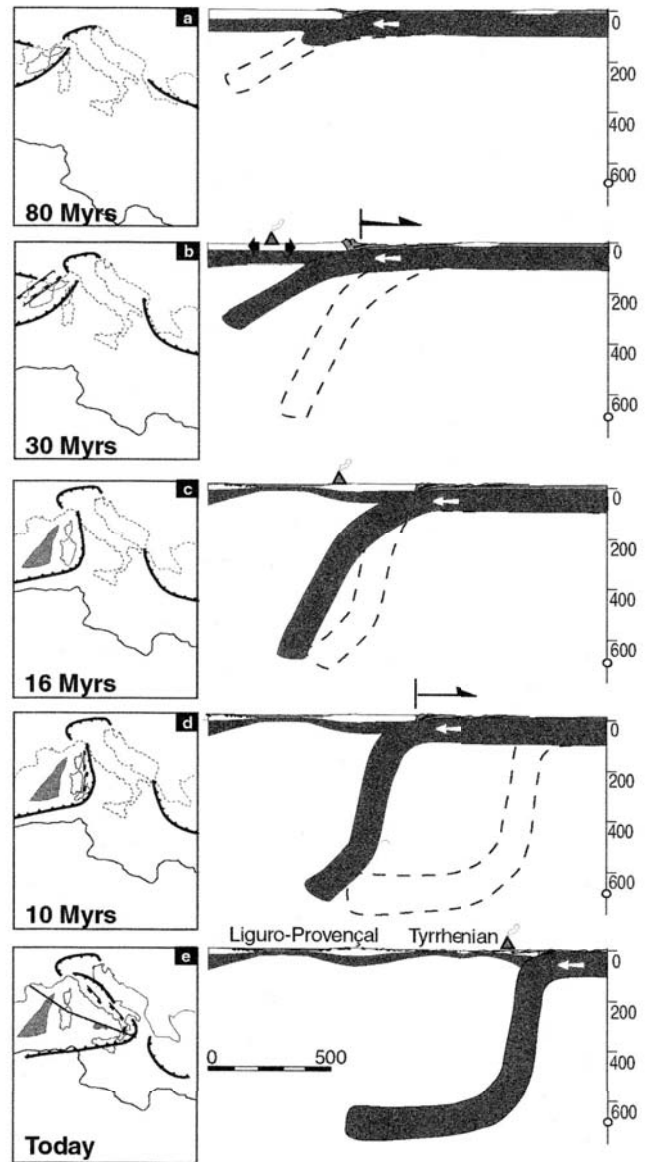


Figure 1-1 (left): General map of the Mediterranean Sea to show the location of the Aegean Sea in relation to the Mediterranean Sea. The Aegean Sea is a product of back-arc extension following the northward subduction of the Apulian microplate under the Eurasian plate.

Figure 1-2 (right): This figure shows the evolution of the subduction and back-arc extension in the Central Mediterranean. The images on the left show the locations of the trenches with respect to a fixed Europe. The cross-sections show the stages of lithospheric subduction with inferred subduction, back-arc extension and trench migration. The dashed line shows the location of the slab in the next frame. The time periods are important transitional time periods in the evolution of the Central Mediterranean. The change in angle of subduction through time and the slab riding on the 660km discontinuity presently is visibly in the cross-sections. (from Faccenna, 2001).



These changes include the consumption of the former Paleotethys and Tethys Oceans to the newly developed back-arc basins that are visible around the Mediterranean Sea, one of which is the Aegean Sea. The tectonic history of the Mediterranean Sea affected Syros through Flysch deposition of sediments and the subsequent creation of back-arc basins during the subduction.

The closure of the Tethys Ocean began in the middle Triassic and by 80 Ma the Apulian microplate began subducting northward under the Eurasian plate. This convergent zone has a historically low rate of movement, about 1-2 cm/year. Over the past 80 Ma this totals to 400-500 km of total subduction resulting in the Alpine buildup (Faccenna et al., 2001). A more in depth look at the evolution of the Mediterranean Sea in the past 80 Ma from Faccenna et al. (2001) is useful (Figure 1-2):

80~30 Ma: This period is marked by slow and continuous northward subduction with Flysch deposition of sediments in the forearc basin. It is not until 32 Ma that there is the indication of volcanism or back-arc extension.

~30-16 Ma: At ~30 Ma there is a change in the overall tectonic setting of the Central Mediterranean from a compressional to an extensional setting; following this, the first back-arc basins begin developing. This corresponds to increased volcanism and the creation of crust in the back-arc basins. This period of extension is what controls the Aegean topography that is seen today.

16-10 Ma: This marks a slow period in the subduction of the Apulian microplate where stretching and subsidence were limited.

10 Ma– present: Extension resumes and back-arc basins continue to form. At present the subduction is slower than average at only a few mm/year. Tomographic imaging shows high-velocity anomalies that seem to indicate that the subducting plate is riding on the 660 km discontinuity.

This timeline is focused on the Central Mediterranean, a more specific timeline concerning the events that have affected Syros shows a similar progression of events (Figure 1-3).

The Aegean Sea and Cycladic Islands are extensional in nature but superimposed on pre-existing compressional structures from the northward migration of the Apulian microplate

Events that influenced (?) rocks on present-day Syros

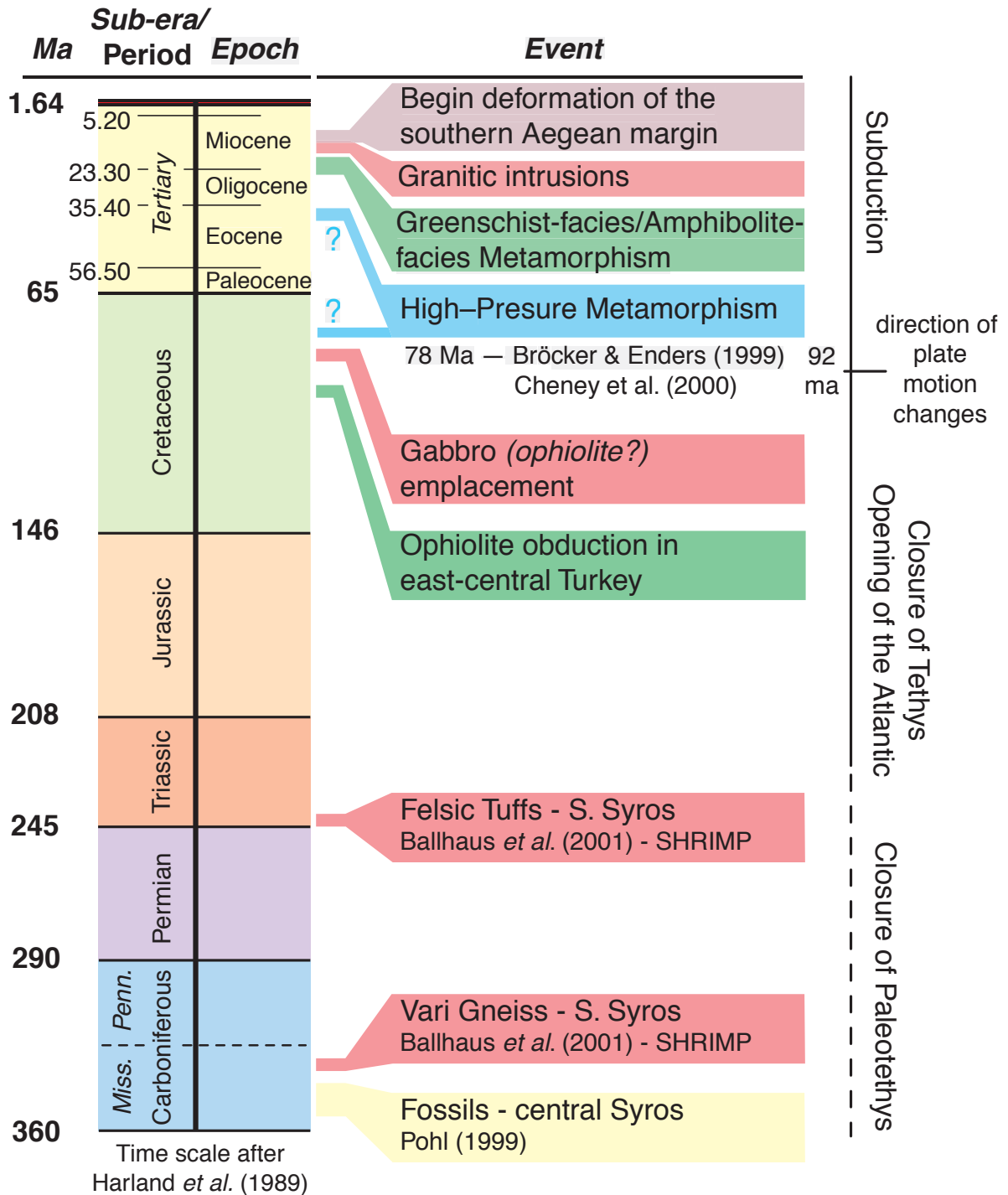


Figure 1-3: This timeline shows a general history of the evolution of Syros, along the left side is time, with events in the center and on the right a reference to the direction of plate motion. The timeline begins with the ages of the protoliths, it then continues through the more recent metamorphism associated with the increased tectonic activity of the last 80 Ma. Authors are cited where appropriate (from Schumacher, personal communication, 2001).

(Figure 1-4). These extensional processes are also associated with the exhumation of the HP/LT rocks that are preserved on a few of the islands in the Cyclades, including Syros. Trotet et al. (2000) suggest that the "extensional mechanism of deformation takes place at depth inside the orogenic wedge prior to the initiation of back-arc extension (30 Ma) of the Aegean crust, during the Paleogene...If this is the case, and assuming an age of 55 Ma, there must be a minimum uplift rate of 128 mm/year" (Trotet, 2000). The exhumation process has not been further constrained.

The island of Syros is part of the Cyclades (Figure 1-5); this ring of islands makes up one of four crystalline complexes in the orogenic arc of the Hellenides - the Attic Cycladic Crystalline Belt (ACCB). This complex is approximately 230x190 km² in area, but most of it lies under the Aegean Sea. It is structurally complicated and includes many thrust faults and nappes. These structural complexities make it difficult to correlate the metamorphic history of the islands in the Cyclades to one another. The three main lithologic units on Syros are separated by faults and have a structurally complex relationship on the island. The repeat of the same lithologic unit throughout the middle of the island is interpreted as an area of tectonic duplication by thrust stacking (Okrusch and Bröcker, 1990).

Much research on Syros has been completed to describe the P/T/t path and the progression of metamorphism, specifically on how the rocks of Syros display the blueschist and later greenschist metamorphism(s). Trotet et al. (2000) gave a succinct description of what they believe to be the four main deformation stages that Syros experienced. The graphitic schists in this study show evidence of the first three stages of metamorphism, but not the fourth.

- Stage 1 (78-53 Ma) corresponds to the end of the prograde path. This end of this time is peak metamorphism and is represented in high-pressure rocks by the relic foliation in S1 garnets. The peak metamorphic conditions are constrained to 12-20 kbar of pressure and 450-500° C (Okrusch and Bröcker, 1990).

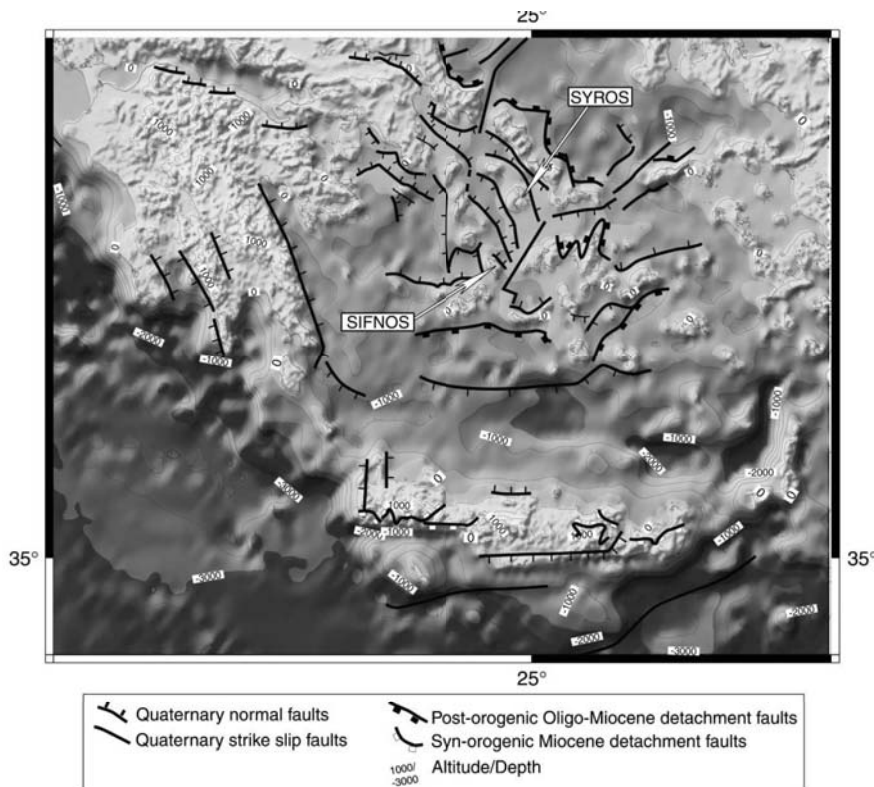


Figure 1-4: This is a simplified map of the Aegean Sea with the islands of the Cyclades as well as mainland Greece, Syros and Sifnos are labeled. The map highlights the major faults (active and fossil) that are throughout the Aegean and that bound the Hellenic trench to the south (from Trotet et al., 2001).

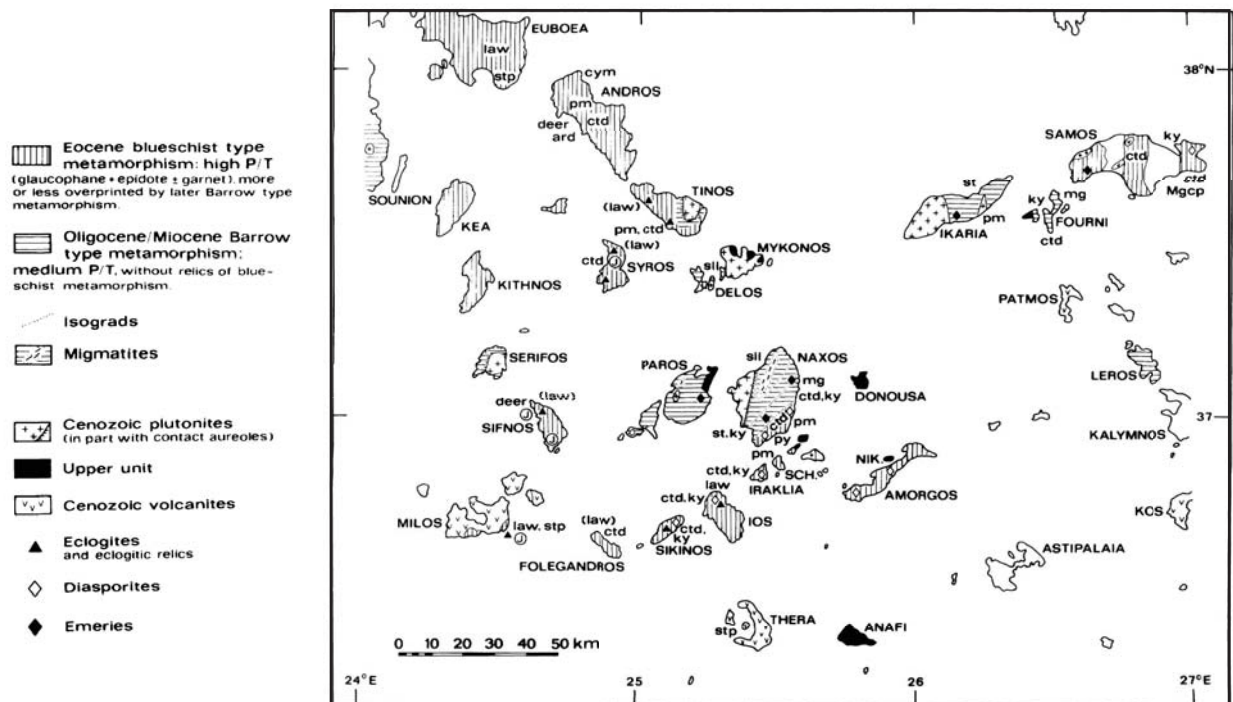


Figure 1-5: This is a map of the Cyclades that shows the primary metamorphic units on the islands. Because of the number of faults, it is difficult to correlate the islands' metamorphic histories to one another (Okrusch and Bröcker, 1990). A wide range of lithologies are preserved on the Cycladic Islands.

- Stage 2 (53-30 Ma) is the first retrogression stage. D2 is responsible for the eclogite/blueschist foliation, S2. It shows strong stretching in an E-W direction on Syros.
- Stage 3 (30-19 Ma) is more localized compared to D2 and kinematic indicators favor top-to-the-NE and E non-coaxial flow.
- Stage 4 (19-0 Ma) is the localized greenschist overprint and is generally absent in northern Syros (Trotet et al., 2000).

At present there are two viable explanations for the greenschist overprint, the first of which, supported by Okrusch and Bröcker (1990), states that there was isothermal decompression of the HP/LT system that led to nominal greenschist metamorphism but it was certainly followed by a separate event of prograde metamorphism. The second theory, asserted by Schmädicke and Will (2003), does not describe that a separate metamorphic event took place; it states that the overprint is a product of partial re-equilibration during the exhumation process (Schmädicke and Will, 2003). These two theories have been neither proved nor disproved and the issue is still debated.

Lithologies

The rocks of the ACCB found on Syros can be divided into three general groups: (I) the metamorphosed sedimentary and volcanic rocks, (II) the thoroughly faulted and deformed remnants of oceanic crust and (III) the Vari gneiss (Schumacher et al., 2008) (Figure 1-6). The graphitic schists of this study are part of Unit I. Okrusch and Bröcker (1990) break the high-pressure lithologies (Units I and II) into three categories: (1) *metabasites and metamorphosed ultramafics*, (2) *meta-acidic jadeite gneisses* and (3) *Metasediments*.

- The *metabasites* are the predominant components of the “metabasite association” (Figure 1-6) but also appear in other units. The main rock types in this category are eclogites and glaucophanites. Eclogites are found interlayered with glaucophanites or as knockers in the mélange area. Glaucophanite is a meta-gabbro that has large amounts of glaucophane.
- *Jadeite-gneisses* are an "important part of the schists of Kampos", which are found in the northern end of the island (Okrusch and Bröcker, 1990). Decompression often altered these rocks to albite.

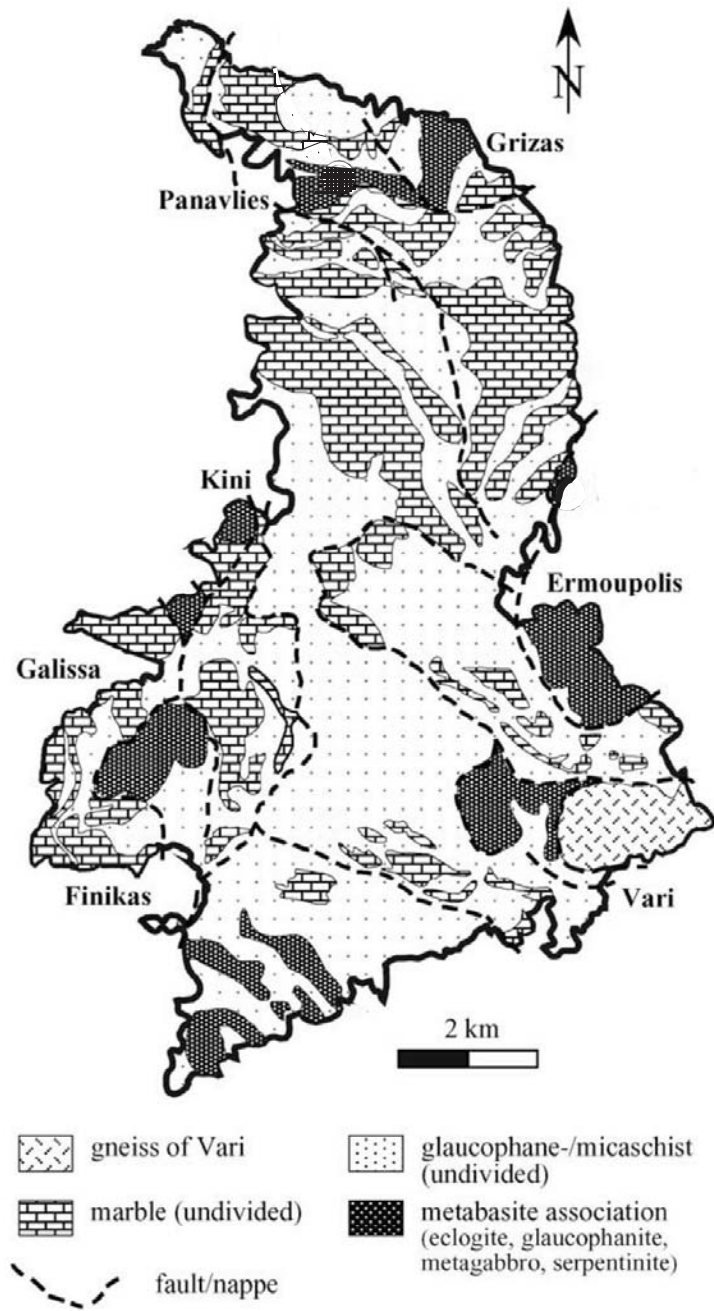


Figure 1-6: This map of Syros shows four general units as well as the larger faults on the island. Putlitz's four units correspond to Schumacher's three units where Unit I is the glaucophane-/micaschists and marbles, Unit II is the metabasite association and Unit III is the gneiss of Vari. The faults on this map give an idea of the frequency and scale of the faulting on Syros. The number of faults through the main section of the island is unknown; here Putlitz has only drawn one (from Putlitz et al., 2005).

- *Metasediments* encompasses a variety of rocks including glaucophane-bearing marbles, glaucophane micaschists, quartzites, manganiferous schists, and lawsonite-bearing schists. This is where the graphitic schists of interest are contained.

The Vari Unit, not a part of the high-pressure lithologies, is the third important lithologic group on Syros, according to Schumacher et al. (2008). Found on the southeastern part of the island, it is interpreted as a tectonic klippe. It is the only possible continental crust found on the island of Syros, though its origin is still debated. The Vari gneiss is made up of greenschist facies orthogneiss, serpentinites, chlorite-schists and metabasic greenschists. The Vari Unit gives Cretaceous ages (70 Ma), which are much younger than the protolith ages of the other rocks on Syros (Trotet et al., 2001). This unit was emplaced by thrust-faulting approximately 30 Ma and sits structurally above the other units (Okrusch and Bröcker, 1990).

Another important region of the island that is not part of the high-pressure lithologies is the *mélange* area, which is made up of a serpentine matrix with knickers of a variety of lithologies isolated in the matrix. This zone is interpreted as a metamorphosed olistostrome or ophiolitic *mélange* (Okrusch and Bröcker, 1990). This zone separates the northern tip of the island from the rest of the island.

Previous Work

The majority of the work that has been completed on the island of Syros focuses on constraining the P/T path and exhumation processes. To do this, petrologists have used the meta-igneous rocks and occasionally the marbles or other meta-sedimentary rocks. No work has been published to date using the graphitic schists.

Dating:

With a goal of constraining the depositional ages of the protoliths of the metatuffaceous and metavolcanic rocks seen in the ACCB, Bröcker and Pidgeon (2007) dated igneous zircons

from rocks on Sifnos, Ios and Andros (other islands in the Cyclades). The dates that they report are Triassic (ca. 237-245 Ma). Putlitz et al. (1985) determined that the protoliths to the schists and marbles of Syros are Paleozoic to Mesozoic in age; these dates are also consistent with the data from Bröcker and Pidgeon (2007). The meta-igneous rocks are found interlayered with the meta-sediments, so these dates also help to constrain the age of the meta-sediments. The Vari Unit has also been dated using zircons by Trotet et al (2001) and others, these zircons yielded Cretaceous ages (~70 Ma), much younger than the meta-sediments.

Exhumation Processes:

Work continues to more explicitly define the evolution of Syros' metamorphic history. Schmädicke and Will (2003) used the assemblages of blueschists and greenschists to constrain the exhumation process. They describe the greenschist overprint as a partial re-equilibration during exhumation. Two possibilities for exhumation are 1) "buoyancy-driven exhumation of small slivers of HP rocks to account for (i) the emergence of deeply subducted continental crust and (ii) for contemporaneous cooling" and 2) "exhumation via return flow of crustal (and mantle) slices in a wedge-shaped subduction channel" (Schmädicke and Will, 2003).

Trotet et al. (2000) describe the exhumation process as continual extension that changed in time from ductile to brittle. They evidence this by shear structures preserved in the rocks. They conclude that the "extensional mechanism of deformation takes place at depth inside the orogenic wedge, prior to the initiation of back arc extension (post-orogenic) of the Aegean crust as indicated by the development of early Miocene basins" (Trotet et al., 2000).

Brady et al. (2002) studied high-pressure marbles that contain what have been interpreted as pseudomorphs after aragonite. The crystals that are interpreted to be pseudomorphs are needle-like in shape and oriented sub-perpendicular to the direction of maximum strain. No

remnant aragonite was found but the conclusion was made based on the evidence of the shape and orientation of the pseudomorphs. The stability range of aragonite falls within the pressure/temperature range of peak metamorphism. "Preservation of the [aragonite pseudomorph] texture limits the amount of deformation experienced by these rocks during exhumation from depths where aragonite is stable" (Brady et al., 2002).

P/T constraints:

Okrusch and Bröcker (1990) used the reaction jadeite + quartz = albite and constrained the P/T conditions to 13.5 kbar and 480°C. The upper pressure limit is given by the presence of paragonite in the absence of kyanite. They also concluded low CO₂ values in the fluid phase because of the former presence of lawsonite and the occurrence of sphene instead of rutile-calcite-quartz.

Schumacher et al. (2008) studied the assemblages in glaucophane-bearing marbles to determine the amount of CO₂ in the fluid during metamorphism. The glaucophane is aligned with the calcite pseudomorphs after aragonite in the rock; this implies that the main phase of deformation occurred in the glaucophane + aragonite stability range (15 kbar and 500 ° C). Constraining the amount of CO₂ in the fluid is important because it affects the stability of the assemblages. Schumacher et al. (2008) determined that the fluid was water rich with XCO₂<0.03 and likely closer to 0.01 for the reported peak P/T.

Purpose of Study

As demonstrated above, the work on Syros has focused primarily on the HP/LT metamorphism and its progression with the rocks of interest being commonly meta-igneous, and rarely metasedimentary. To date, no research has been published on the pseudomorph-bearing graphitic schists on Syros. This lithology is of interest because the pseudomorphs (assumed to

be after lawsonite) are rare on the island and could give new insight into the metamorphism on Syros. The protocrysts of these pseudomorphs is not yet confirmed as lawsonite, determining this protocryst is a main objective. Additionally, studying a different rock type for geothermobarometry is useful to further constrain the peak P/T conditions that Syros, among other islands in the Cyclades, experienced in the Eocene.

Chapter 2: Field Observations and Methods

Field Methods

The samples used in this research were gathered by Frye-Levine in a 2003 Keck project. Her research focused on the graphitic schists and the presence of lawsonite in the rocks, however the short-term nature of her project did not lead to many conclusions. The samples were gathered from the northern end of the island where there is minimal greenschist overprint and the graphitic schist outcrops abundantly; this is an area of about 20 km² (Figure 2-1).

During the 2003 Keck project, Frye-Levine gathered 66 samples, primarily graphitic schists, with or without pseudomorphs. A Global Positioning Satellite unit was used to mark locations where the samples were gathered. A table is provided to describe the hand samples that were still present at Smith College in the summer of 2008 (Table 2-1). The outcrops that were sampled are massive graphitic schist outcrops typically interbedded with marbles.

Visually, the samples vary; some show pervasive cleavage in hand sample while others show little to no cleavage, the frequency and size of pseudomorphs also vary. All samples are gray in color and have a micaceous sheen. The matrix is fine-grained and little detail can be ascertained about the composition in hand sample.

Using this set of rocks, Frye-Levine concluded that it is likely that the graphitic schists are all derived from a single sedimentary protolith and the variations are due to slight variations in local bulk composition, this is evidenced by the compositional similarities throughout the samples. Geothermobarometric calculations were attempted in four locations using a garnet-phengite thermometer (Spear, 2006). Two of the locations resulted in temperatures too high to be consistent with previous data and two were within range (397.1 and 400.3°C).

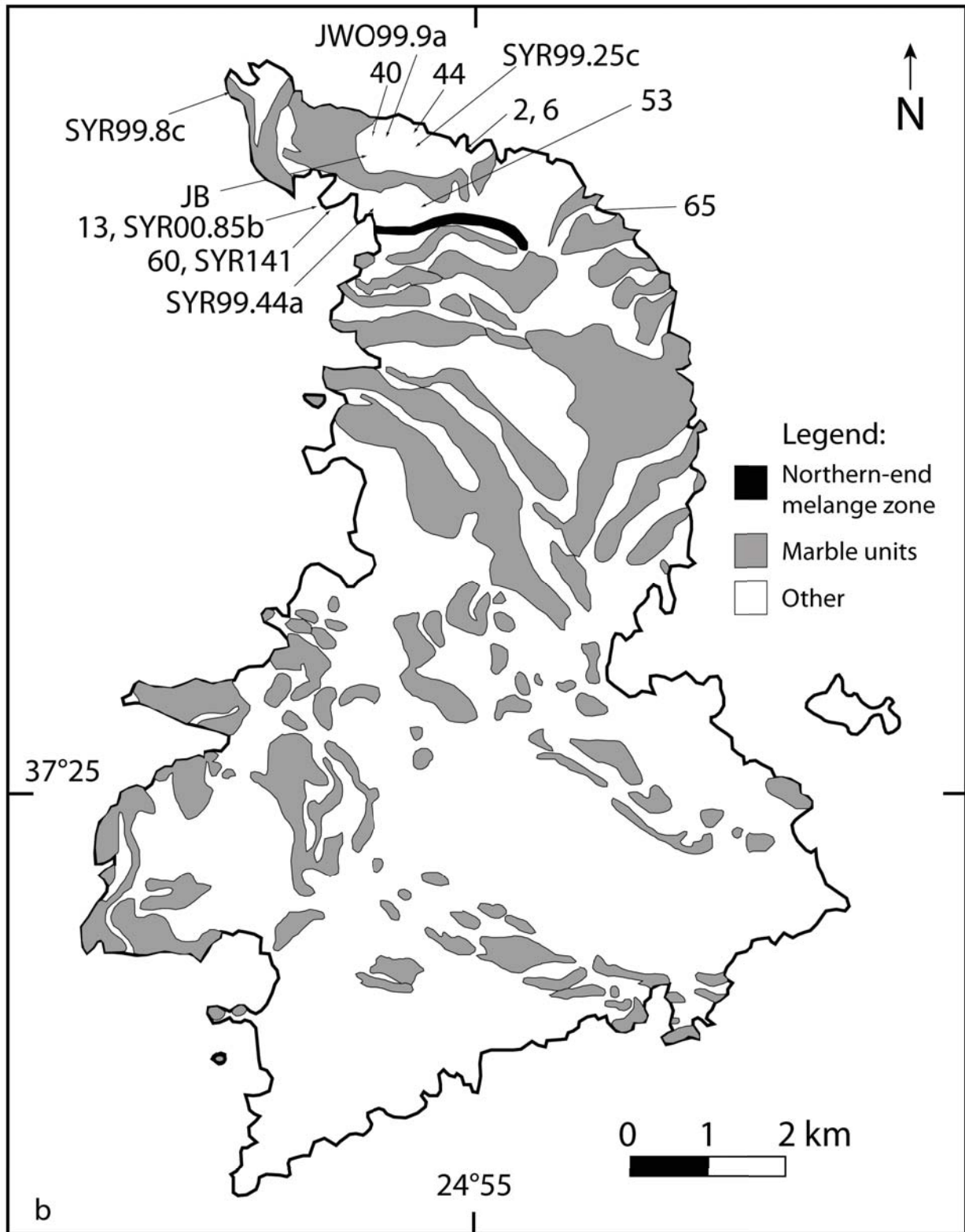


Figure 2-1: This map (adapted from Frye-Levine, 2004) includes the marble units, which bound the graphitic schists, and the other units are left undifferentiated. The marble is in irregular lenses throughout the island but is more pervasive in the northern half of the island. The mélangé zone is drawn here in black. Samples used in this study are located on the map from the GPS coordinates.

Sample	Description	Thin section
LFL01	Visible foliation that is laterally extensive. Quartz clumps up to 4 mm across. Mica- and graphite-rich sample. There are graphite-rich and graphite-poor layers. Garnets (up to 2mm) throughout.	No
LFL02	Mica- and graphite-rich, overall lighter gray color. Microfolds are visible in the graphitic layers. Some crystals are up to 8mm across (many 5-7 mm across) and appear to deflect the foliations. Chlorite-rich sample.	Yes
LFL06	The visible foliation is not laterally extensive. Large crystals up to 7mm in size (most 2-3 mm across). These crystals are dark gray in color. White minerals present in the matrix, but too small for hand sample identification.	Yes
LFL07	Green rock, contains pseudomorphs (up to 7 mm). The pseudomorphs have dark green edges and pink-white centers. The matrix of the rock is chlorite-rich. Not much graphite.	No
LFL09	Omphacite- and glaucophane-rich, not a very graphite-rich rock. Garnets present (up to 3 mm).	No
LFL10	Overall very green color in hand sample, garnets present in the sample, primarily omphacite and muscovite.	
LFL13	Weathered garnets (up to 1 mm), fine-grained mica- and quartz-rich matrix. One large crystal (4 mm) shown in relief.	Yes
LFL17	Mica, chlorite and graphite rich sample with abundant small garnets (1 mm in size). Large crystals that weather in relief (up to 7 mm across), rare.	No
LFL19	Fine grained, micaceous rock. No pseudomorphs or crystals visible. Not very graphite-rich.	No
LFL20	Chlorite- and mica-rich rock with horizons of abundant garnets (up to 3mm in size). No large pseudomorphs visible.	No
LFL21	Graphite and quartz-rich rock with some large crystals visible (up to 5 mm).	No
LFL23	Chlorite-, mica- and quartz-rich matrix with garnets (3 mm).	No
LFL34	Weathered rock, foliations not very distinct	No
LFL40	Well-developed foliation, fine grained aside from quartz clumps.	Yes
LFL44	No large crystals visible. Overall fine-grained schist.	Yes
LFL53	Garnets up to 2mm, some visible foliations	Yes
LFL57	Sparse large crystals (up to 12 mm) in a matrix with many microfolds alternating graphite rich and poor layers.	
LFL60	Large, angular, diamond-shaped crystals that stand out due to weathering, up to 15 mm across. Garnets up to 2mm across. Foliation is well-developed in the hand sample.	Yes
LFL62	Large, gray pseudomorphs (up to 15 mm) that weather in relief to the fine-grained mica- and graphite-rich matrix. Garnets <1 mm throughout. Well-developed foliation in hand sample.	No
LFL65	No hand sample	Yes

Table 2-1: Hand sample descriptions. All rocks have a fine-grained matrix with little information visible in hand sample.

The samples that Frye-Levine gathered were supplemented with graphitic schist thin sections that Professor John Brady of Smith College and Professor Jack Cheney of Amherst College previously gathered from the northern end of Syros. The thin sections do not have corresponding hand samples. The locations of these samples were previously determined and are also located on the map of sample locations.

Lithology - Graphitic Schists:

The lithology of interest in this project is graphitic schist found on the island of Syros, specifically of interest in the schist are mineral clumps that weather in relief, pseudomorphs after an original, unknown protocrust. Outcrops of the graphitic schists are typically interbedded with limestones. The graphitic schist outcrops extensively on the northern end of the island, where all of the samples were gathered. Detailed information about the matrix of the rock is not visible from the outcrop due to the fine-grained nature of the schist. Qualities that are visible are foliation as well as frequency, size and mode of pseudomorphs; this information is important to note at the outcrop/in hand sample (Figure 2-2).

No patterns of pseudomorph location, or the pervasiveness of the foliation around the north end of the island are noted. With this evidence it is plausible that the rocks experienced uniform blueschist metamorphism.

Methods:

Petrography

Of the 66 samples that were gathered by Laura Frye-Levine only 12 of the samples were previously made into thin sections, eight of these were petrographically studied using an Olympus BH-2 petrographic microscope. The eight samples were selected based on the presence of a blueschist assemblage, their pseudomorph content and representative quality of the thin



Figure 2-2: (top) an image of a graphitic schist in Greece, the bumpy surficial texture is visible. These lumps are the pseudomorphs that are seen in the schists as well as other rocks on the island. (bottom) A close-up image of the mineral clumps that weather in relief, approximately 2cm across.

sections. The thin section preparation was completed at Smith College. These eight thin sections were supplemented with those of Professor John Brady and Professor Jack Cheney, as described above. A total of 20 thin sections were petrographically studied.

Of particular interest in the thin sections is the current composition of the matrix and the pseudomorphs, as well as the metamorphic textures preserved in the rocks. An Olympus DP70 camera was attached to the microscope to take photomicrographs of textures and minerals present in the rocks. Details including minerals, modes and metamorphic textures are recorded.

SEM work

The Zeiss EVO 50 SEM with an Oxford INCA EDS system at Amherst College was primarily used to determine the chemical composition of the minerals present in the rocks. The SEM was also used to identify the fine-grained minerals in the pseudomorphs because their fine-grained nature made identification with petrographic techniques difficult.

Element Mapping

The electron microprobe at the University of Massachusetts at Amherst was used to make element maps of pseudomorphs in six thin sections. These maps, combined with chemical compositions from the SEM data, will be used to calculate mass balance equations to assess previously proposed pseudomorphing reactions and attempt to determine the protocry(s) of the pseudomorphs.

Chapter 3: Petrography

A total of 20 thin sections were studied using the Olympus BH-2 petrographic microscope at Smith College. The purpose of the petrographic study was to become familiar with the minerals of the matrix and the current compositions of the pseudomorphs. The petrographic study also revealed textures preserved from the metamorphism that the rock has undergone. The metamorphic textures preserved in the rock lead to a better understanding of the metamorphic history. Ultimately, these details will be used to identify and assess possible pseudomorphing reactions. Appendix 3-1 details the mineralogy and significant features of the graphitic schists.

All of the rocks analyzed are graphitic schists; they have similar bulk compositions with the same minerals present in varying amounts; this was also determined by Frye-Levine in 2003. The typical matrix assemblage for the graphitic schists is calcite + quartz + phengite + sphene + graphite ± clinozoisite ± garnet ± chlorite ± pyrite ± albite ± glaucophane. The pseudomorphs contain assemblages of quartz + phengite ± calcite ± garnet ± sphene. They range in size (from 2mm to 2 cm) and abundance but are present in most samples. The SEM analysis revealed that some of the white mica in both the matrix and pseudomorph assemblages is paragonite, although paragonite could not be distinguished from the phengite in thin section.

The pseudomorphs ubiquitously have smaller crystals than the matrix, but the crystals in the matrix are also very fine, no larger than 2mm and the vast majority much smaller. This does not include the garnets, which range in size from 1mm to 4mm.

Textures

The micas in the matrix of the rocks tend to bend around the pseudomorphs, indicating an episode of deformation following the growth of the pseudomorphs. The mica that bends around the pseudomorphs displays the most recent fabric whereas as the pseudomorphs preserve an

earlier foliation always at an angle to the foliation in the matrix (Figure 3-1). The mica crystals postdate the growth of the protocrust, but it is possible that the protocrust contained inclusions based on the presence of a foliation throughout the pseudomorphs. This difference in foliation angle is indicative of the complexity of the metamorphism that these rocks have experienced. In some places the mica fabric also appears to end by running into the pseudomorphs (Figure 3-2).

Another texture preserved in the graphitic schists is quartz-rich garnets, referred to as skeleton garnets (Figure 3-3). About 30% of the rocks analyzed contain skeleton garnets, and in thin sections where there is one, there are many. The garnets in the matrix commonly have rims of chlorite or are extensively replaced by chlorite.

Most grains inside of the pseudomorphs are smaller than the grains in the matrix and consequently difficult to identify using a petrographic microscope; though this is typical rule, the sphene is the exception (Figure 3-4). The sphene in the thin sections is as large inside of the pseudomorphs as outside of the pseudomorphs. The presence of sphene in the pseudomorphs could indicate a store for the calcium from the lawsonite. If this were true, the lawsonite must have been titanium rich (which is unlikely) or the titanium in the bulk composition of the rock had to be mobilized to enter the pseudomorphs. It is more likely that the sphene is a spectator in the pseudomorphing reactions and that the lawsonite grew after the sphene originally crystallized.

Some of the pseudomorphs show interesting zoning features, particularly identifiable using the interference colors of the minerals in cross-polarized light. The photomicrographs show more mica on the outer edge of the pseudomorph displaying an overall higher birefringence, and an area of low birefringence in the center of the pseudomorph (Figure 3-5).

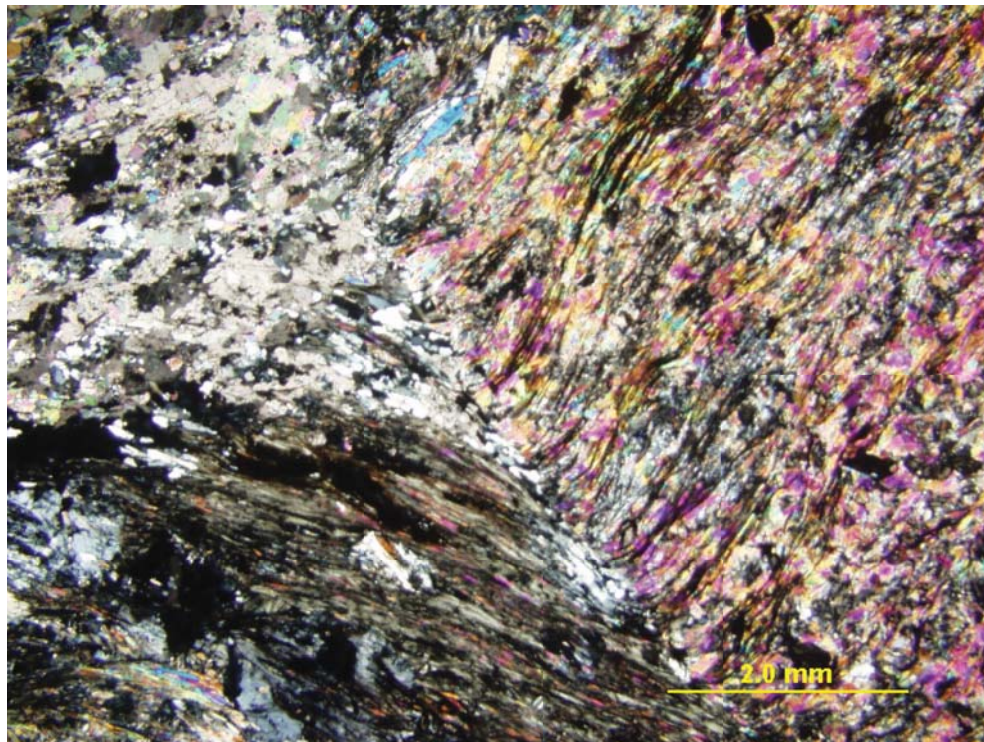
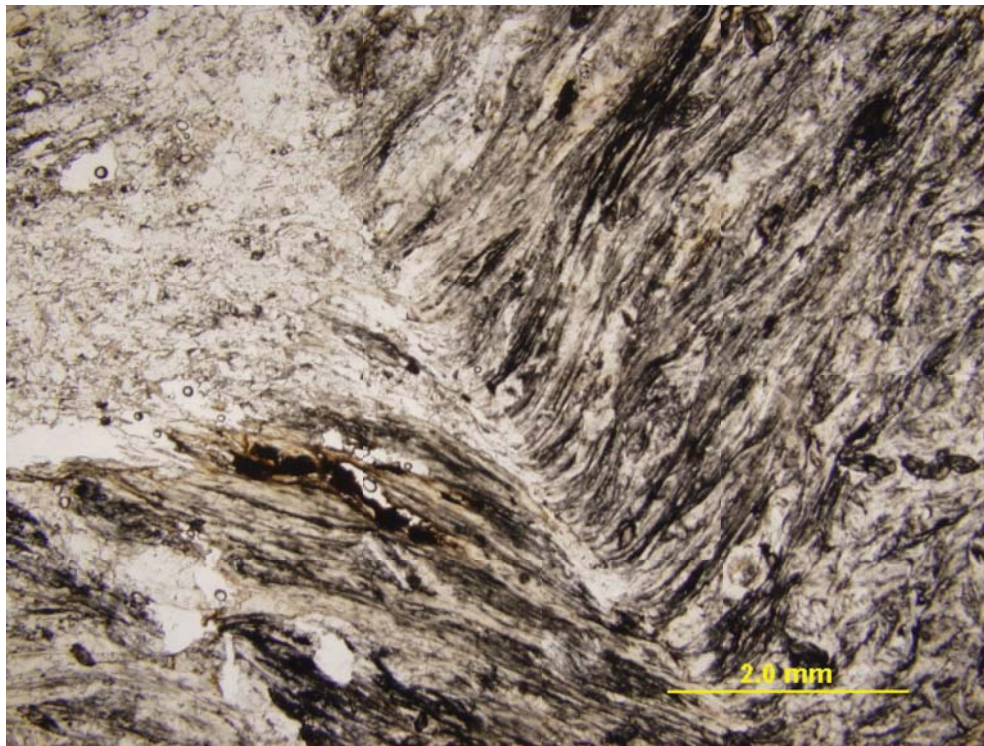


Figure 3-1: Photomicrographs of SYR99.25C. (A) The edge of a large (19 mm) pseudomorph is visible on the right in this image, as well as the mica bending around the pseudomorph at an angle to the overall fabric preserved in the pseudomorph. There are two layers in the matrix, a chlorite-, mica- and graphite-rich layer (below) and a calcite-rich layer (above). (B) The crossed-polarized image shows the high interference colors of the mica in the pseudomorph in contrast to the gray/green colors of the chlorite-rich matrix and the calcite-rich layer.

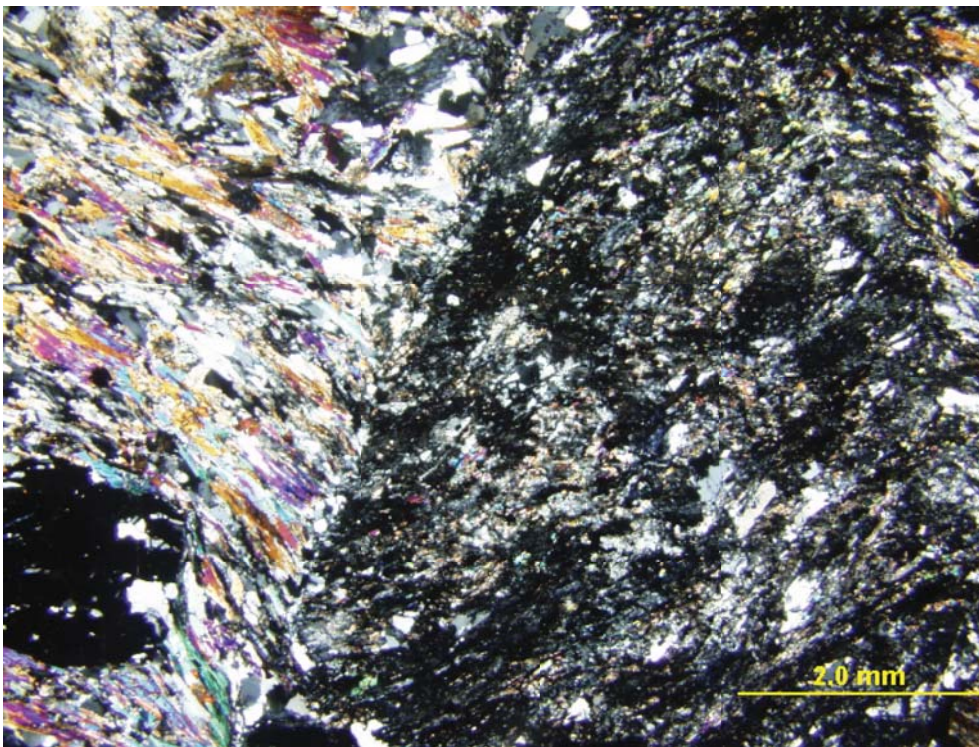
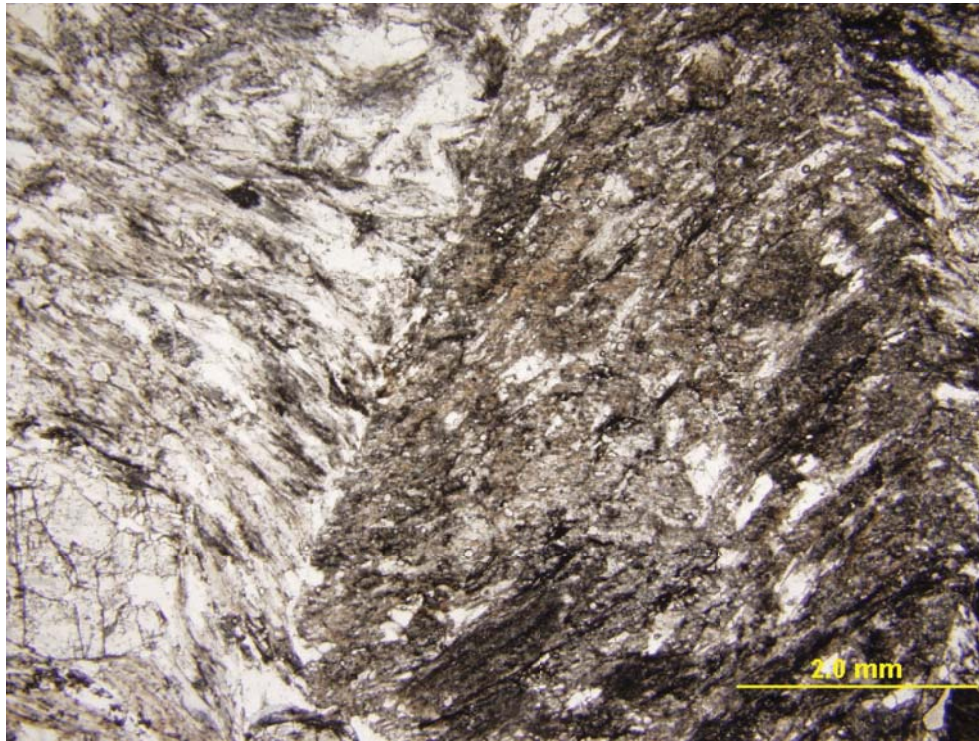


Figure 3-2: Photomicrographs of JBB00-33C. (top) The pseudomorph on the right is more graphite-rich than the matrix, and it has a well-defined boundary. The quartz in the thin-section is graphite free. (bottom) This image shows the edge of a pseudomorph with the mica fabric in the matrix running into the edge of the pseudomorph, the mica fabric runs through the pseudomorph but at an angle to the matrix fabric. The fine-grained quality of the pseudomorph is especially visible with the polarizers crossed. The generally low interference colors in the pseudomorph are primarily clinozoisite crystals with some high-interference mica visible.

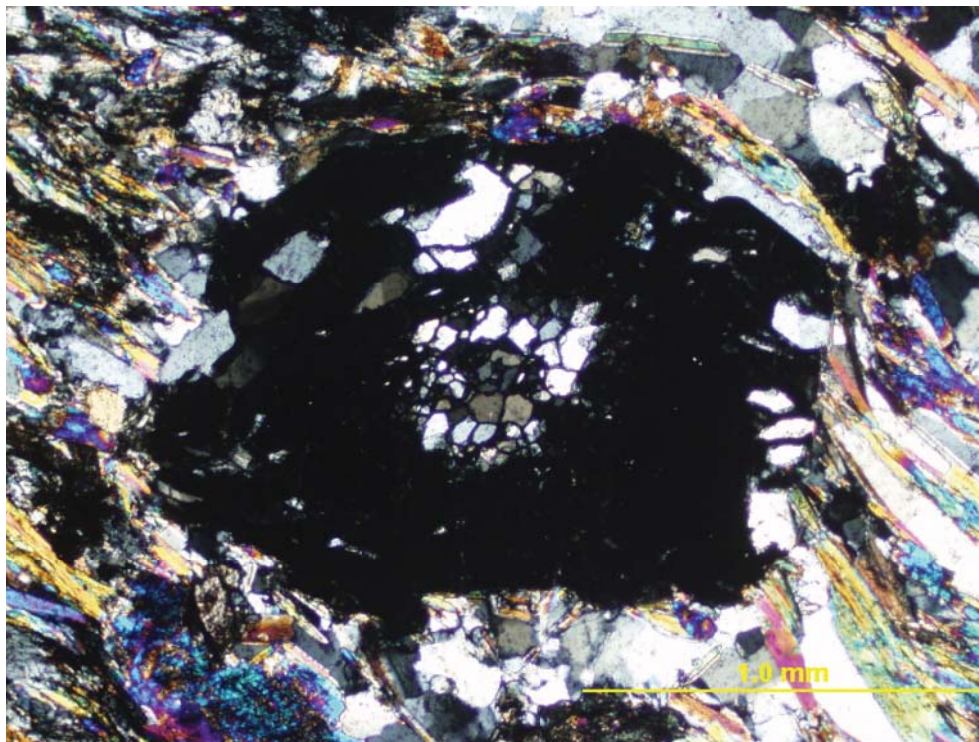
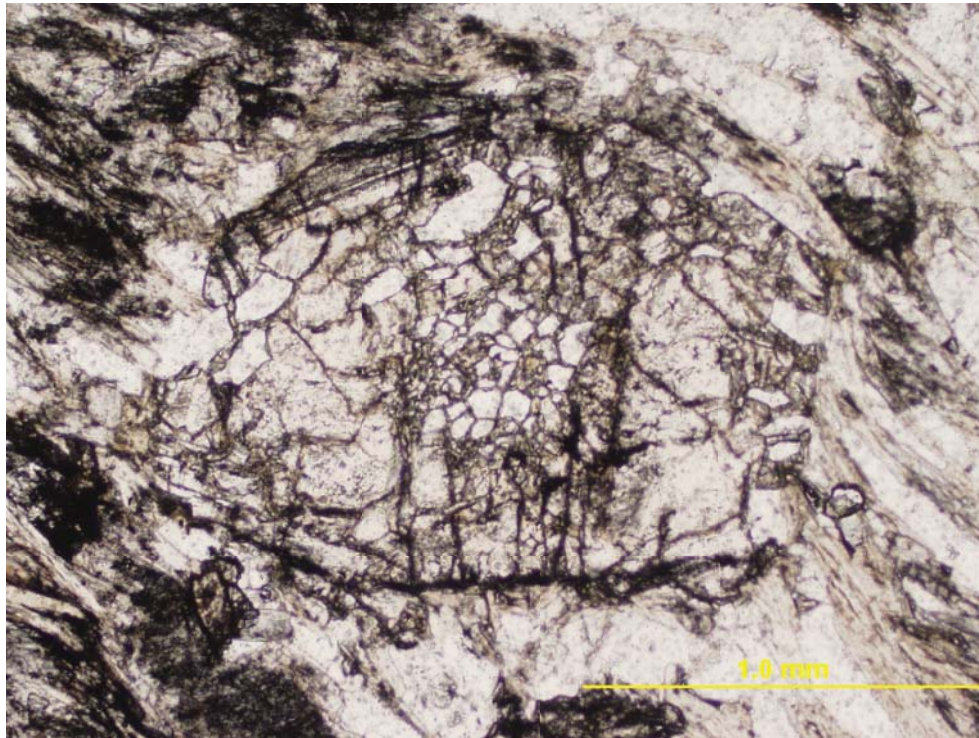


Figure 3-3: Photomicrographs of JBB00-33C. (top) A garnet is located in the center of this image that is fractured and contains numerous inclusions. A slight mica fabric is visible to the right of the garnet. (bottom) In cross-polarized light the quartz inclusions are visible in the center of the garnet, and on the edges, as well as the mica fabric to the right of the garnet. This is a skeleton garnet, found in many of the thin sections.

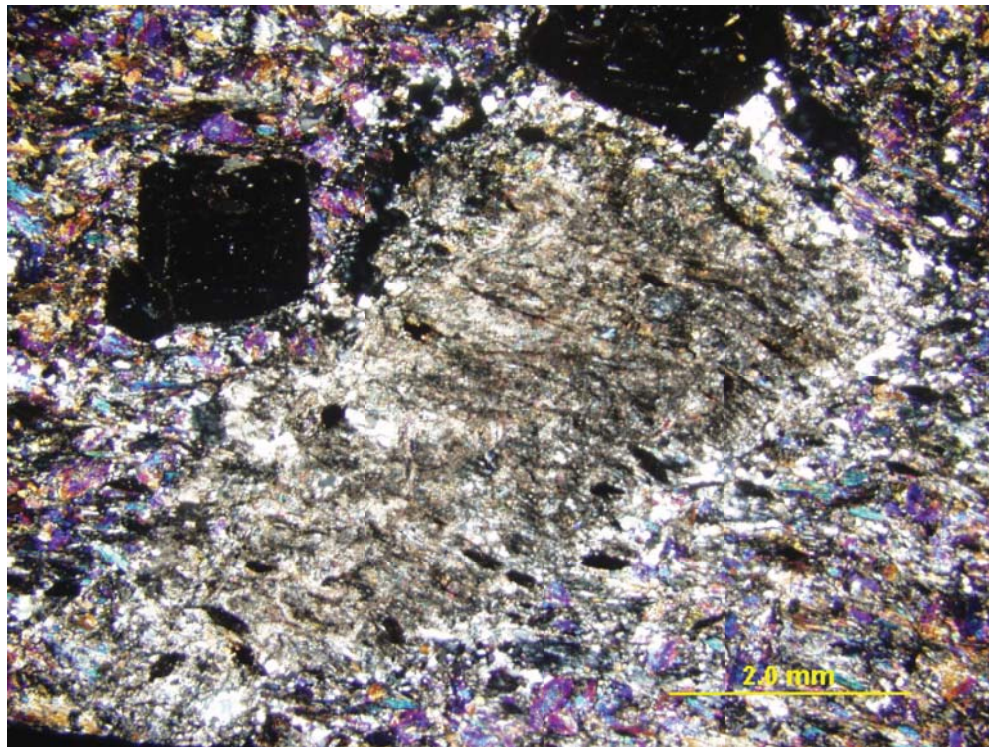
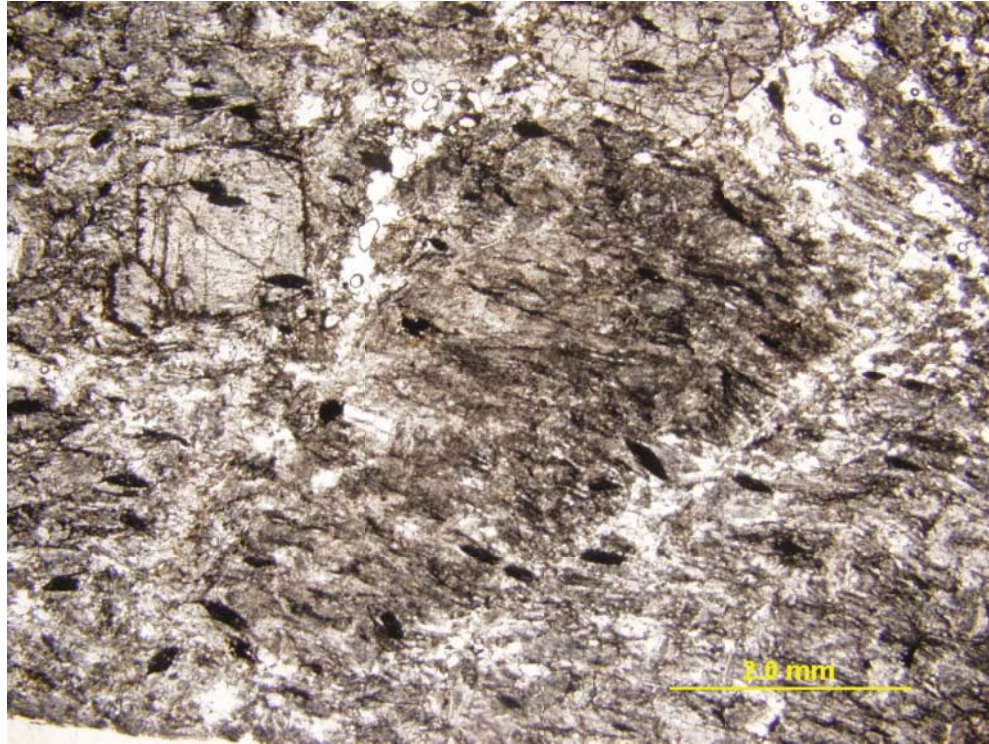


Figure 3-4: Photomicrographs of SYR141F. (top) The pseudomorph, in ppl, is defined by a slight halo of graphite free area. The sphene in the matrix is equal in size to the sphene inside of the pseudomorph. The sphene is also found as inclusions in the garnets. (bottom) In cross-polarized light the pseudomorph shows lower birefringence (clinzoisite rich) than the matrix (glaucophane rich). The crystals inside of the pseudomorph, other than the sphene are all very fine grained.

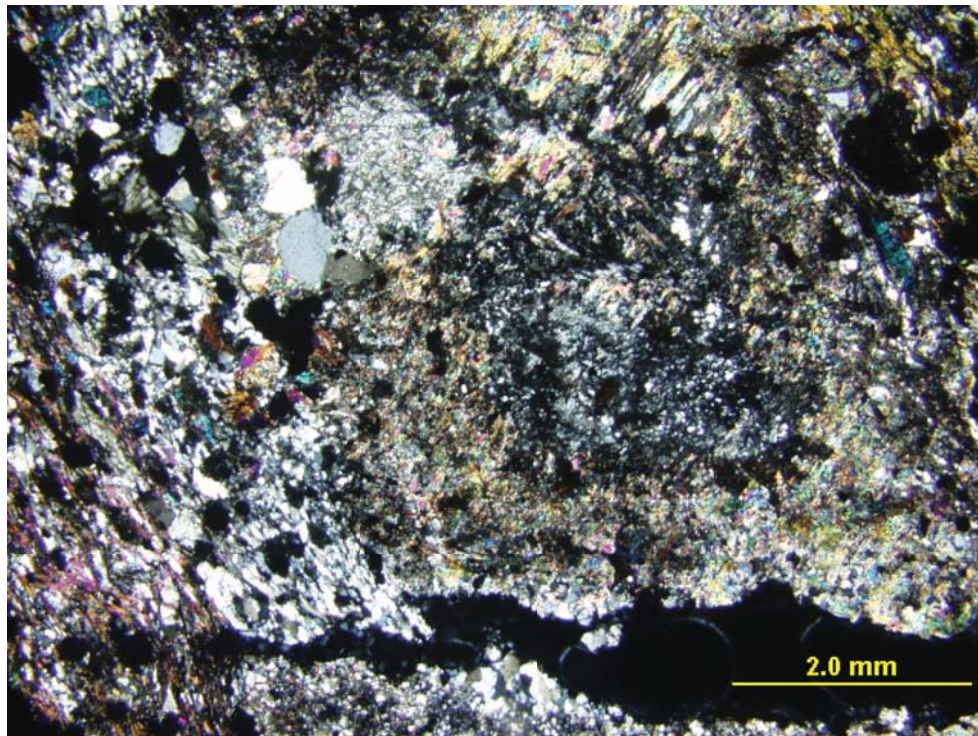
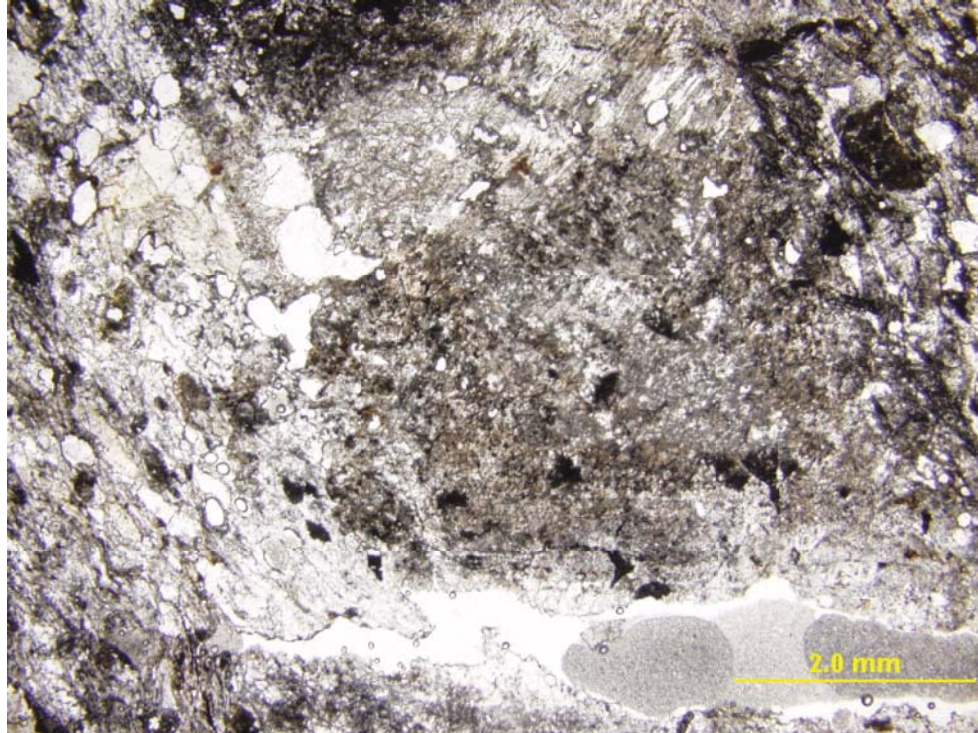


Figure 3-5: Photomicrographs of JBB00-33A. (top) in ppl, the edge of the pseudomorph is not very visible, but it still appears very graphite-rich. In the lower-left corner of the pseudomorph there is an indication of zoning by graphite concentration. (bottom) Under crossed-polars a mineralogic zoning is visible with the outer edge of the pseudomorph showing higher birefringence and the inner part of the pseudomorph displaying first-order interference colors. This mineralogic zoning is explored further with the SEM.

Chapter 4: Chemical Analysis

Methods:

Fourteen graphitic schist samples were analyzed on Amherst College's Zeiss EVO 50 SEM with an Oxford INCA EDS system. The 14 samples were selected out of the original 20 because of their pseudomorph content as well as representative quality of the thin section. The goal of the SEM analysis was to characterize the chemical compositions of the minerals present by identifying a compositional range. Spot analyses were completed for gathering data. Images were gathered where spectra were taken. In each of the 14 thin sections all minerals found, aside from quartz and calcite, were quantitatively analyzed. Below, minerals found in both the matrix and pseudomorphs are discussed. Appendix 4-1 displays all SEM data. The garnet, albite and sphene present in the rocks maintained a similar composition throughout all of the samples. The mica, chlorite, glaucophane and clinozoisite varied in composition throughout individual samples and between thin sections.

Mineral Description and Chemical Compositions:

Graphite

All of the rocks that were analyzed are graphitic schists, so they contained a significant amount of graphite (C) as compared to the other rocks on the island of Syros. The amount of graphite contained in each of the samples is hard to define because of the small size of the numerous graphite crystals, because the SEM requires a carbon coating, and because the SEM cannot give quantitative analyses for elements lighter than sodium. The presence of the graphite indicates an organic-rich environment of deposition.

Quartz

The habit of the quartz (SiO_2) in thin sections varies from veins to individual grains, all of which are virtually graphite free. Quartz is present in the matrices all of the samples; its mode ranges from 10 - 40%. Quartz is also common in the pseudomorphs ranging from 7-20%.

Calcite

Calcite (CaCO_3) is a major constituent (up to 40%) in the matrix of some of the rocks, but non-existent in others. The calcite observed in the matrix contains only Ca, no other form of carbonate was identified. Previous research concluded that it is likely that the rocks all have similar bulk compositions and that the variation in the amount of calcite is due to local depositional setting (Frye-Levine, 2004). This assumption is explored below by plotting the bulk compositions of the rocks. Calcite is not found in the pseudomorphs.

Albite

The albite ($\text{NaAlSi}_3\text{O}_8$) in these rocks is found in both the matrix and the pseudomorphs. Okrusch and Bröcker (1990) suggest a retrograde origination of the albite with the greenschist overprint that followed the blueschist metamorphism. In the matrix, the albite ranges from 3 to 20% when present. Inside of the pseudomorphs there was nearly always a small amount of albite present. The percent of the pseudomorph that is albite ranges from 0 to 10% (commonly near 10%). The SEM analyses show that the albite remains at end member composition $\text{NaAlSi}_3\text{O}_8$.

Sphene

The graphitic schists contain a substantial amount of sphene (CaTiSiO_5), both inside and outside of the pseudomorphs. The sphene percentage in the matrix is small, ranging from 1% to 5%. However, the presence of sphene indicates that there is an excess of Ti, enough to make the observed amount of sphene. The sphene crystals contained many graphite inclusions. The

samples that contained the smallest mode of sphene correspond to the samples that have the most glaucophane. This could be because glaucophane can accommodate some Ti in its structure, although SEM analyses yield only trace amounts of Ti.

The pseudomorphs commonly contained sphene in similar modes to the matrix. The SEM analyses showed a constant chemical composition for the sphene, inside and outside of the pseudomorphs: $\text{Ca}_{1.00}\text{Ti}_{0.94}\text{Al}_{0.06}\text{OSiO}_4$. High-pressure sphene can contain a small amount of aluminum; here this small proportion remained constant. The presence of sphene in similar amounts and with consistent compositions indicates that sphene probably grew before the protocrysts and was not involved in the pseudomorphing reactions.

Garnet

Garnets of similar form and composition are found in both the matrix and the pseudomorphs of these rocks; this is evidence that the garnets likely are not participating in the pseudomorphing reactions. Garnet is present in the matrix in percentages ranging (when present) from 5 to 25%. Garnet was found in pseudomorphs of 2 thin sections where they account for 5-20% of the pseudomorphs. The chemical composition of the garnet did not vary between the matrix and pseudomorph, quantitatively supporting garnet as a spectator mineral. The SEM gives an average composition of 62% almandine, 29% grossular, 7% pyrope and 3% spessartine.

Mica

Through petrography only one type of mica was identified, a white, phengitic mica. This was assumed because of the occurrence of phengite in other rocks from Syros (Okrusch and Bröcker, 1990). Upon SEM inspection two different micas were revealed: (1) phengite, a white mica that has a higher Si:Al ratio than muscovite, found mostly in the matrix and (2) paragonite (Na-rich mica), contained primarily within the pseudomorphs. The chemical composition of the

phengite that resulted from the SEM analyses is $K_{1.54-1.73}Na_{0.05-0.17}Al_{3.91-4.71}Mg_{0.44-0.87}Fe_{0.17-0.37}(Si_{6.68-7.00}O_{20})(OH)_4$. The chemical composition of the paragonite that resulted from the SEM analyses is $K_{0.09-0.38}Na_{1.49-2.02}Al_{5.46-5.82}Mg_{0.02-0.10}Fe_{0.03-0.10}(Si_{6.06-6.21}O_{20})(OH)_4$. The paragonite contains smaller amounts of Mg, Fe, Si and K and much larger amounts of Al and Na. The higher Al content of the micas inside of the pseudomorphs is consistent with past research (Brady, 2003) and is indicative of growth from a more aluminous source, such as the aluminous protocrysts that are observed in the element maps.

Chlorite

In these rocks the chlorite $((Mg,Al,Fe)_3(Si,Al)_4O_{10}(OH)_2 \cdot (Mg,Al,Fe)_3(OH)_6)$ appears principally as a secondary texture from the garnets. The chlorite can be seen as rims on garnets, or even fully replacing garnets. Not all chlorite appears to be retrograde, it has a similar habit to the micas in the rock, and is commonly found in micaceous layers. The mode of chlorite in the matrix ranges from about 3 to 7%. The chlorite composition did vary within and between thin sections. The Fe and Mg values varied the most. The chemical formula is $(Mg_{4.06-6.59}Al_{2.32-2.39}Fe_{2.66-4.96})(Si_{5.61-5.82}Al_{2.18-2.39})O_{20}(OH)_{16}$.

Variation in chlorite composition is not systematic, disparities occur within thin sections and between thin sections. There is no difference in the chlorite composition between the matrix and pseudomorphs. All of the chlorite plots in the same area with no ordered variation.

Glaucophane

Glaucophane (Na amphibole) is a typical mineral in the meta-igneous rocks found around Syros, though not typically found in large amounts in the graphitic schists. Ten samples of the 20 analyzed contained glaucophane. The typical mode of glaucophane was 7% but it ranges up

to 40%. Glaucofanane was not found in the pseudomorphs. The chemical composition range is $\text{Na}_{1.76-1.94}\text{Ca}_{0.09-0.23}\text{Mg}_{1.94-2.38}\text{Fe}_{0.91-1.32}\text{Al}_{1.8-1.85}\text{Si}_{7.94-8.01}$.

Clinozoisite

Clinozoisite (Ca, Fe³⁺, Al silicate) serves as a store for the calcium that was released when the structure of lawsonite becomes unstable and as such is primarily contained within the pseudomorphs. It is a mineral that has been found in pseudomorphs after lawsonite on Syros (Able, 2003). The largest amount of clinozoisite in the matrix is 3%. Dissimilarly, most pseudomorphs contain clinozoisite in larger amounts, from 20 to 50%. The composition of the clinozoisite, given by the SEM analyses has the range $\text{Ca}_{1.93-2.06}\text{Fe}_{0.04-0.48}\text{Al}_{2.54-2.90}\text{Si}_{3.03-3.13}$.

The more Fe-rich clinozoisite is typically found in the matrix, while the clinozoisite inside of the pseudomorphs is low-Fe. This trend is reasonable if the clinozoisite in the pseudomorph is from a lawsonite protocryt during conditions where iron is not mobile, thus remains in the matrix.

Opaques

In these graphitic schists most samples contain a small amount of opaques, other than graphite, (when present <1%). The shape of the opaque minerals in thin section is square, suggesting pyrite. However, upon further examination with the SEM, the composition of the opaques is only Fe and O, hematite (Fe₂O₃). The opaques are not abundant enough to have any impact on the pseudomorphing reactions, so they were not extensively studied.

Other

In addition to the minerals that were mentioned, there is apatite, zircon and bits of allanite found in small amounts in a variety of the thin sections. The allanite was found exclusively within larger clinozoisite crystals contained in the pseudomorphs.

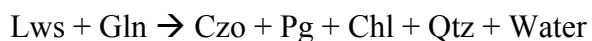
Chapter 5: Microprobe Analysis

Of the 14 samples studied on the SEM, six were mapped using the electron microprobe at the University of Massachusetts at Amherst. The six samples sent to UMass were selected on the basis of the presence of pseudomorphs as well as the minerals present in the pseudomorphs. The six map areas were solely pseudomorphs or suspected pseudomorphs.

The element mapping was used to look at the larger distribution of minerals present in the pseudomorphs for quantitative analysis combined with the point analyses from the SEM. The SEM chemical data was combined with the maps to do quantitative analyses to determine the protocryt to the pseudomorphs.

Previously Proposed Reactions:

Following a 2000 Keck project, pseudomorphing reactions were proposed by Brady et al. (2001) using the mineral assemblages that were documented. Two proposed reactions fit the mineralogy of these rocks, and will be tested:



Based on the pseudomorph modes, these reactions require some compounds to enter the pseudomorph, namely K_2O , Na_2O , MgO and Fe_2O_3 , and other compounds to leave the pseudomorphs: SiO_2 and H_2O (Figure 5-1). Since water is a product in the reaction, the recrystallization of the protocrysts is interpreted as occurring with rising temperature (prograde).

The plausibility of specific reactions will be tested by counting pixels (using the program ImageJ NIH) of the minerals contained within the pseudomorphs to determine the modes and compare them to the modes necessary to create an equal size lawsonite protocryt.

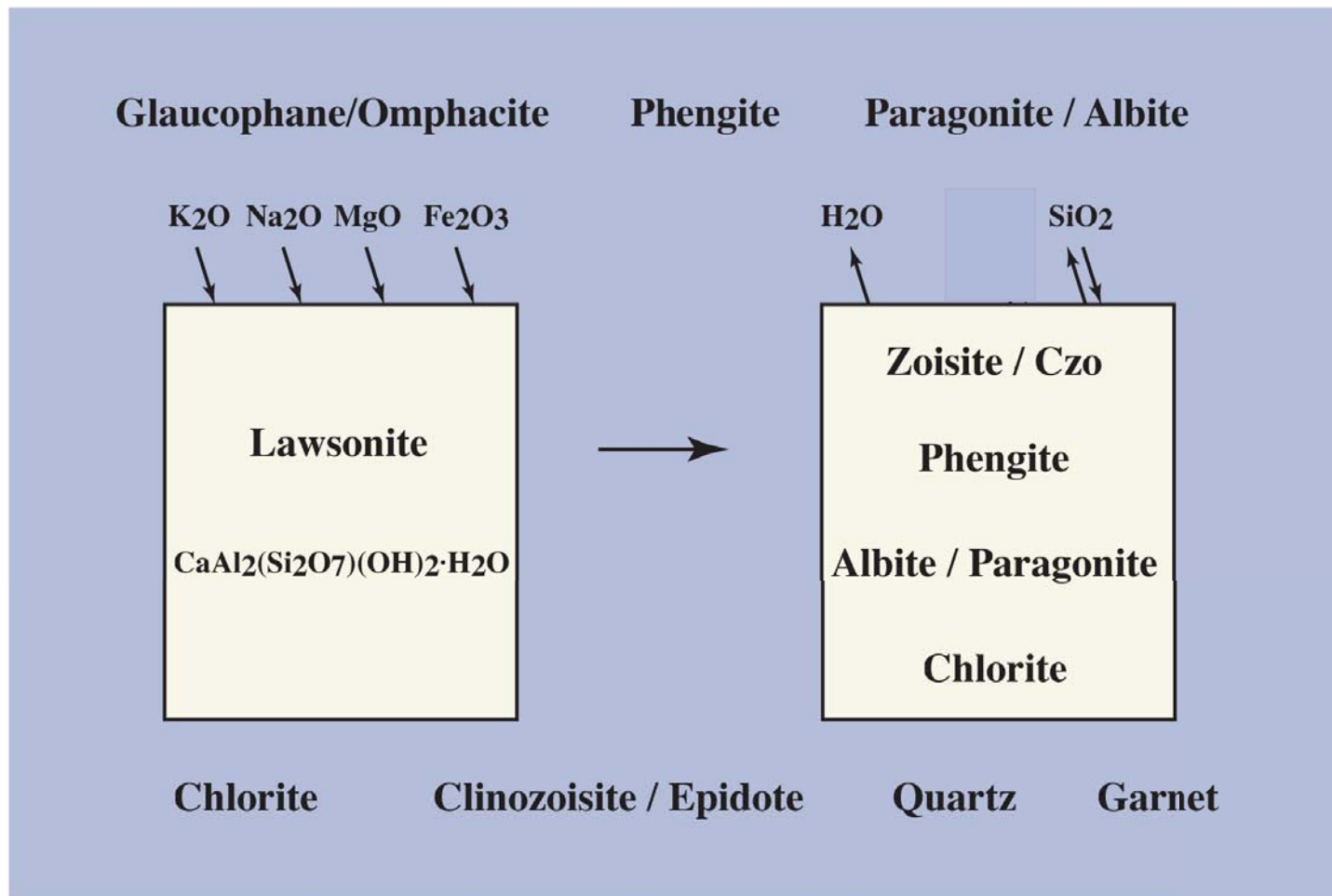


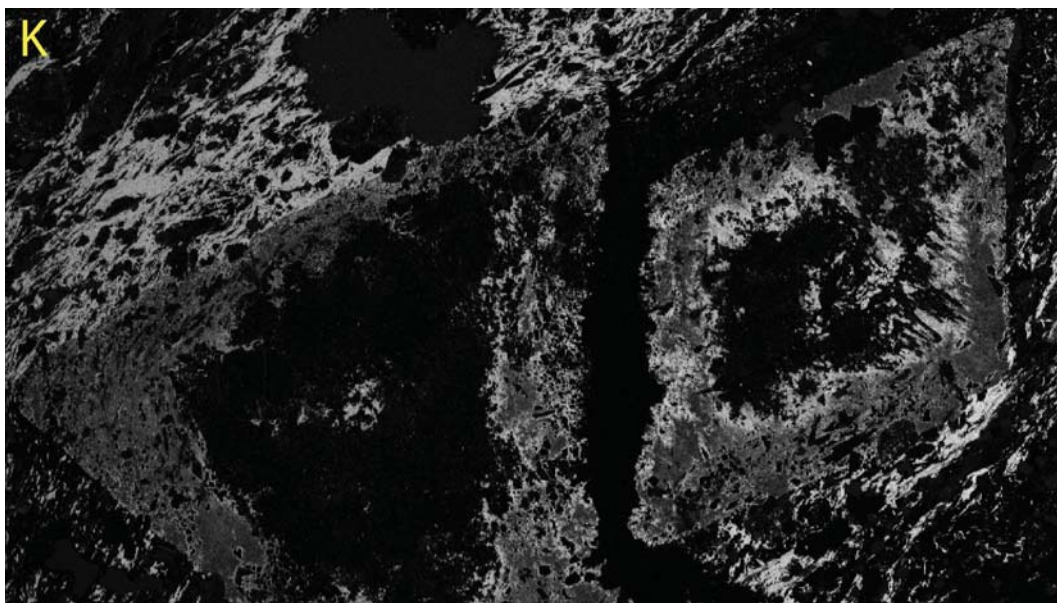
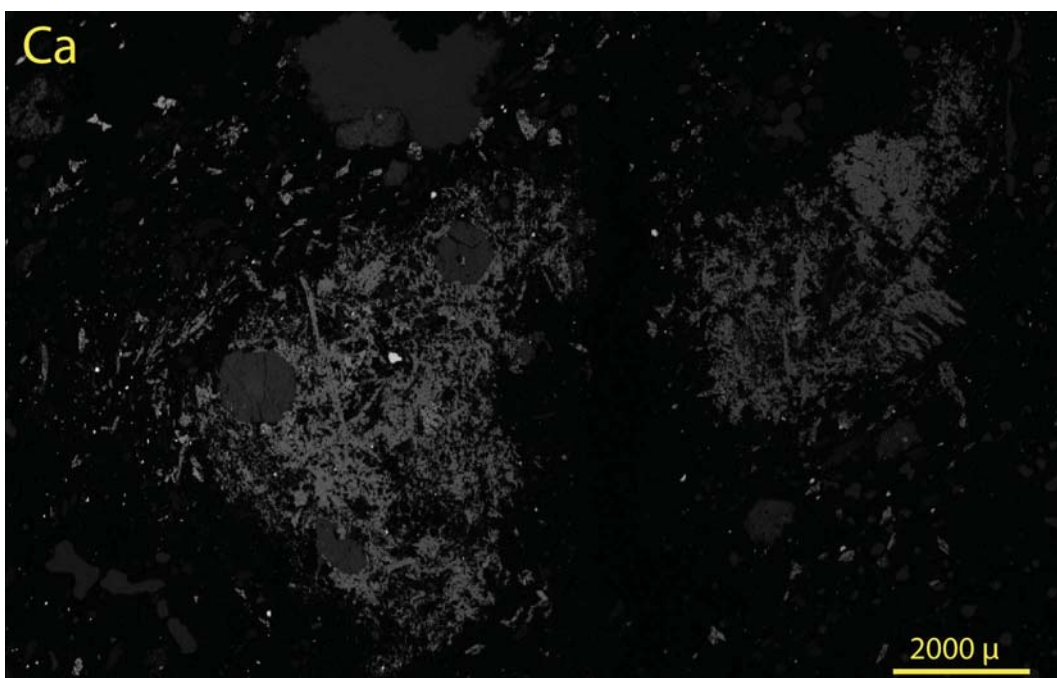
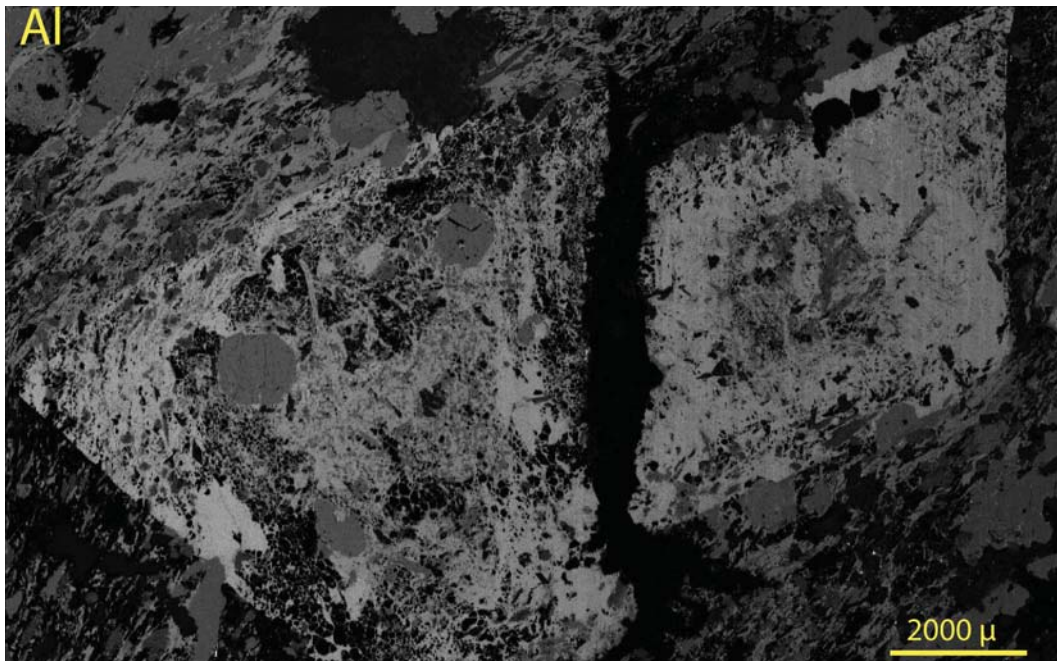
Figure 5-1: This image is a schematic drawing of what compounds are needed to enter the system in order to drive the reaction of lawsonite forward to achieve the assemblages that are seen in the pseudomorphs currently. The small square represents a lawsonite crystal with the background representing the matrix and its more or less stable composition. K_2O , Na_2O , MgO and Fe_2O_3 enter the system, while H_2O and/or SiO_2 leave the system. Because water leaves the system, this reaction is interpreted as prograde (Brady et al., 2001). Other reactions that are similar to the cartoon's depiction are listed in the text.

Microprobe Images:

A total of eight element maps were taken from six thin sections: (1) JBB00-33A, (2) SYR99.25C, (3) JBB00-33C, (4) SYR141F, (5) JBB00-33B and (6) LFL02. The UMass microprobe has five detectors and five elements were picked to analyze: K, Ca, Al, Fe and Mg. The goal was to differentiate between the minerals identified in the pseudomorphs through the SEM analysis. The maps show the element proportion in grayscale where black is a reading of zero and white shows the largest abundance. Black areas on all element maps indicate the presence of *quartz*. K indicates the presence of *mica*, different intensities of K are seen between the Na-rich and -poor mica. A strong Ca reading indicates *calcite*. Where Ca and Al coexist with minor Fe is *clinozoisite*. Solely Al indicates *albite*. The presence of Mg, Fe and Al indicates *chlorite*. *Glaucophane* is identified by its blocky habit and contains smaller amounts of Mg, Fe and Al than chlorite. *Garnets* are best indicated by their habit but also contain Ca, Al, Fe and Mg. *Sphene* is indicated by the presence of Ca and its habit. The eight sets of area maps give a variety of insights into the mineral qualities and textures within the pseudomorphs that are not visible with a petrographic microscope or the SEM images. A summary of the maps and the information that they display is included below (Figures 5-2 to 5-9).

In addition to the qualitative analysis of the pseudomorphs, a quantitative analysis was completed using ImageJ, pixel-counting software. Both the pseudomorphs and matrix were analyzed with ImageJ. The pixel analysis had internal checks because of Maps 1a/b and 3a/b, a similar result for the pseudomorph and the matrix from the (a) and (b) sites is likely because of the close proximity of measurements. The matrix measurements were also compared to the petrographically measured modes to check for internal consistency. The pie charts below show the composition of the pseudomorphs and the matrix around them for comparison (Figure 5-10).

Figure 5-2



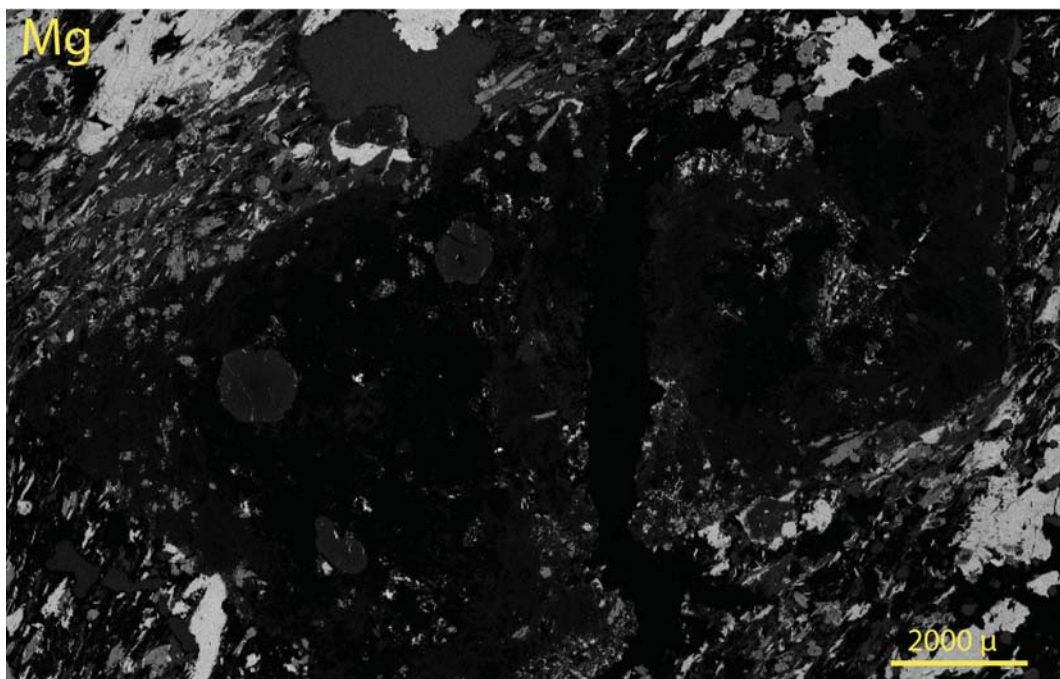
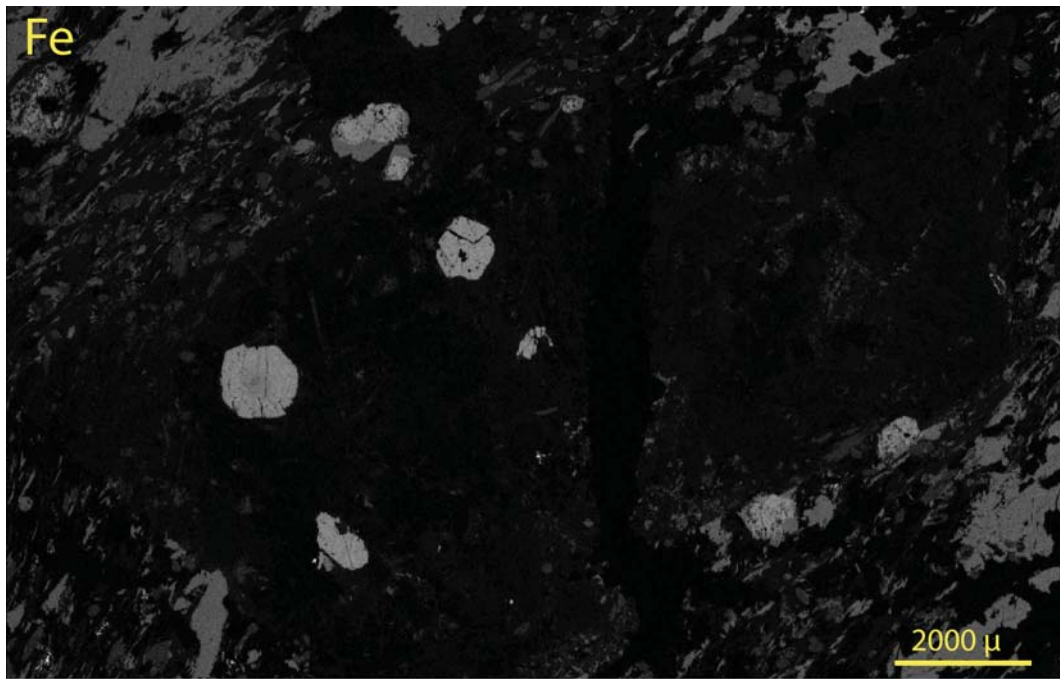
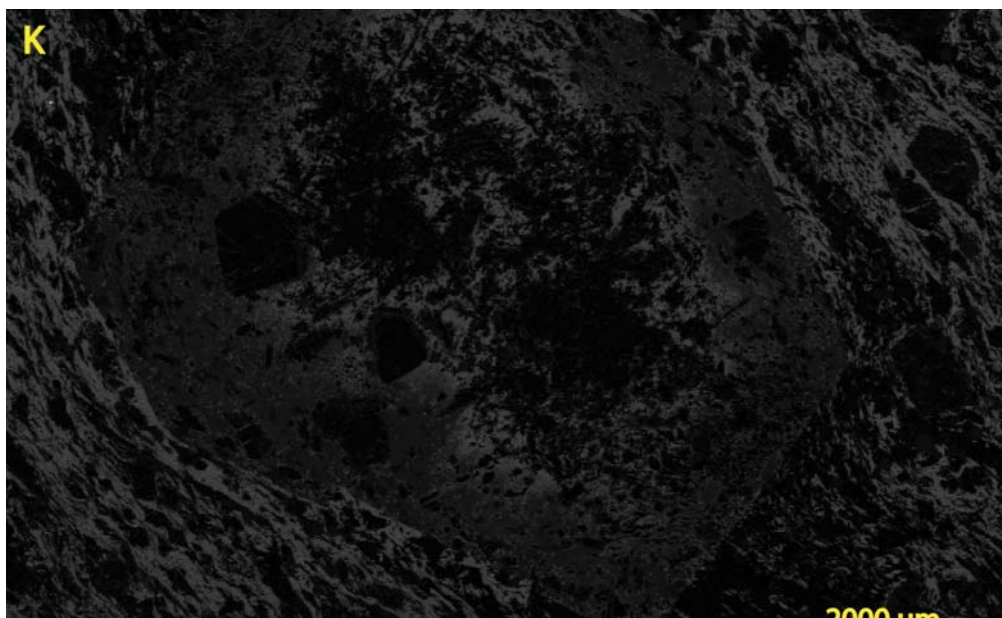
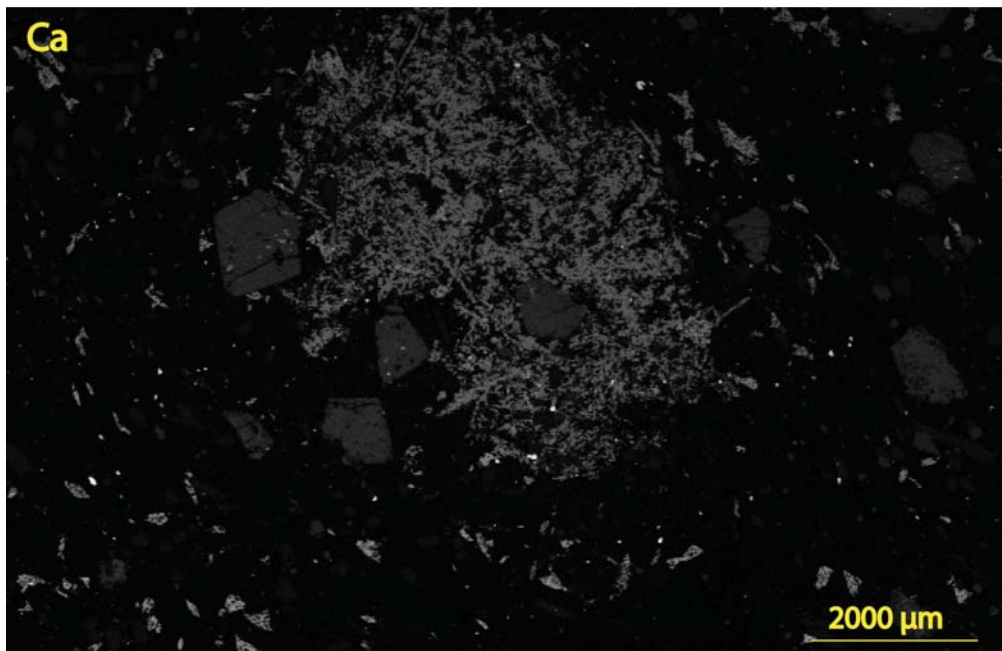
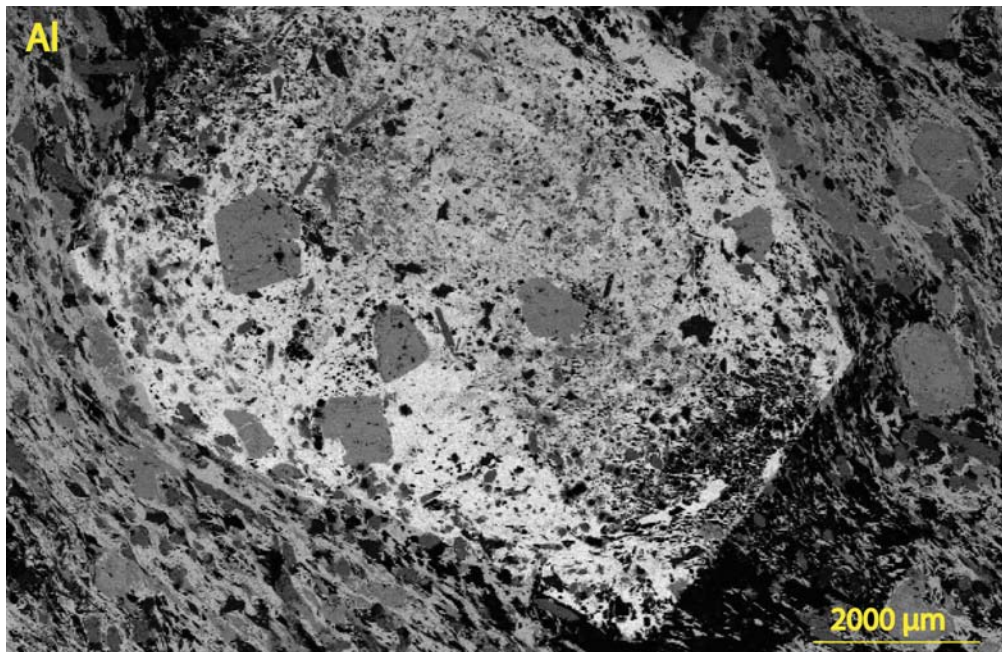


Figure 5-2: This thin section (JBB00-33A) contains four large pseudomorphs (up to 8 mm) two of them are shown here, slightly separated. Aluminum is abundant in the rock with even more aluminum in the pseudomorphs themselves. The Fe map shows that there is not much iron throughout the pseudomorphs, but there is iron in the garnets that are contained within the pseudomorph. The Mg map shows a similar pattern as the Fe map; there is low Mg inside of the pseudomorph (aside from the garnets), and the matrix is relatively rich in Mg. The Ca and K maps show a different pattern. The outer edges of the pseudomorphs are rich in K and the center of the pseudomorph is rich in Ca, mica and clinozoisite respectively. This mineralogic zoning in the pseudomorph was unexpected but could be explained by bringing K into the protocryt to drive the reaction from lawsonite to mica and an epidote group mineral.

Figure 5-3



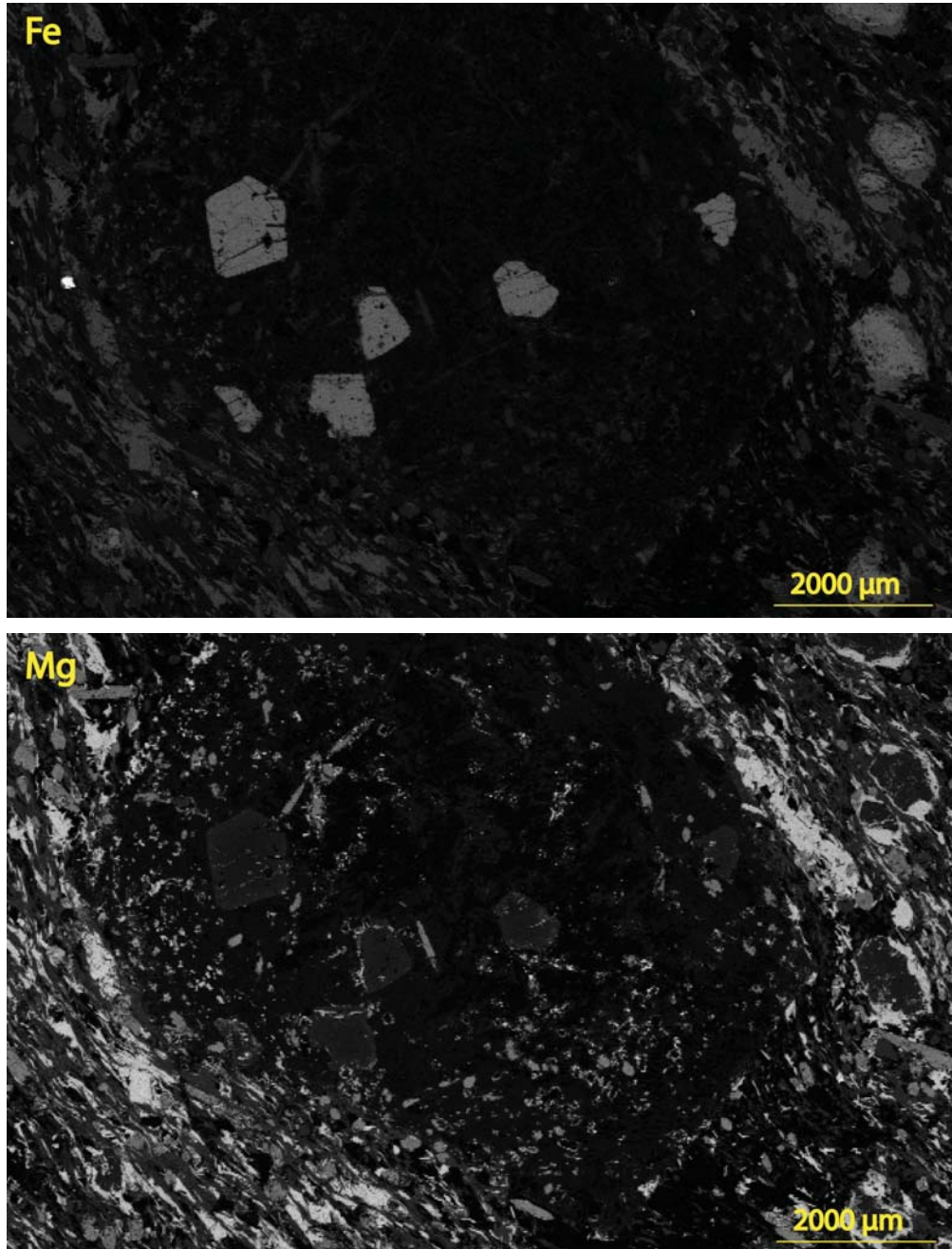
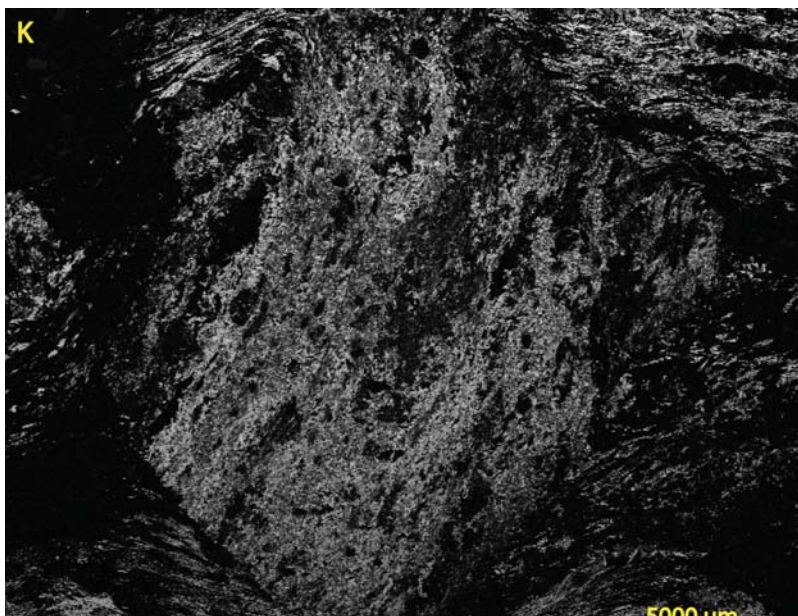
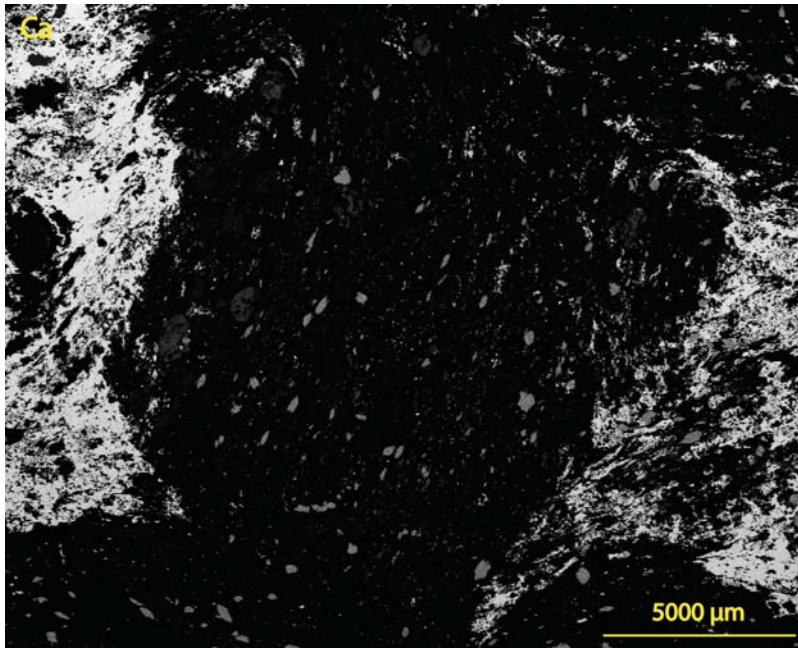
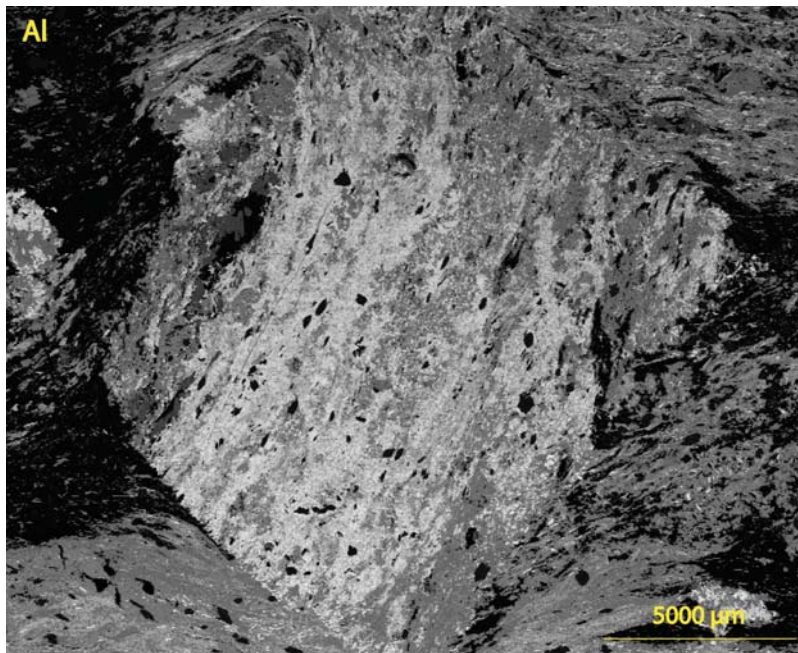


Figure 5-3: This pseudomorph is from the same thin section (JBB00-33A) and shows a similar pattern to Figure 5-1 where there is a higher concentration of Ca in the center of the pseudomorph and K on the edge. In addition, this pseudomorph contains more Mg throughout, though still small in comparison to the amount in the matrix. Another texture worth noting is that the garnets contained inside of the pseudomorph do not have rims of retrograde chlorite, but the garnets outside of the pseudomorphs do have chlorite rims, this could be because the pseudomorph engulfed the garnets prior to retrograde metamorphism and protected the garnets from the replacement that has occurred in the matrix.

Figure 5-4



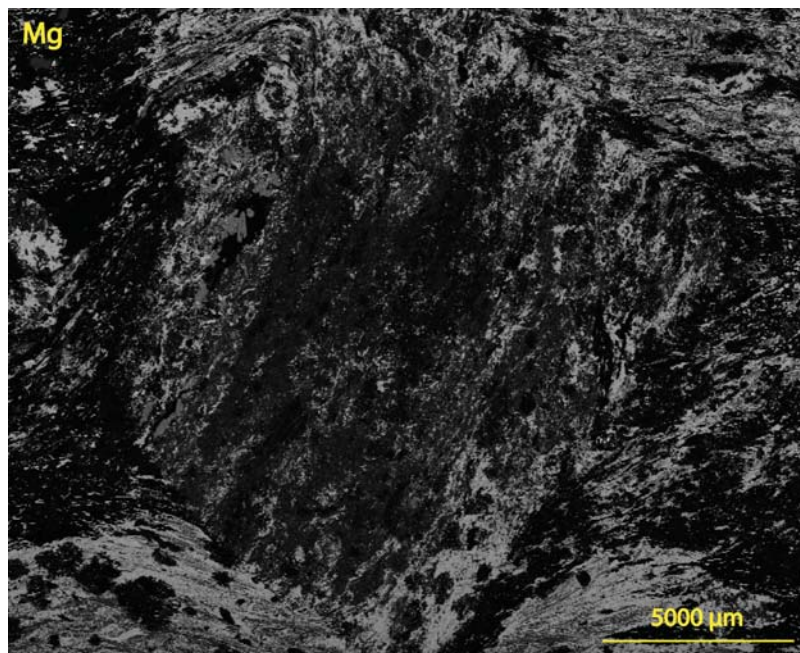
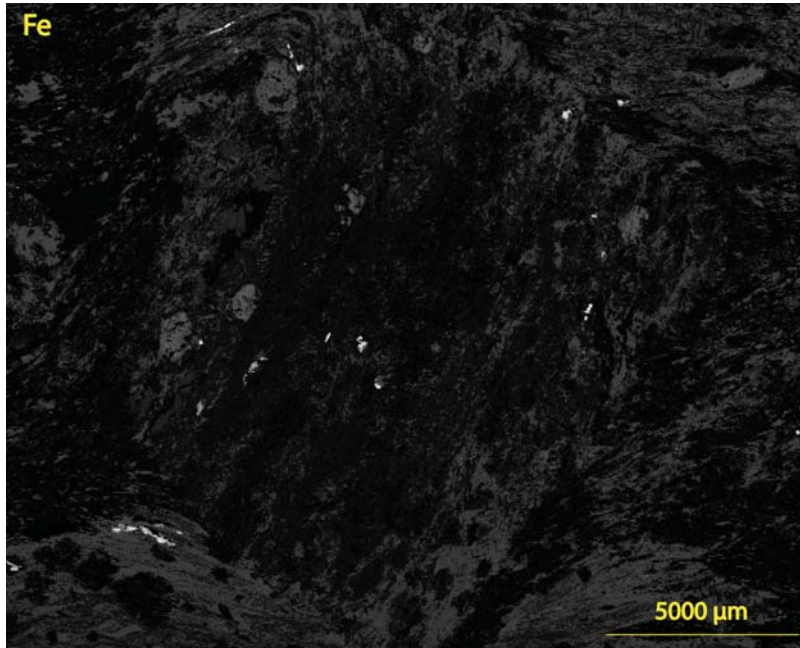
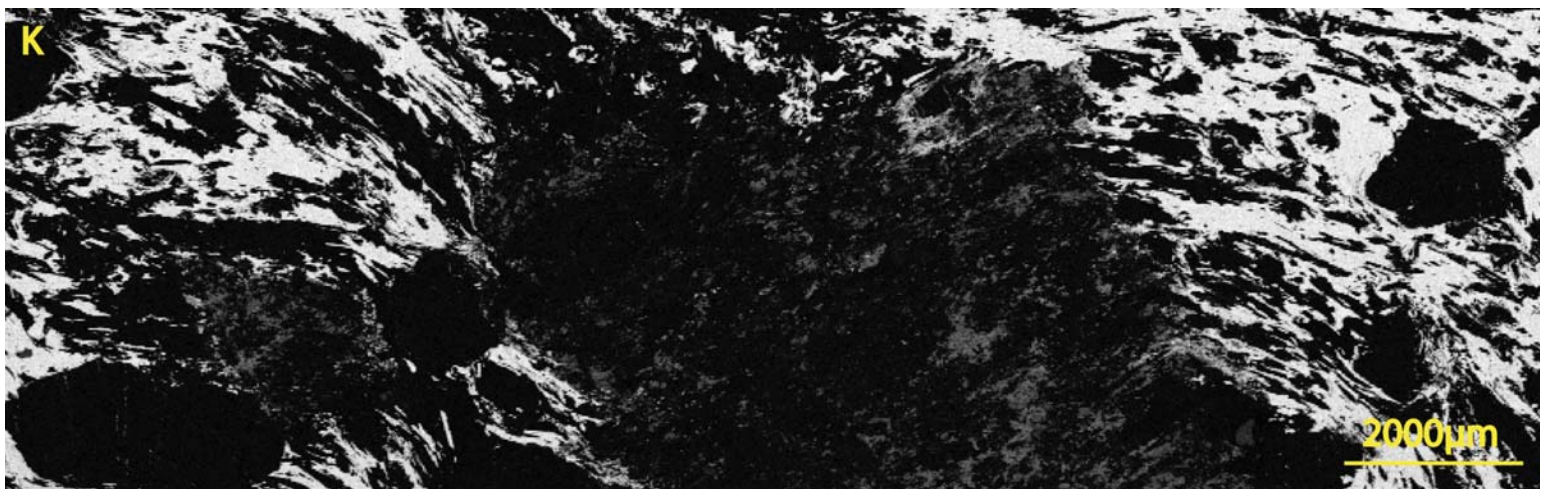
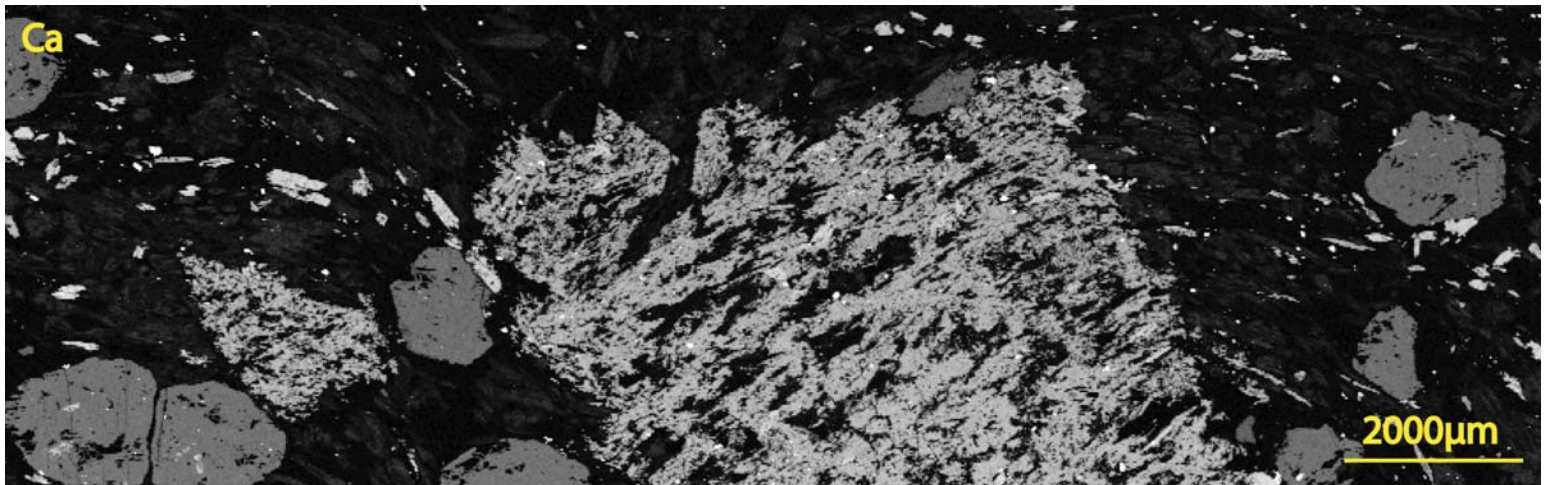
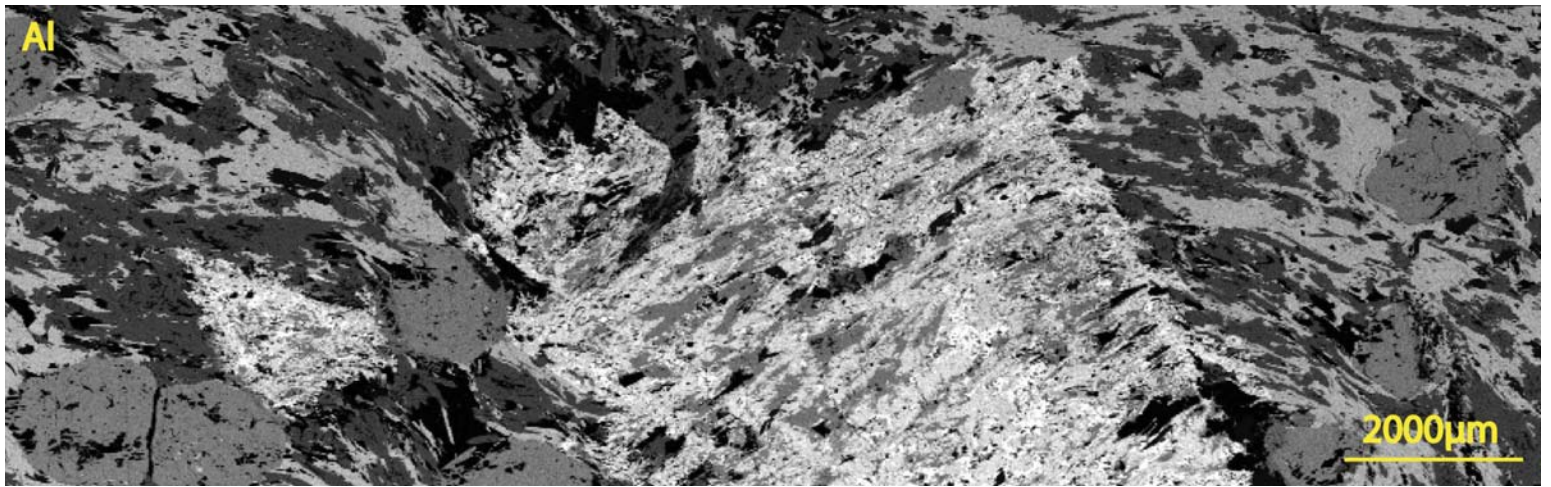
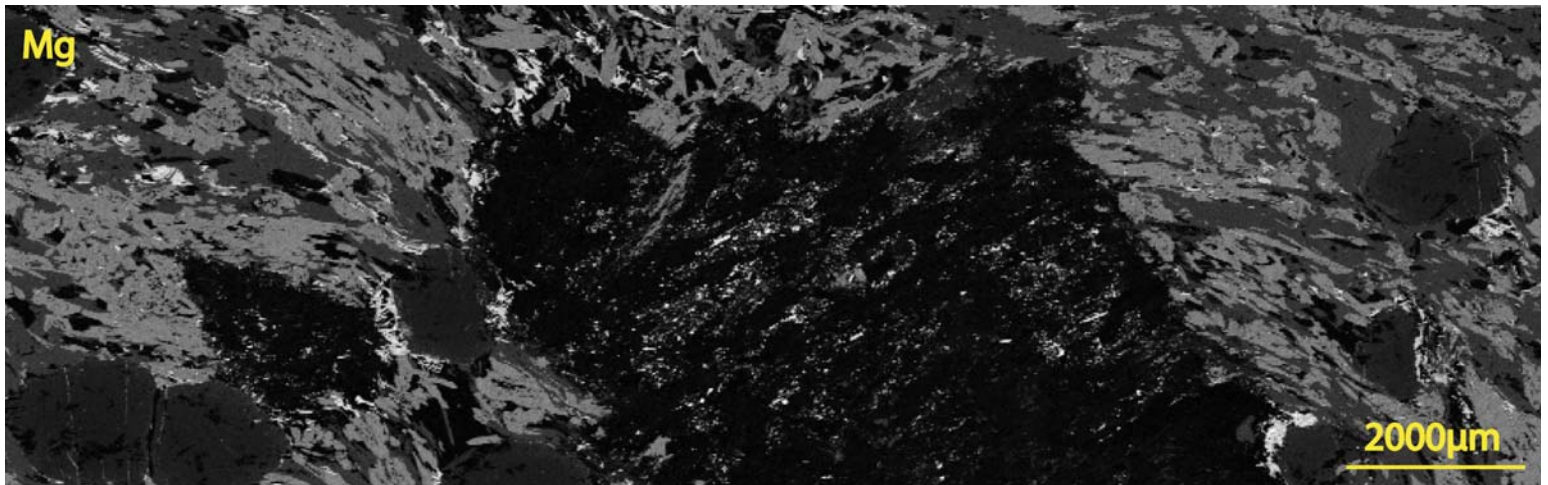


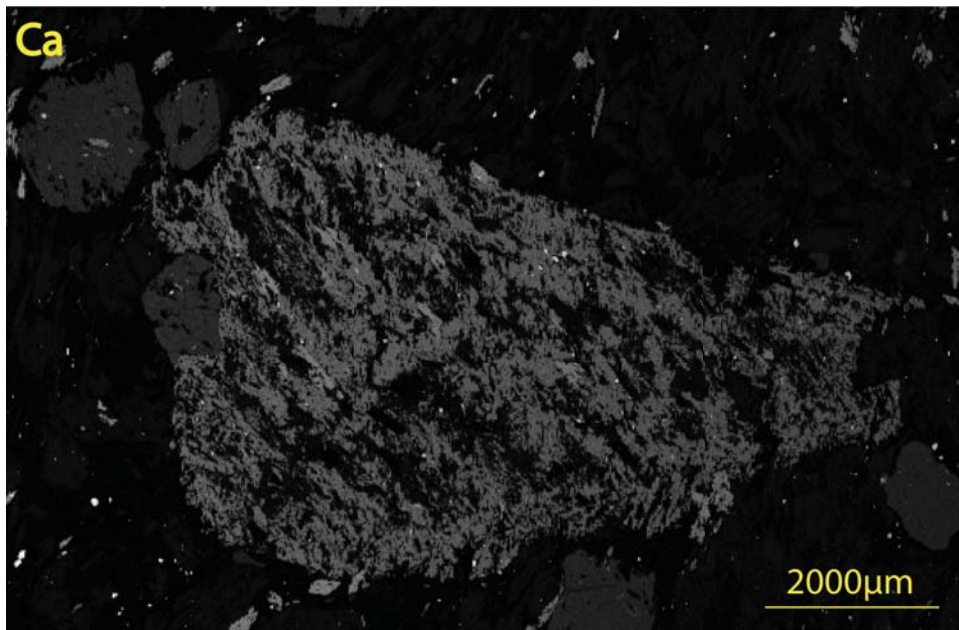
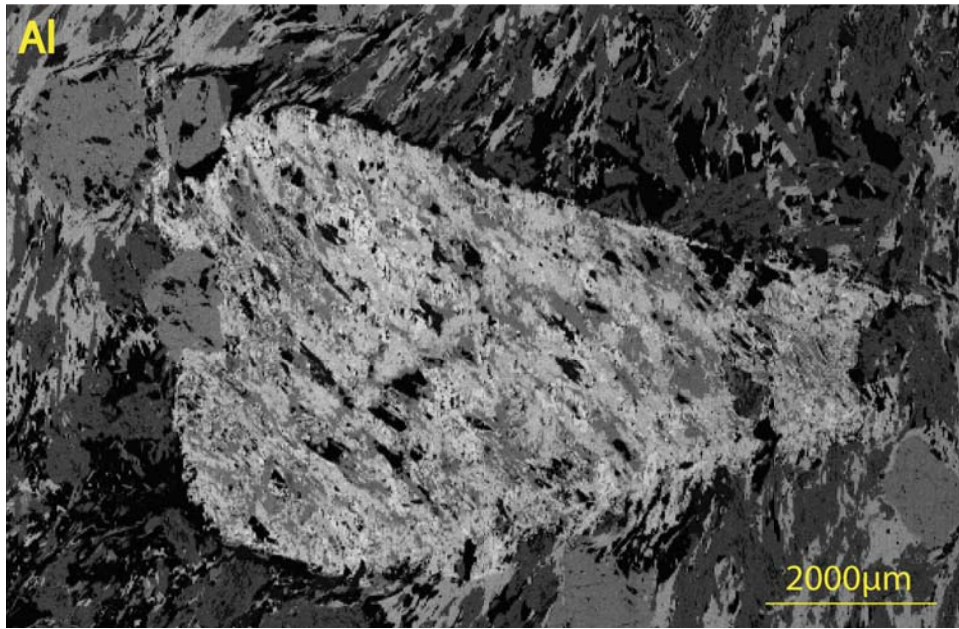
Figure 5-4: This pseudomorph is from the thin section SYR99.25C: it has one large pseudomorph (19 mm) in a mica- and calcite-rich rock. The element maps show that the pseudomorph is largely micaceous. Al, K and Mg are located throughout the pseudomorph following the foliation that is visible based on the orientation of the sphene. Fe is found throughout but in relatively small amounts. This combination of elements is representative of a pseudomorph composition of primarily mica with some chlorite. The Ca map shows a minimal amount of Ca stored in the pseudomorph – it almost exclusively occurs in the sphene, which is thought to be a spectator mineral. The overall lack of Ca lends itself to further questioning. If the protolith to this pseudomorph was lawsonite, where did the Ca go? If the protolith was not lawsonite, then what was it?





5-5: This pseudomorph is located on the edge of thin section JBB00-33C. There is an increased amount of Al in the p as compared to the matrix of the rock; this corresponds primarily to the location of the Ca in the pseudomorph. Th at this pseudomorph is made up primarily of clinozoisite and contains small amounts of mica and chlorite (shown b j maps). To the left of the larger pseudomorph, there appears to be another small triangular pseudomorph as well wh it distributions similar to the larger pseudomorph.

Figure 5-6



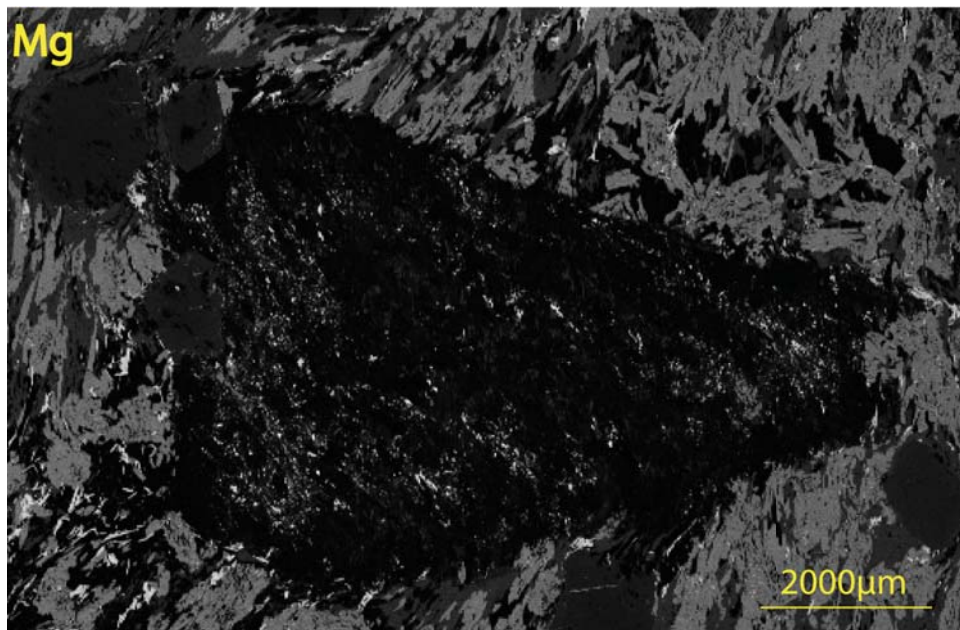
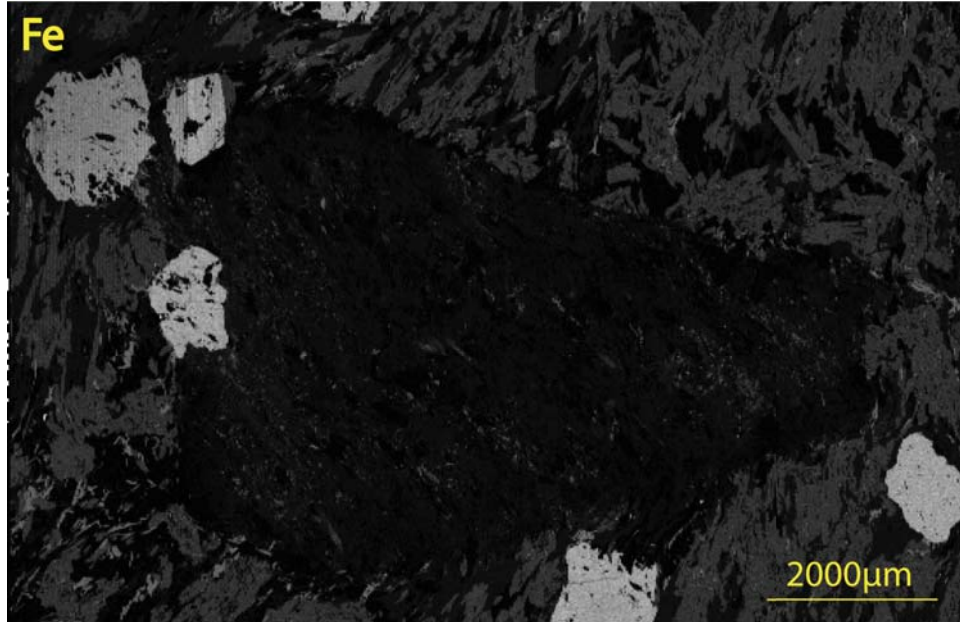
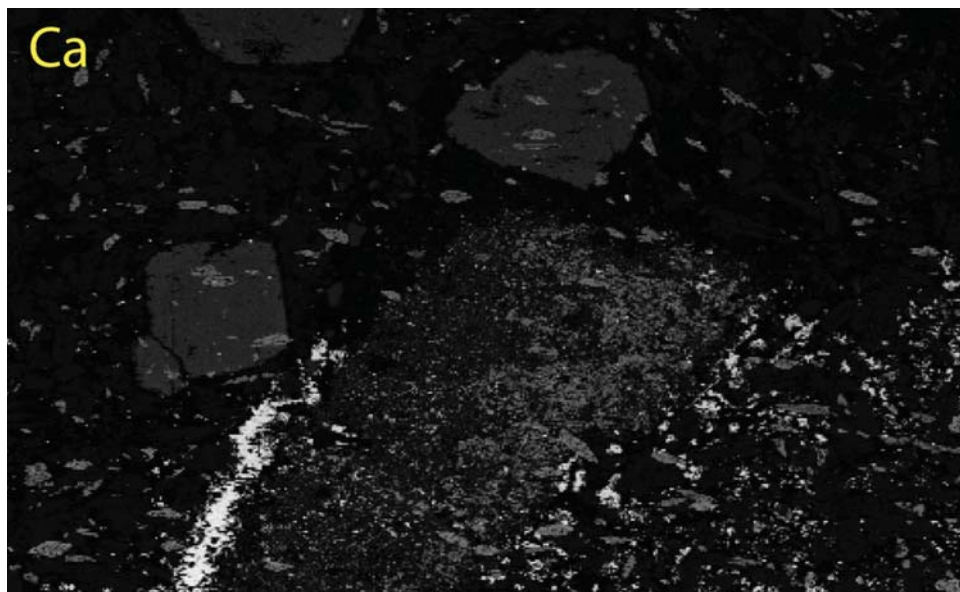
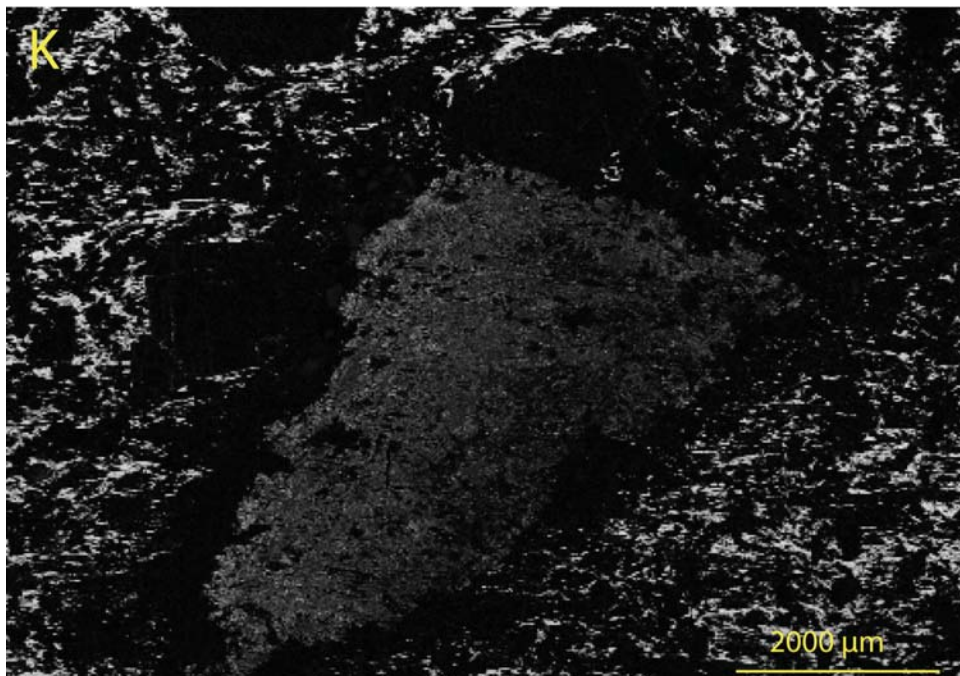
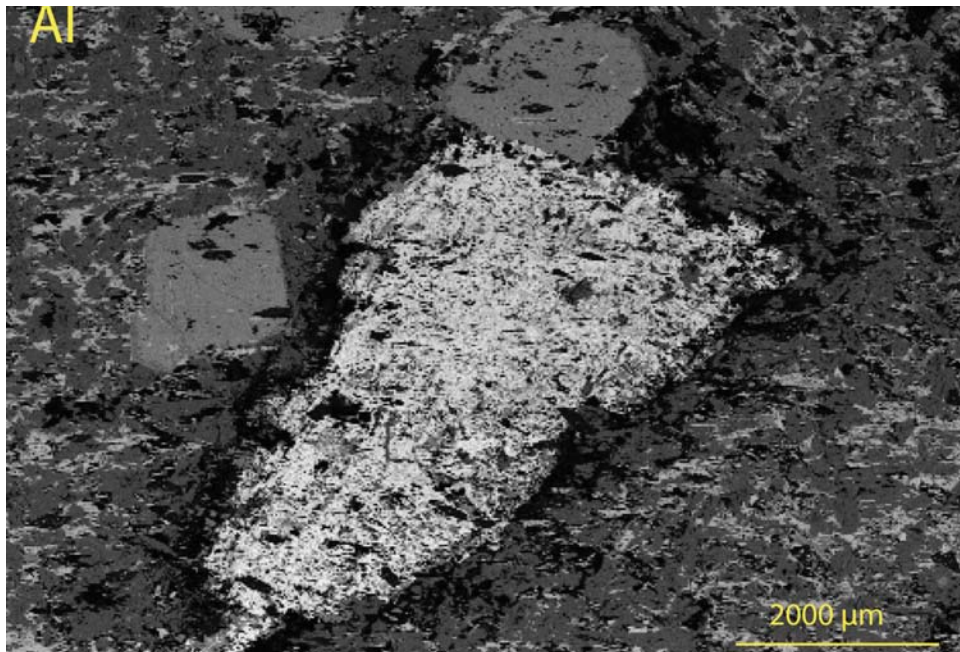


Figure 5-6: This pseudomorph is located on the edge of thin section JBB00-33C. There is an increased amount of Al in the pseudomorph as compared to the matrix of the rock; this corresponds primarily to the location of the Ca in the pseudomorph. This indicates that this pseudomorph is made up primarily of clinozoisite and contains small amounts of mica and chlorite (shown by the K and Mg maps). To the left of the larger pseudomorph, there appears to be another small triangular pseudomorph as well which has element distributions similar to the larger pseudomorph.

Figure 5-7



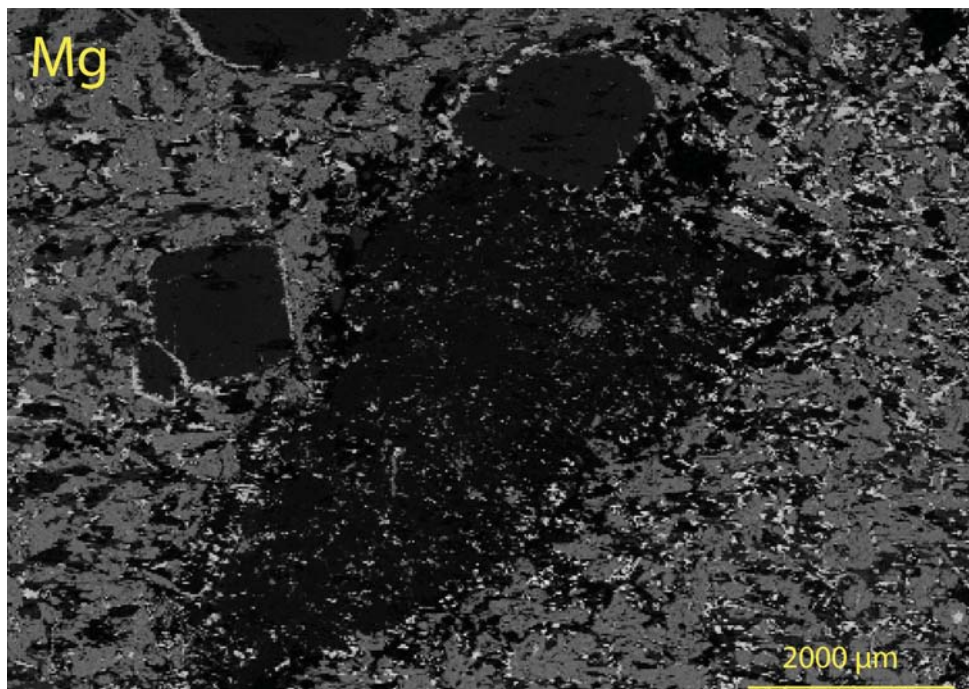
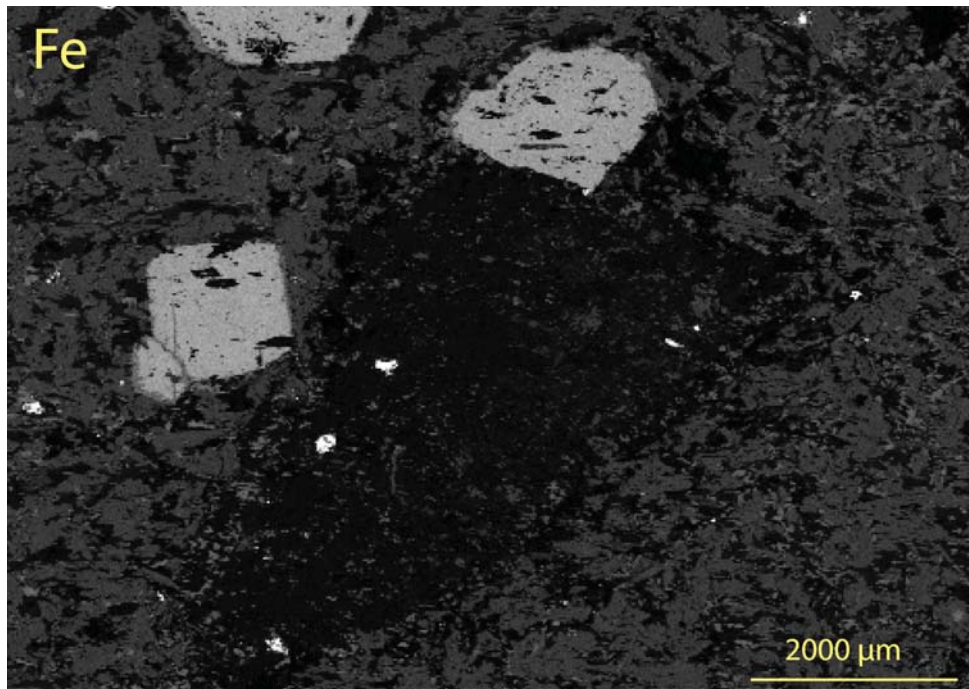
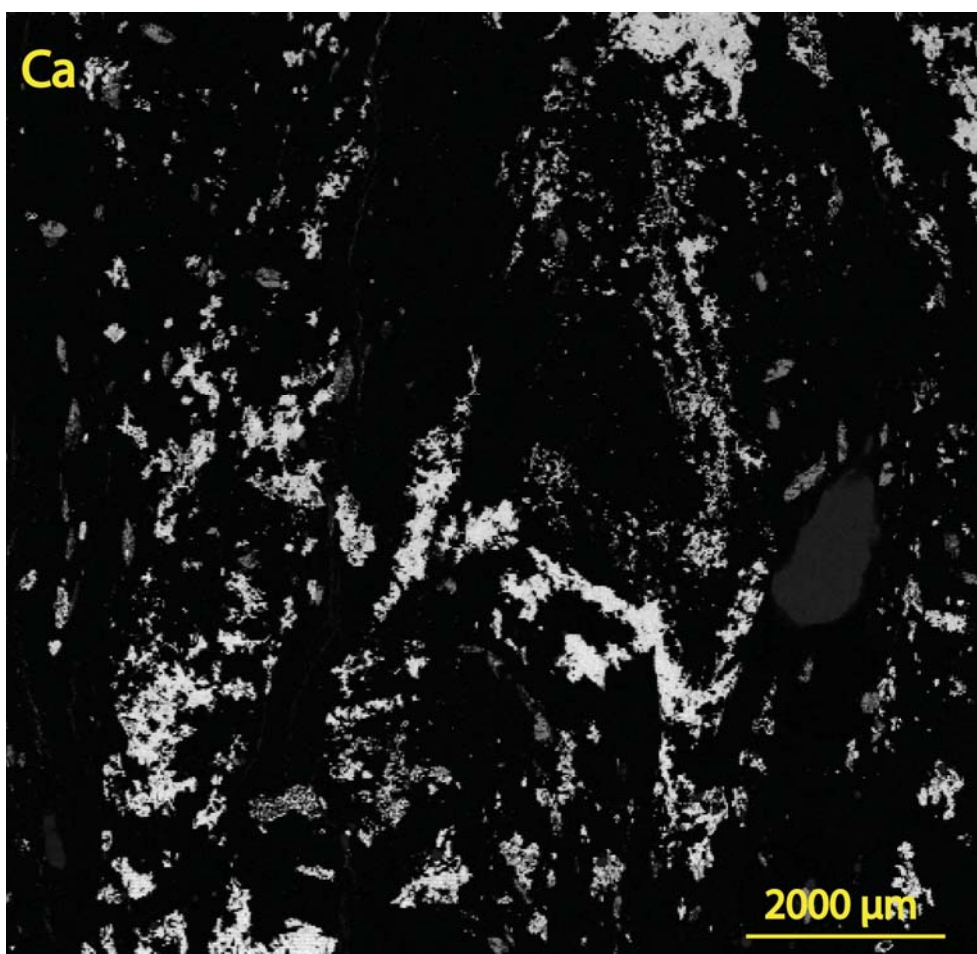
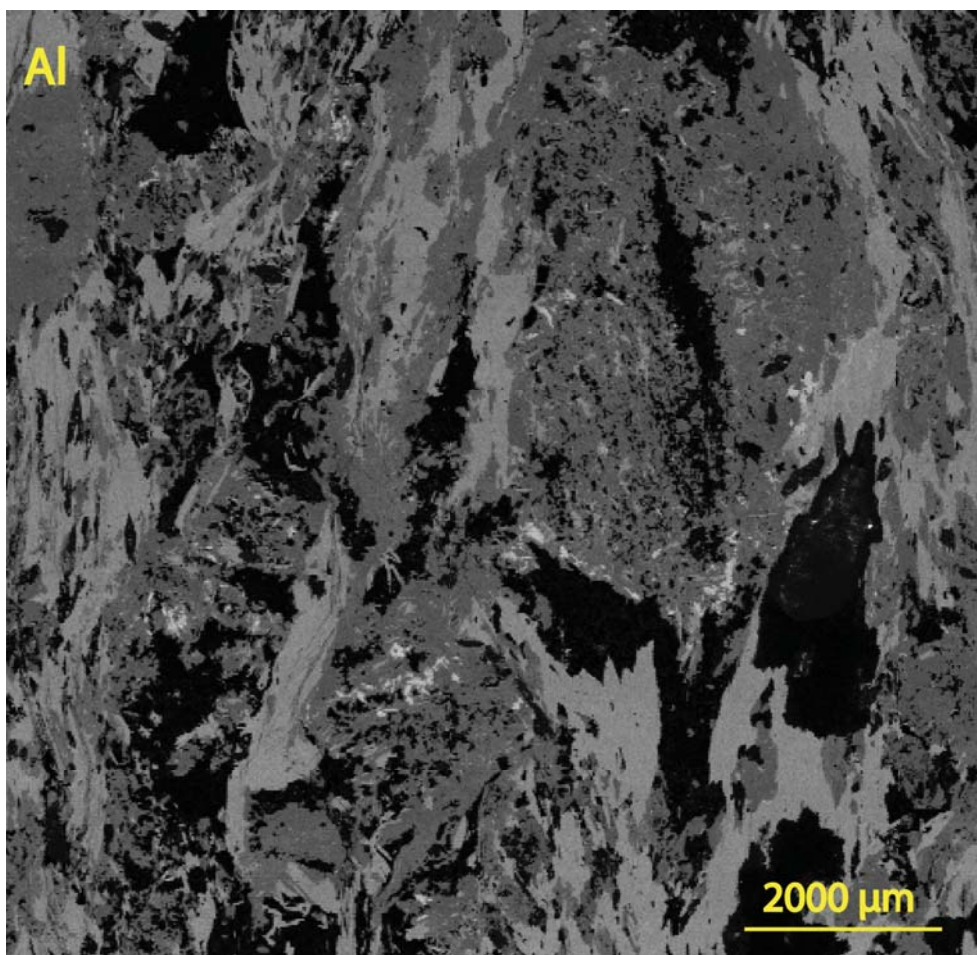
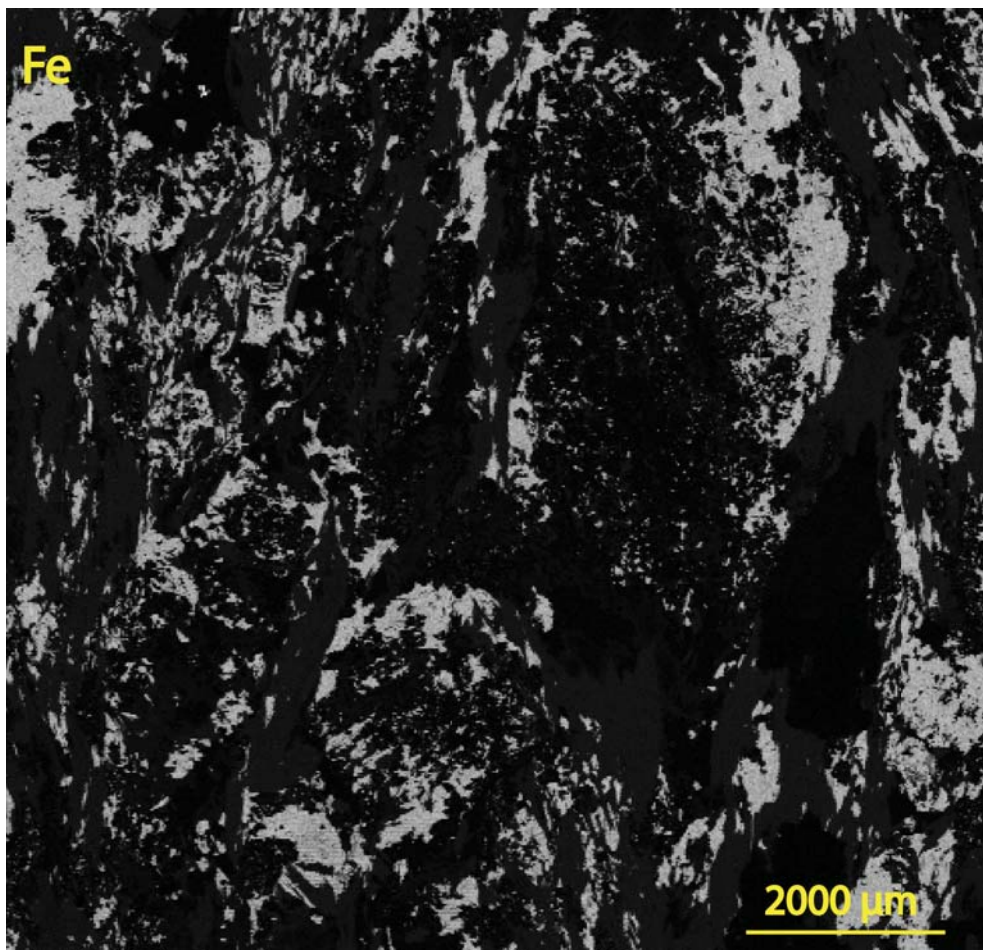
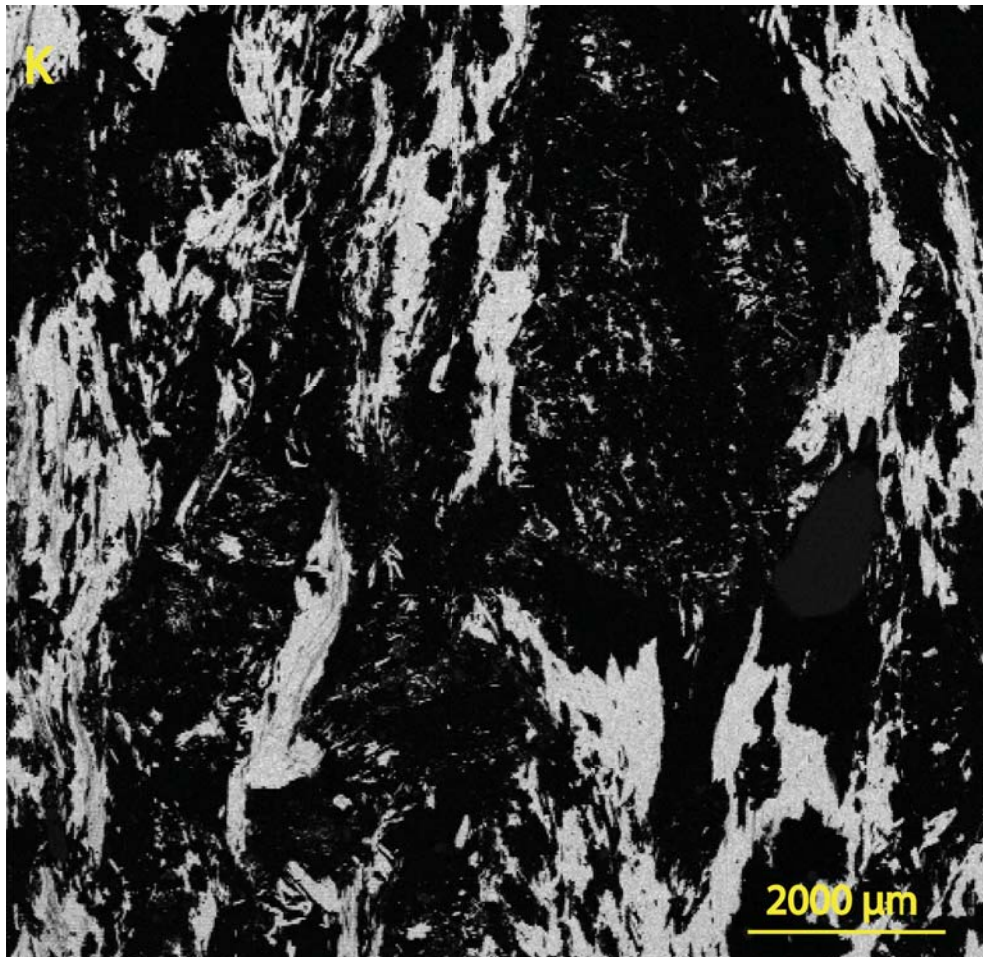


Figure 5-7: This pseudomorph is from thin section SYR 141F. It shows a much higher aluminum concentration than the surrounding matrix but lower amounts of Fe and Mg. The distribution of Ca shows more clinozoisite on the right side of the pseudomorph. The K element map shows more mica on the left side of the pseudomorph, opposite of the location of the clinozoisite. Also, surrounding the pseudomorph on the K map there is a K depleted area compared to the pseudomorph as well as the matrix; this area is primarily chlorite and quartz. The absence of K in a ring around the pseudomorph gives more evidence to the hypothesis of bringing K into the protocryt to drive the reaction forward.

Figure 5-8





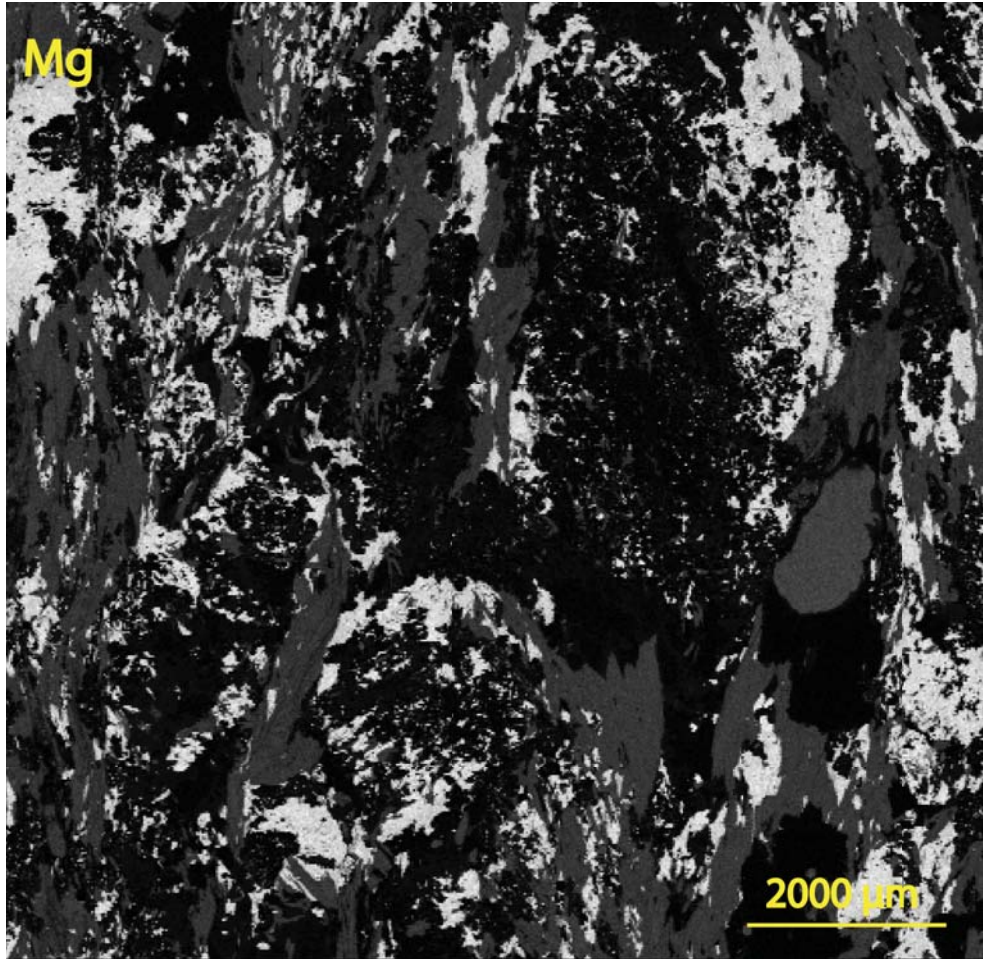
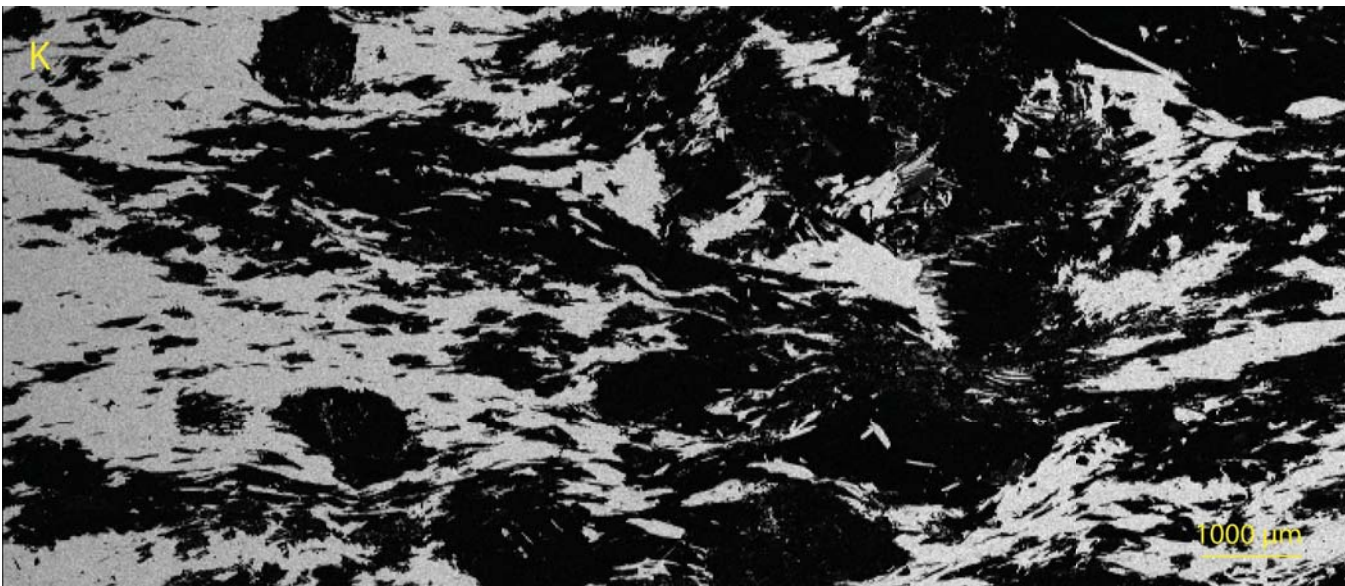
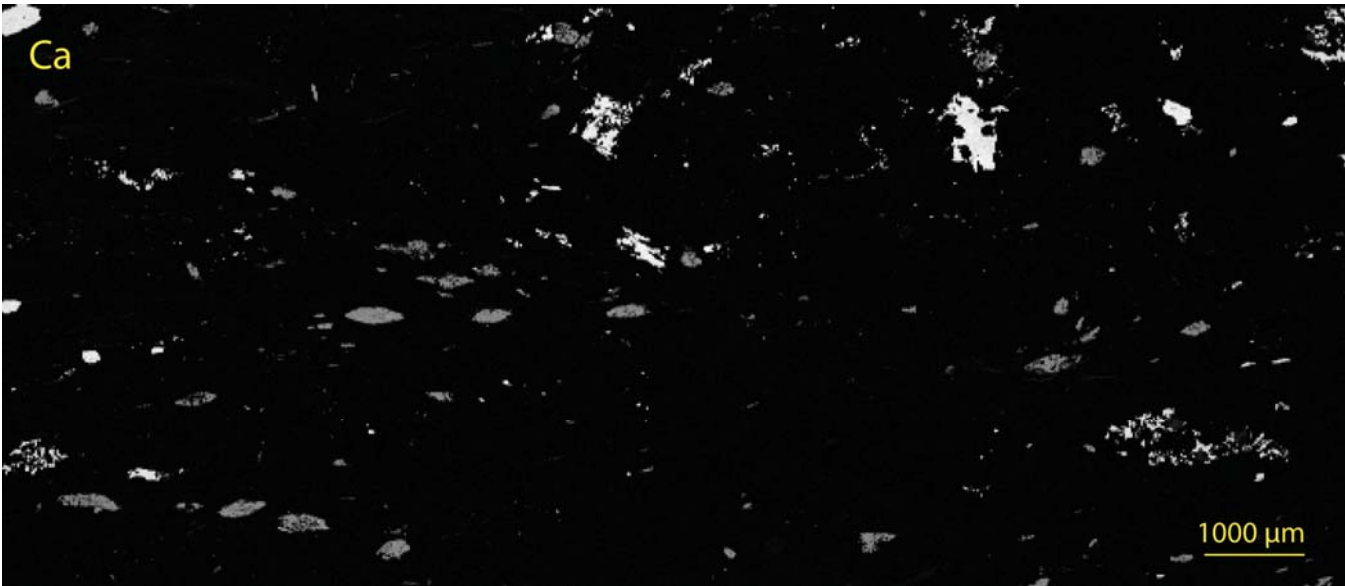
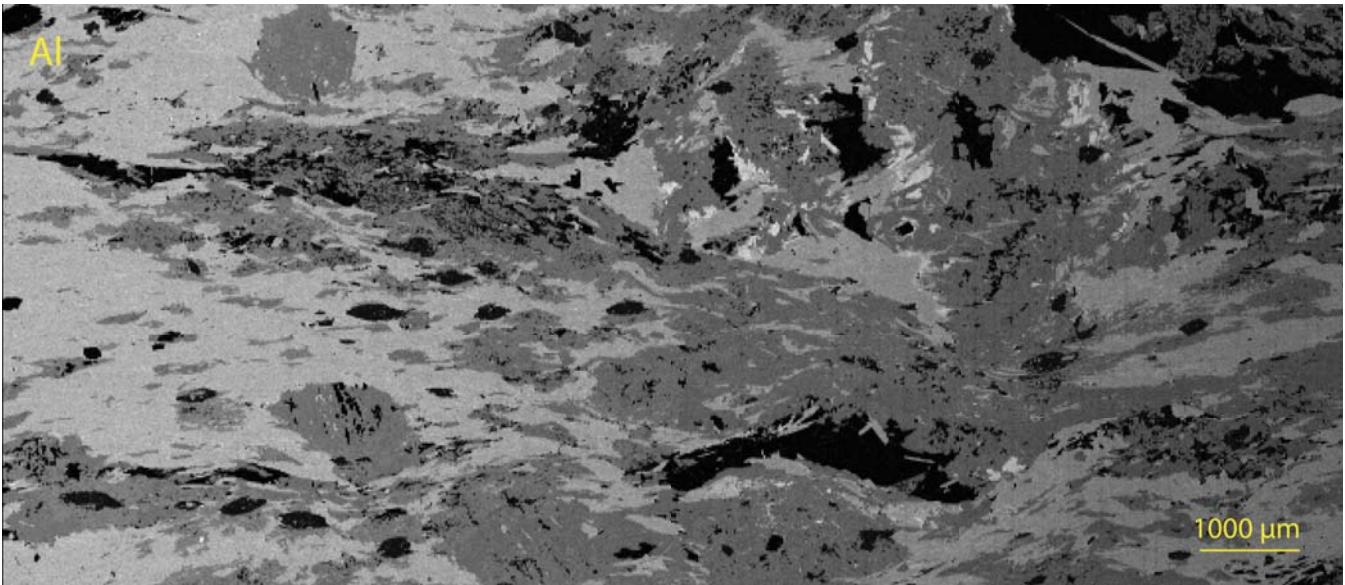


Figure 5-8: The mapped area is from JBB99-33B, this thin section contained many rhombohedral and circular mineral masses that looked similar to pseudomorphs. This series of element maps shows that these suspected pseudomorphs are not from the same protocrust. The top pseudomorph is primarily albite with some chlorite on the right edge. Not only does this pseudomorph vary from the other pseudomorphs in this map area, it does not contain Ca or K like the pseudomorphs in Figures 5-1 to 5-4, and likely does not share the same protocrust.

The bottom pseudomorph is more Fe and Mg rich; this, in conjunction with petrographic analyses, shows that it is made up primarily of chlorite. The shape and other textures, such as mica bending around the chlorite-rich clump, indicates that this is a chlorite-replaced garnet.

Figure 5-9



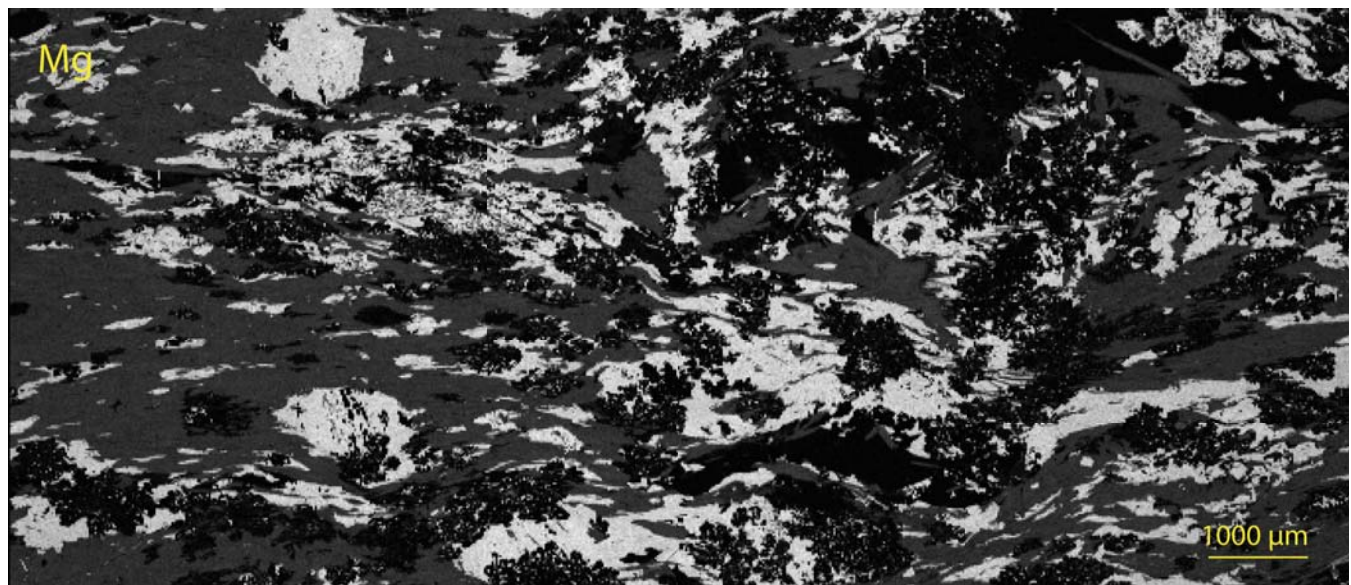
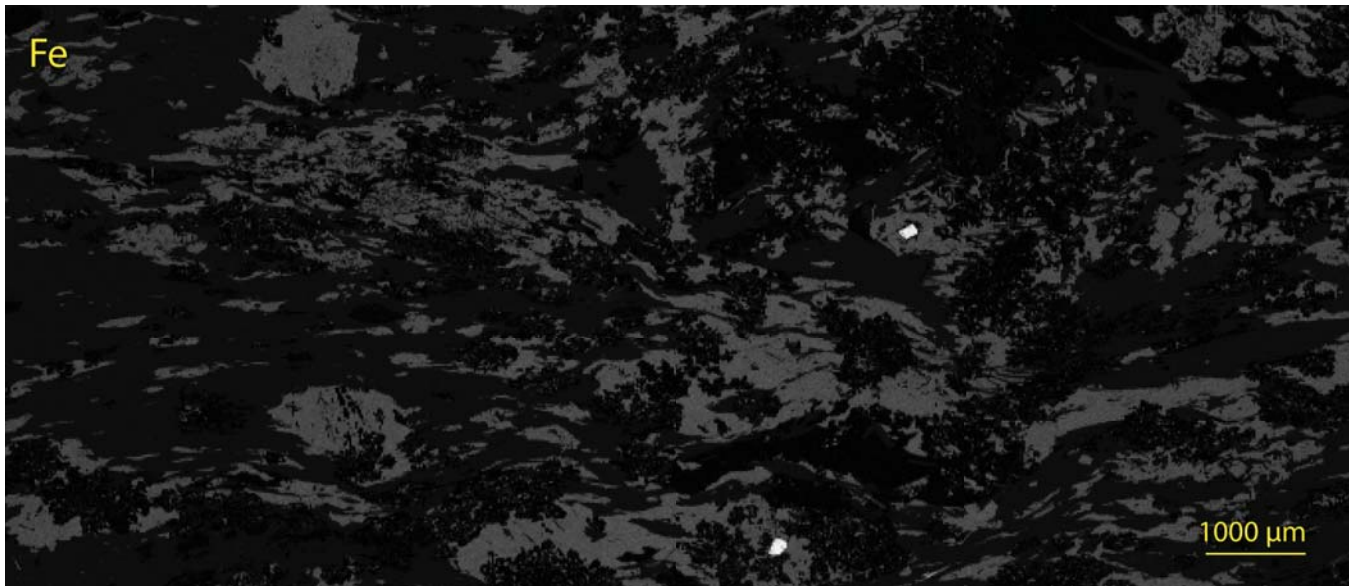


Figure 5-9: This series of maps is from LFL02, it was mapped because it was suspected to contain pseudomorphs due to the distribution and shape of mineral. This set of area maps confirms that the anhedral mineral throughout LFL02, LFL65 and JBB99-33B is albite. However, the element maps do not show that these clusters are pseudomorphs because their composition is no different from the rest of the rock. This rock has large amounts of albite and likely underwent more greenschist metamorphism than the other rocks in the suite.



Discussion:

In order to assess whether or not it is plausible that the protocry of the pseudomorphs was lawsonite, mass balance calculations were completed. To do these calculations, a fundamental assumption was made that the Ca present in clinozoisite now is equal to the amount of calcium that was present in the protocry. It is likely that the aluminum that was originally in the protocry remained in the pseudomorph, however, there are other aluminous minerals in the matrix, the micas in particular. So it is more likely that there was aluminum added to the pseudomorph during metamorphism than calcium. Calcium is a large cation and given the low X_{CO_2} values ($X \sim 0.01$) calculated by Schumacher et al. (2008) it is unlikely that the calcium in the original protocry was used to grow calcite. This means that the clinozoisite present in the pseudomorphs dictates the amount of lawsonite that was originally present because it is the only mineral that is storing the Ca. With the assumption, the calculations can be completed.

In order to determine the relative amount of Ca present in the pseudomorphs as compared to what would be expected for a lawsonite protocry two pieces of information are needed: (1) the area of clinozoisite and the area of the total pseudomorph from the pixel counting and (2) the percentage of the volume that is taken up by calcium in the lawsonite or clinozoisite, respectively. Using this data, the following table was generated that shows the percent of lawsonite and inferred percentage of inclusions in the pseudomorph, assuming that what was not lawsonite was inclusions (Table 5-1).

Table 5-1: Results of the calculations representing the amount of calcium present in the pseudomorphs currently and the amount of lawsonite that this calcium can generate. This is

	JBB00-33A	JBB00-33A	JBB00-33A	SYR99.25C	JBB00-33C	JBB00-33C	SYR141F
Area Cz	10369	20666	403284	0	26669	25247	4203
Area Ca - from Cz	1481	2952	57612	0	3810	3607	600
Hyp. area laws	14813	29523	576120	0	38099	36067	6004
Area PS -from map	74066	121563	2122546	192677	74082	72134	35021
Percent laws of PS	20	24	27	0	51	50	17
Percent inc of PS	80	76	73	100	49	50	83

compared to the size of the pseudomorphs that are observed in the rocks. What is not lawsonite in the protocryt is assumed to be inclusions.

The largest percentage of possible lawsonite in the pseudomorph area observed in the thin sections is from JBB00-33C, 51%. This pseudomorph, the most calcium-rich with regards to size of the pseudomorph, only has enough calcium to make a protocryt of 51% lawsonite, 49% inclusions. The other pseudomorphs from JBB00-33A and SYR141F contain enough calcium to make approximately 20% of the protocryt be lawsonite.

The pseudomorphs in JBB00-33A showed distinct mineral zoning with a clinozoisite - rich center (Figures 5-1, 5-2 and 5-3), this could be representative of the original size of the lawsonite protocryt with other minerals either included or added on to the pseudomorphs. This hypothesis was tested using the hypothetical area of lawsonite from Table 5-1 and comparing it with the area of the central, clinozoisite-rich section of the pseudomorphs. The results vary, but on average the amount of lawsonite is similar to the area in the central zone of the pseudomorphs, especially the third pseudomorph tested in JBB00-33A. This evidence supports the idea of a lawsonite protocryt and the calcium control of the original size of the lawsonite protocryt.

	Map 1a PS1	Map1a PS2	Map1b
Area Laws - from Ca	14813	29523	576120
Area PS in	19695	47376	636764
Percent Laws/PS	75	62	90

Table 5-2: Results of calculations representing the hypothetical area of lawsonite in the protocryst compared to the area in the clinozoisite-rich center in pseudomorphs (JBB00-33A).

Map 2 stands out in composition and mode from all of the other maps, this is visible in the pie charts (Figure 5-10) as well as Table 5-1. The pseudomorph contains no clinozoisite and very little calcium (3%); the rock itself is also Na-poor. It is unlikely that the calcium in the pseudomorph, especially all of the calcium, was removed. This indicates that it likely has a different protocryst than the pseudomorphs in the other three thin sections.

Even though JBB00-33A, JBB00-33C and SYR141F contain clinozoisite as a calcium sink and appear to have a large amount of clinozoisite, they do not have nearly enough calcium for a pure lawsonite protocryst with a size equal to the current pseudomorph. However, the occurrence of lawsonite in other rocks on Syros, shape of lawsonite porphyroblasts and overall Ca and Al content of the pseudomorph still support the idea of a lawsonite protocryst. In order to assert that the protocrysts were originally lawsonite, an explanation must be made for the lack of calcium currently present that is required for the lawsonite protocrysts. Three logical arguments can be made:

(1) A foliation is preserved in many of the pseudomorphs that are seen. This indicates that the lawsonite overgrew a foliation and possibly contained numerous inclusions. The only way that the pseudomorphs could preserve a fabric is if the protocryst overgrew a fabric. If the lawsonite was full of inclusions when it grew, it could lead to the low numbers for calcium that are observed in Table 5-1. The inclusions would likely be of a similar composition to the current

matrix. The garnets and sphene that are included within the pseudomorphs but do not participate in the reactions support the theory of lawsonite containing numerous inclusions.

(2) A portion of the calcium that was contained in the lawsonite pseudomorphs could have been removed through the reactions, contrary to the original assumption. This is especially possible given that the metamorphic history of the rocks is widely unknown. Removing some calcium from the protocrust is a possibility; but the low X_{CO_2} values suggested by Schumacher et al. (2008) state that it could not be combined with the CO_2 and precipitate calcite. The removal of some Ca from the system could account for some of the calcium deficiency, but not a complete lack of calcium as with Figure 5-3.

(3) If the pseudomorphs are zoned, as is observed in JBB00-33A and LFL60, then the location of the cross-section in thin section could affect the observed composition of the pseudomorphs. It is possible that the Ca-poor area of the pseudomorphs is being measured and there are more clinozoisite -rich (and thus Ca-rich) areas in the pseudomorphs, this would increase the total value for calcium present in the pseudomorphs.

(4) A fourth scenario would be K metasomatism from a K-rich fluid. This has been cited as the explanation for lawsonite replacement in the Southern Urals from the relationship: lawsonite + garnet + K-bearing fluid \rightarrow clinozoisite + chlorite + phengite (Schulte and Sindern, 2002). This reaction looks very similar to the reactions being explored in this research, however other evidence refutes this as a likely possibility. The pseudomorphs occur frequently on the island of Syros and the research suggests that the lawsonite has gone through a similar reaction; it is not likely that the K fluid would uniformly permeate through all of the rocks and create the same reaction that is observed around the island. Additionally, metasomatism decreases in grade

away from the source, so one would expect a zonation of the lawsonite reaction if this were the case, this is not observed on the island.

There are more aspects of the pseudomorphs and the rocks that could be investigated to better support or refute the lawsonite protocry. Here are some points that should be investigated: Does the matrix composition vary with respect to the distance from the pseudomorphs? Does the mica composition vary with respect to distance from the pseudomorphs? Why or why not? Do the rocks that have glaucophane in the matrix have pseudomorphs that are Ca-poor? Could this be evidence for the presence of a more Na-rich protocry? There is one consideration to keep in mind: because it is not easily feasible to see in 3-D, knowing how far one pseudomorph is from another is difficult. This adds complexity to quantifying variations in the matrix.

Chapter 6: ACFN and ACF Diagramming

Locating the bulk composition of the rocks and pseudomorphs on a diagram is helpful to assess whether or not the bulk compositions of the rocks are in fact similar, and if they vary, how. It also highlights how the rocks that have pseudomorphs compare to those that do not. A ternary diagram does not cover all of the variables that are important to the relationships of the rocks in this study. FeO+MgO, Al₂O₃, CaO and Na₂O need to be considered in order to fully explain the variations in bulk composition and assess the composition of the pseudomorphs. For this, a tetrahedral plotting program was used to look at all of the variables involved in the rocks (Tetlab). The bulk compositions of all of the rocks were plotted in molar averages on the diagrams. Additionally, the end member minerals found in the matrix and pseudomorphs were added to the diagram to help visualize the pseudomorphing reactions that may have taken place.

The first diagram (Figure 6-1) shows a traditional ACF view where it is apparent that there are two groups of bulk compositions plotting in two areas, one on the lower left and one on the right side of the triangle. There is one exception to this rule, the point located in the middle of the diagram. The tilted diagram shows the Na content in the rocks (Figure 6-2), the sample that does not fit into the two plotting areas stands out as the most Na-rich sample. This sample clearly has a different bulk composition than the other rocks, and because only one sample falls here, trends cannot be concluded.

In combination with the bulk rock compositions, tie lines were drawn to show a potential reaction that the protocrust experienced (Figures 6-3 and 6-4). The head-on ACF (Figure 6-3) shows that the lawsonite + glaucophane tie line divides the two groups of rocks. This could account for the lack of clinozoisite-rich pseudomorphs in the pseudomorphs below the lawsonite + glaucophane tie line. It is possible that the assemblage could have been calcite + clinozoisite +

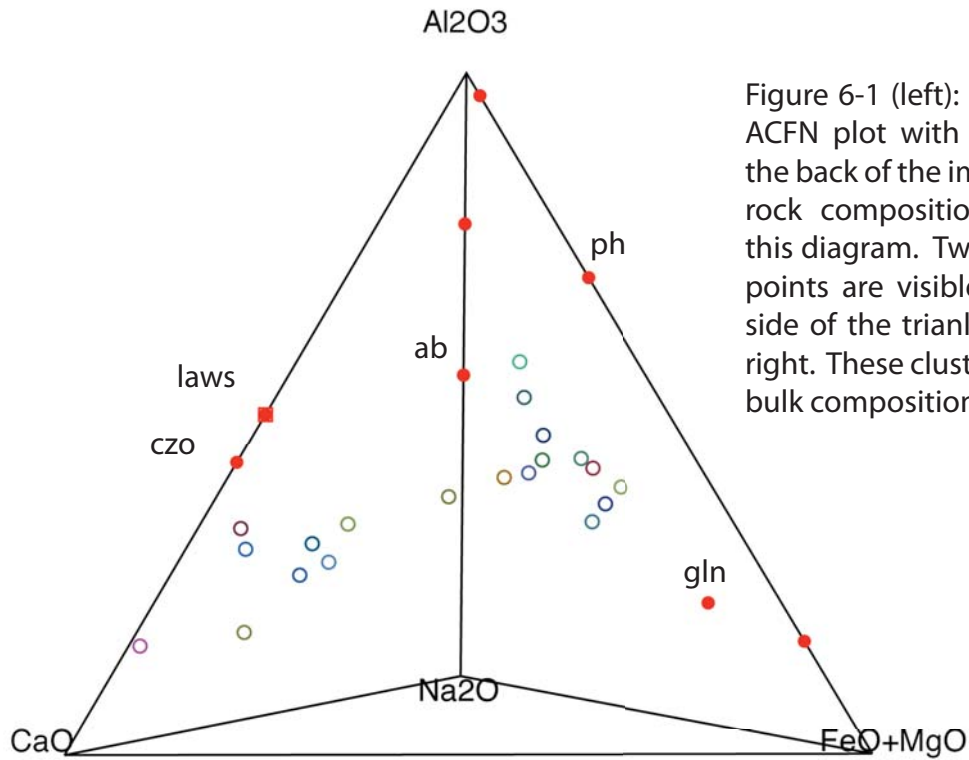


Figure 6-1 (left): An ACF view of the ACFN plot with the Na₂O point at the back of the image. All of the bulk rock compositions are plotted on this diagram. Two distinct groups of points are visible. One on the left side of the triangle, the other on the right. These clusters display different bulk compositions.

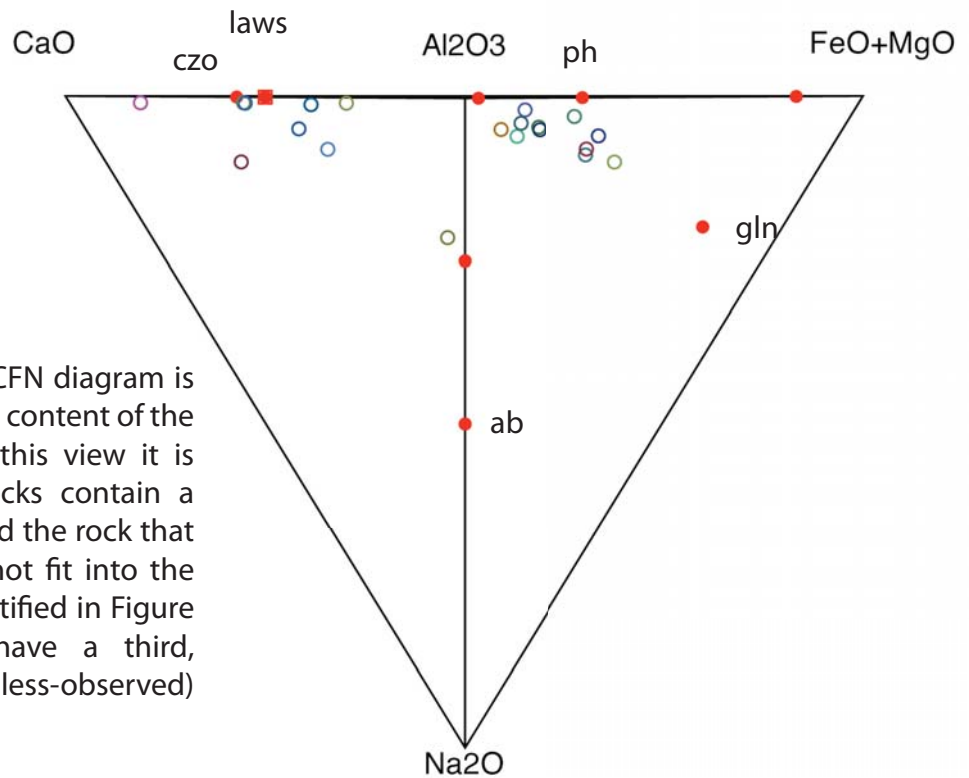


Figure 6-2 (right): The ACFN diagram is now tilted to view the Na content of the bulk compositions. In this view it is established that the rocks contain a limited amount of Na and the rock that has the most Na does not fit into the two distinct groups identified in Figure 6-1, this rock must have a third, distinctly different (but less-observed) bulk composition.

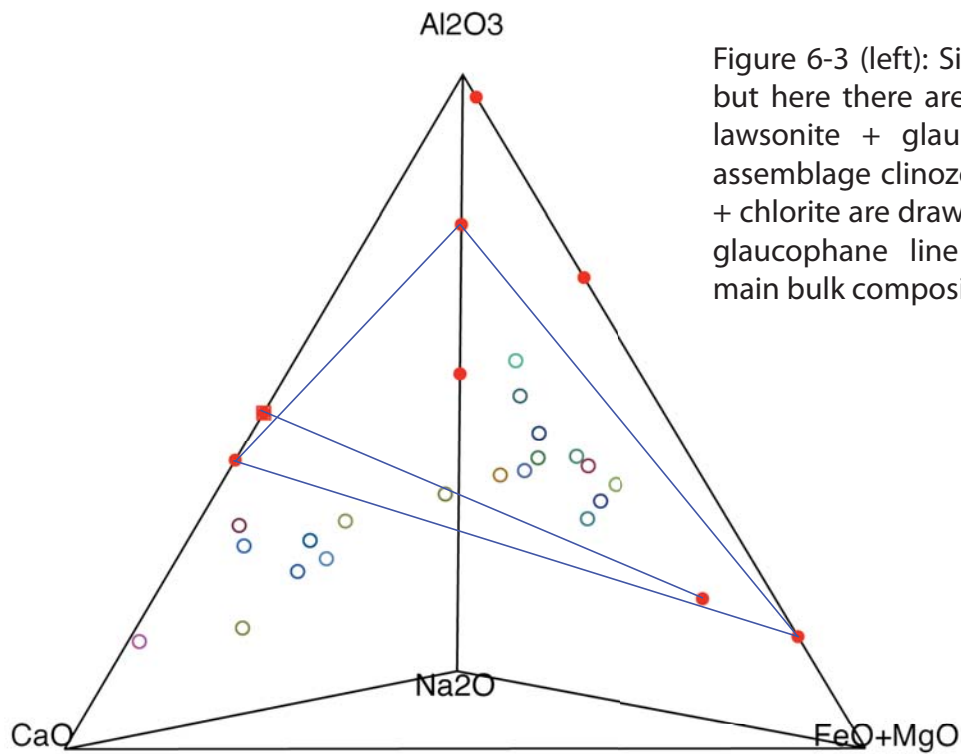
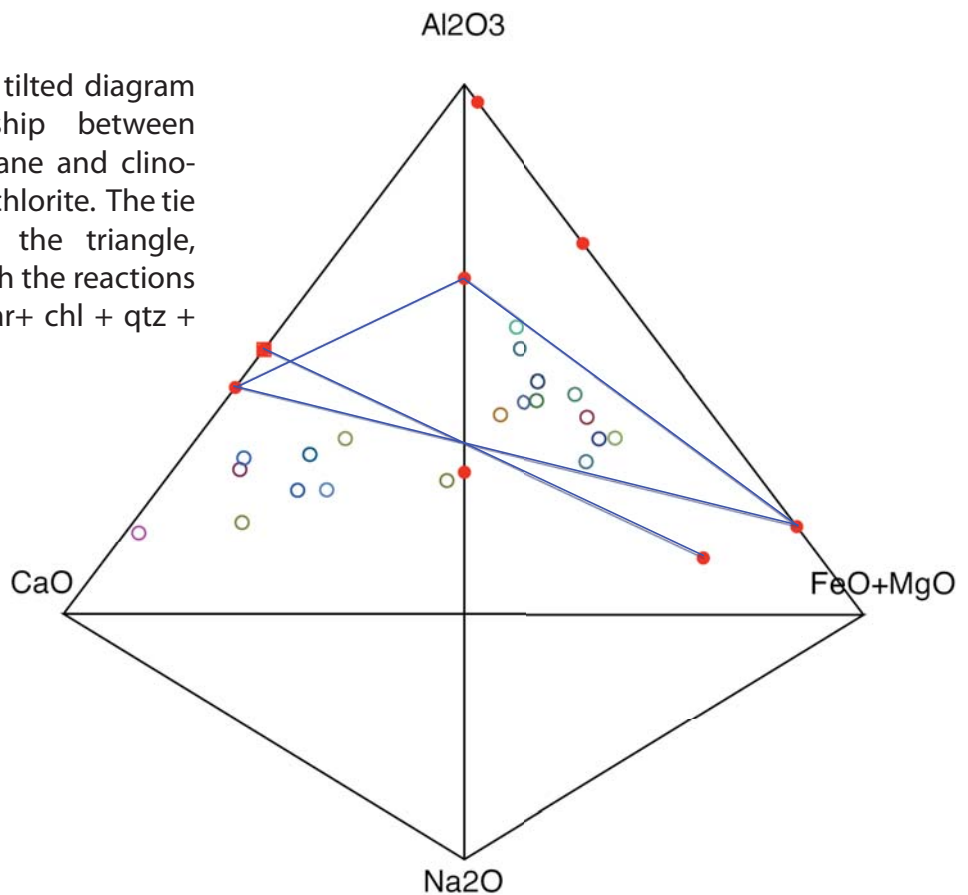


Figure 6-3 (left): Similar to Figure 6-1 but here there are tie lines between lawsonite + glaucophane and the assemblage clinozoisite + paragonite + chlorite are drawn. The lawsonite + glaucophane line divides the two main bulk compositions.

Figure 6-4 (right): This tilted diagram shows the relationship between lawsonite + glaucophane and clinozoisite + paragonite + chlorite. The tie line crosses through the triangle, which is consistent with the reactions $lws + gln \rightarrow Czo + par + chl + qtz + water$.



glaucophane and the clinozoisite has since been reacted, providing that clinozoisite was stable under these conditions. The tilted diagram (Figure 6-4) shows that the lawsonite + glaucophane tie line crosses through the clinozoisite + paragonite + chlorite tie lines – the observed assemblage for some of the pseudomorphs.

Because the tetrahedral plots show that many of the rocks do not contain a substantial amount of Na, the ternary ACF diagram can be used to show the effects of bulk rock chemistry on the pseudomorph assemblages. Using molar averages, the bulk compositions of all rocks were plotted. The four thin sections that showed well-developed pseudomorphs (JBB00-33A, JBB00-33C, SYR99.25C and SYR141F) are plotted on their own diagram to show the location of the pseudomorph composition, matrix composition, and weighted average of the bulk rock composition. The bulk rock compositions of these rocks plot in the same regions as the majority of the thin sections (Figure 6-5). The lawsonite + glaucophane line divides the rocks into two groups, and most fit into the triangle delimited by the clinozoisite + glaucophane + chlorite assemblage. A weighted average for the thin sections that were mapped was generated to plot the matrix composition, the pseudomorph composition and the average bulk rock composition for these much studied samples (Figure 6-6). All rocks that contained pseudomorphs (as observed through the petrographic study) were plotted on a final ACF diagram to compare their bulk compositions to the pseudomorphs observed (Figure 6-7). The rocks that contain Ca-rich (in the form of clinozoisite) pseudomorphs all plot above the lawsonite + glaucophane line. These are believed to be pseudomorphs after an original lawsonite protocryt that was full of inclusions.

The rocks with bulk compositions that plot below the lawsonite + glaucophane line contain pseudomorphs that are Ca-poor, despite the fact that the matrix is richer in Ca- than the

former group. These pseudomorphs are believed not to be after lawsonite, but have a different protocryst that has not yet been identified. The protocryst to these pseudomorphs needs to be aluminous and have a diamond-shaped cross-section, but not be Ca-rich. The rocks in the lower left of the triangle do not follow the same reaction that the previous rocks do, because of their location outside of the clinozoisite + glaucophane + chlorite triangle.

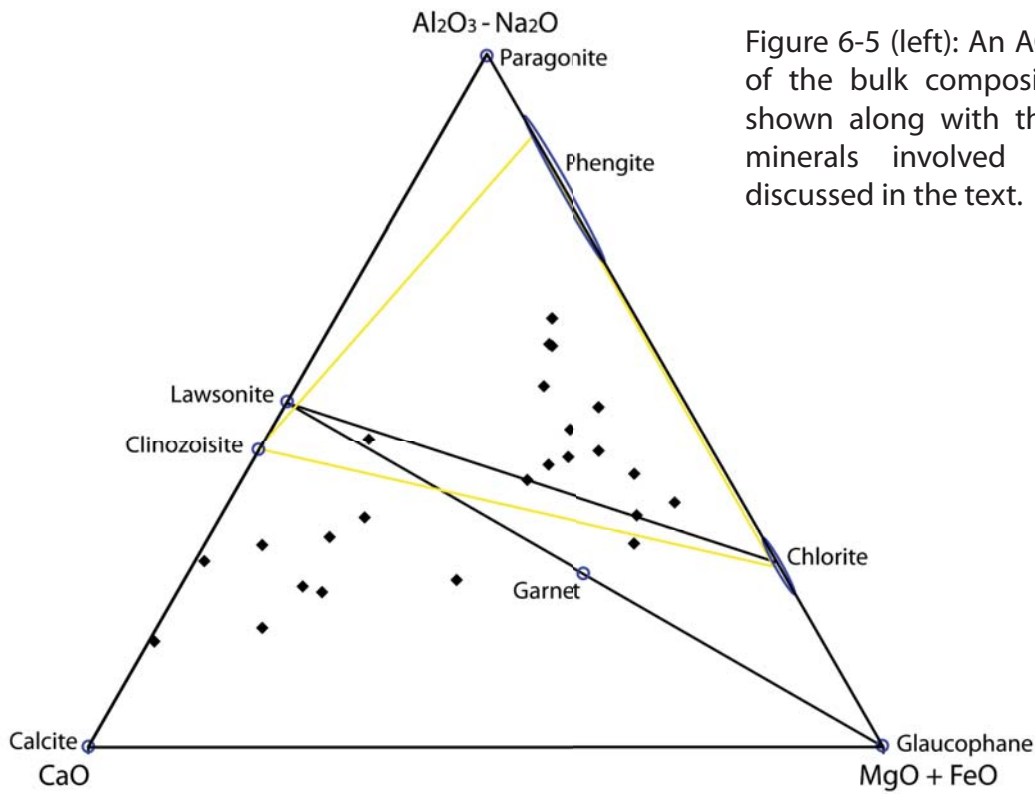
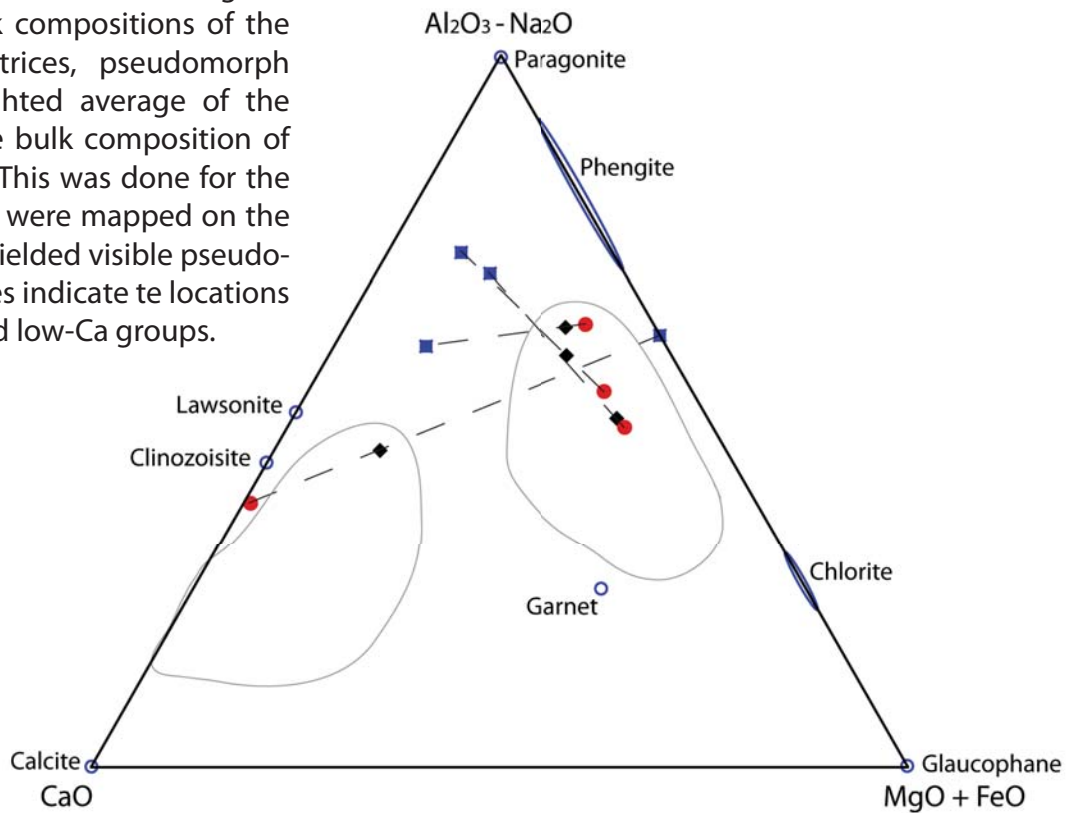


Figure 6-5 (left): An ACF diagram with all of the bulk compositions of the rocks shown along with the compositions of minerals involved in the reactions discussed in the text.

Figure 6-6 (right): An ACF diagram showing the bulk compositions of the thin section matrices, pseudomorph modes and weighted average of the two (showing the bulk composition of the whole rock). This was done for the four samples that were mapped on the microprobe and yielded visible pseudomorphs. The circles indicate the locations of the high-Ca and low-Ca groups.



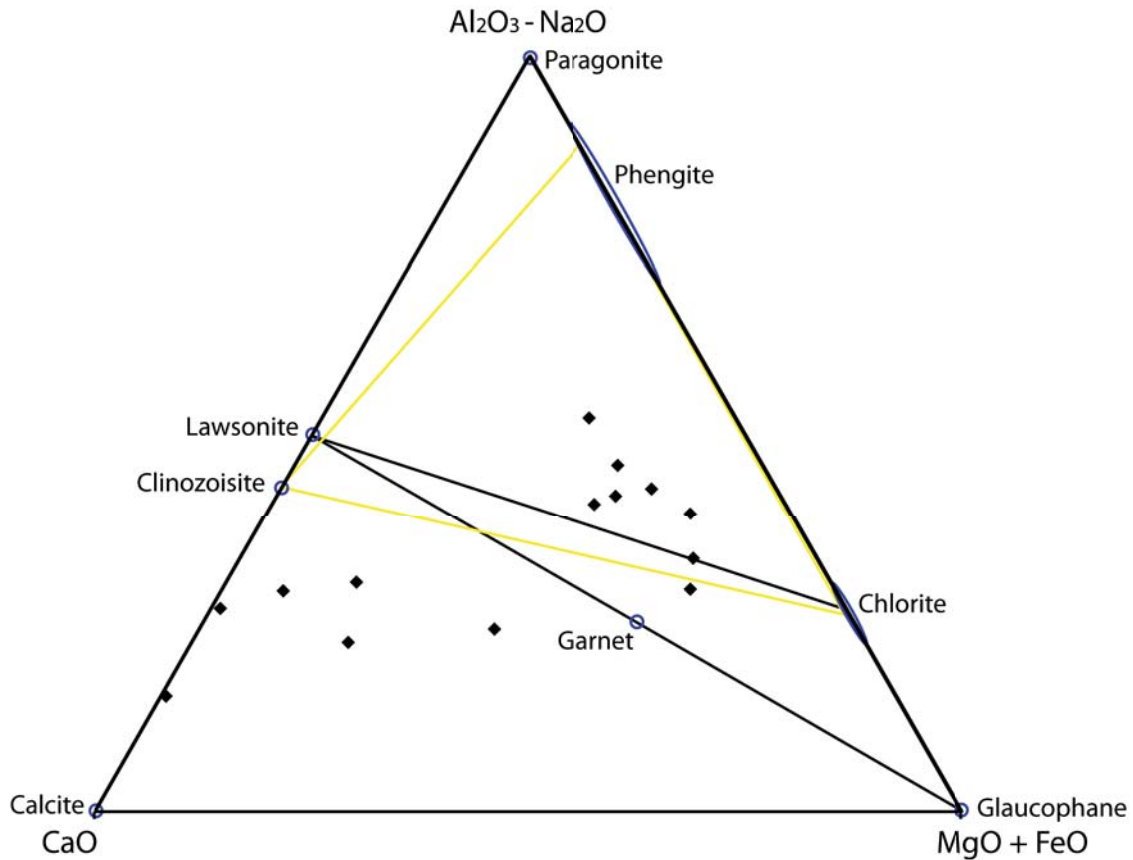


Figure 6-7: This ACF diagram has only the rocks plotted on it that displayed pseudomorphs through petrographic studies. Most of these rocks fall in the clinzoisite + phengite+ chlorite field. The rocks that fall below the lawsonite + glaucophane line all have Ca-poor pseudomorphs. Conversely, the bulk compositions that plot above the lawsonite + glaucophane line have Ca-rich (in the form of clinzoisite) pseudomorphs.

Chapter 7: Geothermobarometry

In order to add to the data on P-T information for Syros, a geothermobarometric analysis was attempted using Frank Spear's (RPI) program: GTB (Geothermobarometry, 2006). The thermometer that was employed was the garnet-phengite (Fe-Mg exchange) thermometer calibrated by Hynes and Forest (1988). This reaction is useful because there is a small change in volume, and thus a small dependence on pressure, which is important given the pressure range for peak metamorphism. It was tested with the average garnet sample and a variety of phengite samples from different thin sections and inside and outside of the pseudomorphs to look at patterns of temperature.

In general, the phengite inside of the pseudomorphs gives a lower temperature than the phengite outside of the pseudomorphs (Figure 7-1), however these trends are not statistically significant. The geothermobarometry assumes that equilibrium is achieved between the phengite and garnet, and given that the garnet is pre-existing, this may not be an appropriate assumption for the phengite inside of the pseudomorphs. All of the temperatures ascertained are near the range of what has been published to date, in general on the lower side. These data are also consistent with the geothermobarometry data that Frye-Levine gathered in 2003.

Plotted on the geothermobarometry graph is a lawsonite out reaction, which locates where lawsonite becomes unstable and changes into other mineral combinations. The P-T path must cross this, or a similar, reaction lines to create the assemblages that are seen in the rocks.

Phengite In		Phengite Out	
Sample	Temp	Sample	Temp
LFL06	389.3	LFL06	379.4
LFL60	361.9	LFL60	352.8
LFL60	336.5	JB	375.9
JB	388.0	SYR99.88C	405.6
JB	383.0	SYR99.8C	401.6
JB	349.9	SYR99.25C	394.3

Table 7-1: Temperatures reported by GTB of the garnet-phengite thermometry. These values do not change in the 10 kbar range displayed in the graphs as the lines are essentially vertical.

Geothermobarometry Plot

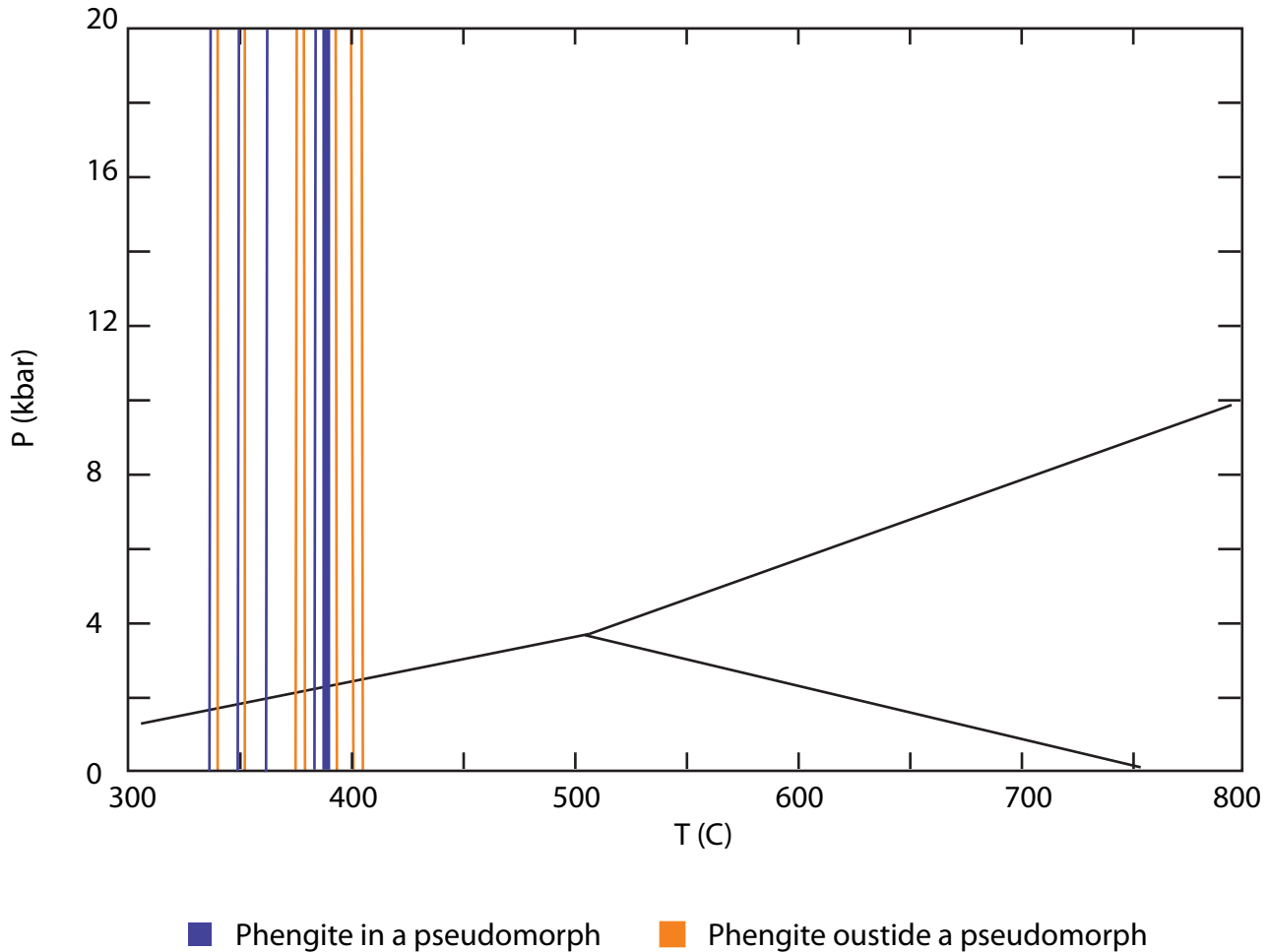


Figure 7-1: This geothermobarometry graph that shows the ascertained temperatures of growth of the phengite in the rocks. The phengite in the pseudomorph tends to be at a slightly lower temperature than the phengite outside of the pseudomorphs, however this statement is not stastically significant. The data on the whole are lower than would be typically expected. This could be because the garnet and phengite were not in equilibrium.

Ch. 8 Summary

Syros has undergone a complicated metamorphic history that is displayed in the metamorphic rocks on the island. Scientists have been, and still are, investigating the evolution of Syros and its metamorphic history. The meta-igneous (and meta-sedimentary rocks by association) have been dated as Triassic (273-245 Ma) (Bröcker and Pidgeon, 2007), while the Vari unit is dated at 70 Ma (Trotet et al., 2001; Jolivet et al., 2003). The peak metamorphism recorded in rims of zircons in both of these units is dated to 52 Ma (Tomaschek et al., 2001). The peak P/T constraints have been narrowed to 12-16 kbar and 450-500 degrees C (Okrusch and Bröcker, 1990; Schumacher, 2008), but the exhumation process is less understood. Syn-orogenic exhumation inside of the orogenic wedge has been cited by Trotet et al. (2000) as the mechanism for exposing the blueschist rocks on the surface. They assert that the extrusion began under a continuing compressional regime, prior to the back-arc extension of the Aegean Sea (ca. 50 Ma). The meta-igneous rocks (including meta-gabbros and eclogites) and marbles have been studied to gather this data and help with understanding the metamorphic history of the island, however the schists have been largely ignored to date.

The graphitic schists, found interbedded with marbles throughout the northern end of the island contain pseudomorphs that weather in relief to the rest of the rock. The typical matrix assemblage for the graphitic schists is phengite + quartz + calcite + sphene + graphite ± paragonite ± albite ± garnet ± clinozoisite ± glaucophane ± chlorite ± opaques. The pseudomorphs contain assemblages of phengite + quartz ± paragonite ± albite ± garnet ± clinozoisite ± chlorite ± sphene. Garnet and sphene are interpreted as spectator minerals that were not part of the pseudomorphing reactions that took place. This was concluded because the

sphene is present in the pseudomorphs and matrix in the same amounts, and the garnet compositions do not vary from inside to outside of the pseudomorphs.

The pseudomorphs range in size (from 2mm to 2 cm) and abundance but are present in most samples. Many pseudomorphs preserve an earlier foliation indicating that there was a metamorphic texture throughout the rock prior to the growth of the protocrust. Following the growth of the protocrust, a metamorphic fabric with a new orientation grew and is easily seen in the matrix of the rock at an angle to the fabric preserved within the pseudomorphs.

The microprobe maps of the pseudomorphs show a variety of textures. Some pseudomorphs are homogenous throughout and clinozoisite-rich (SYR141F), others are homogenous throughout and clinozoisite-poor (SYR99.25C); and still others are mineralogically zoned with clinozoisite -rich centers and mica-rich outer edges (JBB00-33A, JBB00-33C). Two maps do not show pseudomorphs that are calcium-rich, or even distinguished from the matrix (JBB99-33B, LFL02). These pseudomorphs are albite-rich and appear to be after a different protocrust.

The pseudomorphs in this rock were assumed to be after lawsonite. This is because of the presence of remnant lawsonite in other rocks on Syros, its association with HP/LT metamorphism and the shape of the crystal. This hypothesis was tested using mass balance equations. Clinozoisite is the only Ca-bearing mineral in the pseudomorphs, and due to the low X_{CO_2} values ($X \sim 0.01$) reported by Schumacher (2008) there was not a sufficient amount of CO_2 in the fluid to facilitate calcite growth. Thus, it is likely that the calcium in the clinozoisite present in the pseudomorphs now is virtually equal to the amount of calcium that the protocrust contained.

The mass balance calculations show that the size of the pseudomorphs that are displayed were originally only 20 to 50% lawsonite and the rest was likely inclusions. These numbers are based on the amount of calcium that is inside of the pseudomorph. These values show that there is a range of calcium present in the pseudomorphs, but there is not near enough to assert that the protocry of the pseudomorphs was pure lawsonite.

The implications of this result could be that the protocry for these pseudomorphs was not lawsonite at all, or there is an explanation for the low calcium values. Some proposed explanations for the lack of calcium in the pseudomorph are: (1) the protocry of lawsonite was full of inclusions; (2) some calcium was removed from the pseudomorph, (3) the zonation of the pseudomorphs is not considered and the cross-section of the pseudomorph that is seen in is calcium-poor and other areas of the pseudomorph are calcium-rich, or (4) any combination of these three ideas.

It is likely that the pseudomorphs in Figures 5-1, 5-2, 5-4, 5-5, and 5-6 are after lawsonite, but the protocry had to be full of inclusions and possibly in conjunction with another controlling factor. It is not likely that the pseudomorph in Figure 5-3 is after lawsonite because of its complete lack of calcium. An alternative protocry may be dolomite or ankerite because of the rhombohedral shape, however more research must be completed to test this hypothesis. The pseudomorphs in Figures 5-7 and 5-8 are albite-rich and have a third protocry and a different bulk composition because most of the rocks in this study are relatively Na-poor. The protocry to these other pseudomorphs have not been investigated and will be a focus in the future.

ACFN and ACF diagrams display the bulk compositions in a 3-D and 2-D setting; these diagrams yield a better understanding of the pseudomorphing reactions and how the bulk compositions of the rocks relate to each other. The ACFN and ACF diagrams show that the

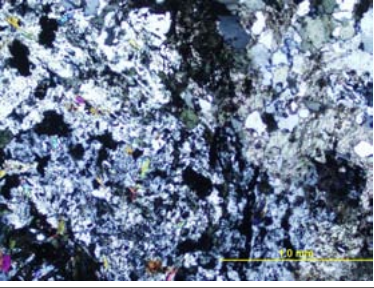
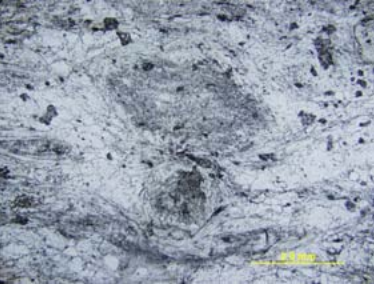
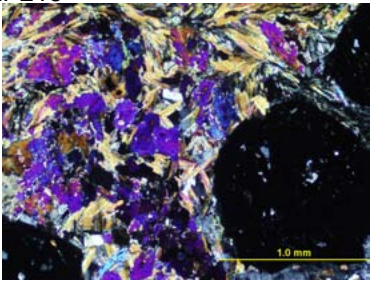
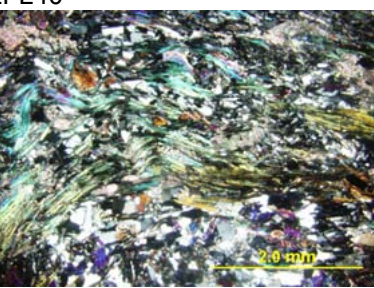
rocks, in fact, do not all stem from a similar bulk composition; they plot in two distinctly different regions of the diagrams. One is more calcite-rich and the other more aluminous. The calcite-rich bulk compositions yielded pseudomorphs that are clinozoisite-poor and mica-rich (SYR99.25C) while the aluminous rocks yielded the pseudomorphs that are clinozoisite- and mica-rich (JBB00-33A, JBB00-33C, SYR141F). This data also supports the assertion that the pseudomorphs from JBB00-33A, JBB00-33C and SYR141F are from a lawsonite protocrust that was rich in inclusions. Dissimilarly the pseudomorph from SYR99.25C does not have a lawsonite protocrust and does not share the assemblages that are seen in the pseudomorphs after lawsonite.

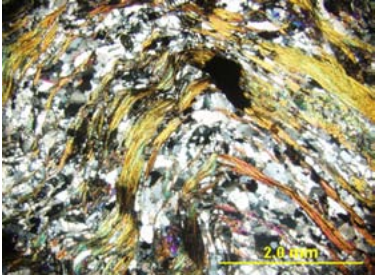
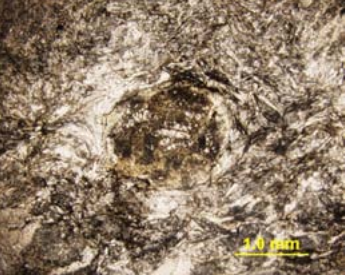
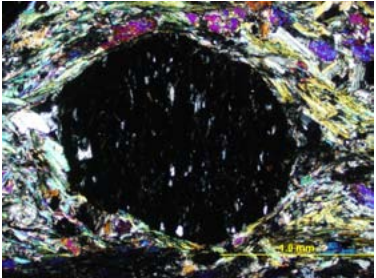
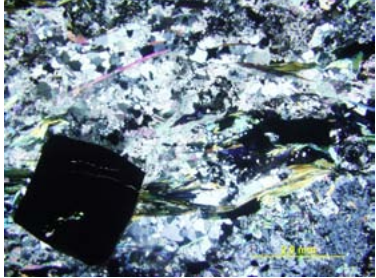
Geothermobarometry was attempted using Spear's GTB (2006). The garnet-phengite thermometer last calibrate by Hynes and Foreset (1988) was used with an average garnet sample and numerous phengite samples from different thin sections as well as inside and outside of the pseudomorphs. The program yielded temperatures ranging from 340 to 410 °C. These data are on the lower range of what would be expected, but are similar to other temperatures that have been reported (450-500°C; Okrusch and Bröcker, 1990). The geothermobarometry assumes equilibrium between the phases, this assumption may not be appropriate for the phengite inside of the pseudomorphs and may lead to temperature data outside of the generally accepted range.

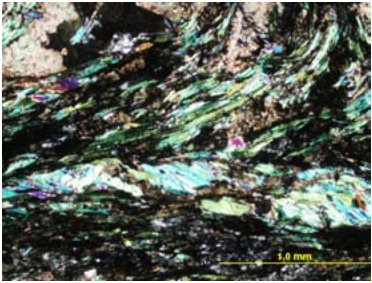
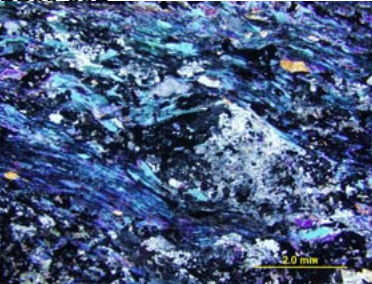
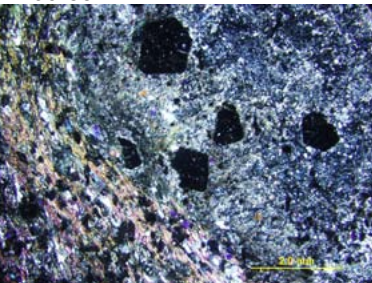
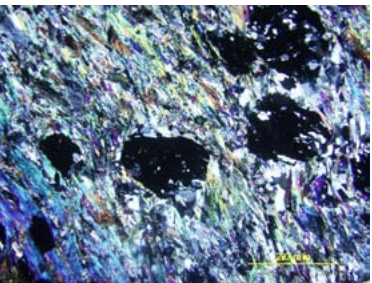
References:

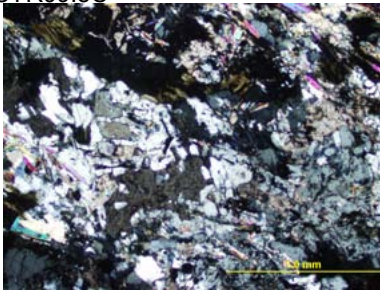
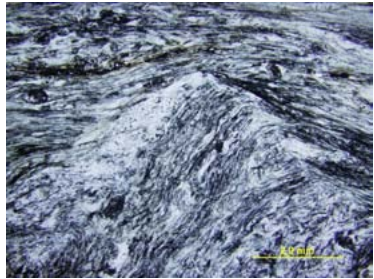
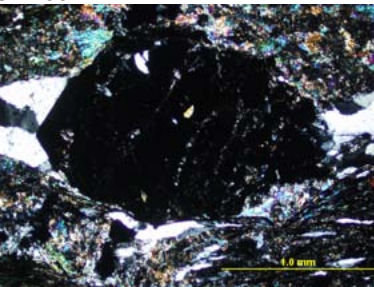
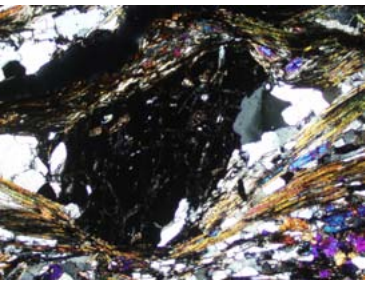
- Able, L. (2004) Lawsonite pseudomorphs in the schists, of Syros, Greece: in Palmer B.A., coordinator, 17th Annual Keck Research Symposium in Geology, Proceedings, Keck Geology Consortium, Carleton, MN.
- Appel, Peter. Tetlab: <http://www.ifg.uni-kiel.de/339.html>
- Brady, J.B., *Able, L.M., Cheney, J.T., *Sperry, A.J., and Schumacher, J.C. (2001) Prograde lawsonite pseudomorphs in blueschists from Syros, Greece: Geological Society of America Abstracts with Programs 33, 6, 250-251.
- Brady, J.B., Markley, M.J., Schumacher, J.C., Cheney, J.T. and Bianciardi, G.A. (2002) Aragonite pseudomorphs in high-pressure marbles of Syros, Greece. *Journal of Structural Geology*, 26, 3-9.
- Bröcker, M., and Pidgeon, R.T. (2007) Protolith Ages of Meta-igneous and Metatuffaceous Rocks from the Cycladic Blueschist Unit, Greece: Results of a Reconnaissance U-Pb Zircon Study. *The Journal of Geology*, 115, 83-98.
- Faccenna, C., Finicciello, F., Giardini, D., and Lucente, P. (2001) Episodic back-arc extension during restricted mantle connection in the Central Mediterranean. *Earth and Planetary Science Letters*, 187, 105-116.
- Frye-Levine, L. (2004) Graphitic Schists of Syros, Greece: in Palmer, B.A., coordinator, 17th Annual Keck Research Symposium in Geology, Proceedings, Keck Geology Consortium, Carleton, MN.
- Jolivet, L., Faccenna, C., Goffé, B., Burov, E., Agard, P. (2003) Subduction tectonics and exhumation of high-pressure metamorphic rocks in the Mediterranean orogens. *American Journal of Science*, 303, 353-409.
- Laurent, J. (1999) The Mediterranean basins : tertiary extension within the Alpine Orogen; an introduction. Geological Society special publications, 156, 1-14.
- Okrusch, M., and Bröcker, M. (1990) Eclogites associated with high-grade blueschists in the Cyclades archipelago, Greece: A review. *European Journal of Mineralogy*, 2, 451-478.
- Putlitz, B., Cosca, M.A., Schumacher, J.C. (2005) Prograde mica ⁴⁰Ar/³⁹Ar growth ages recorded in high pressure rocks (Syros, Cyclades, Greece). *Chemical Geology*, 214, 79-98.
- Schmädicke, E., and Will, T.M. (2003) Pressure-temperature evolution of blueschist facies rocks from Sifnoes, Greece, and implications for the exhumation of high-pressure rocks in the Central Aegean. *Journal of metamorphic Geology*, 21, 799-811.

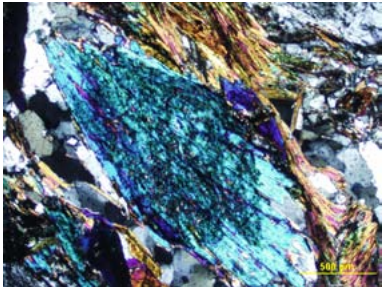
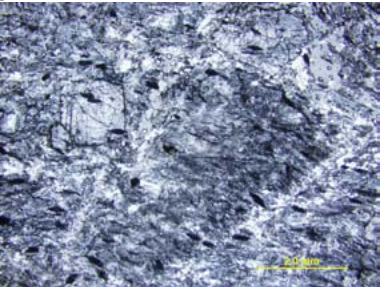
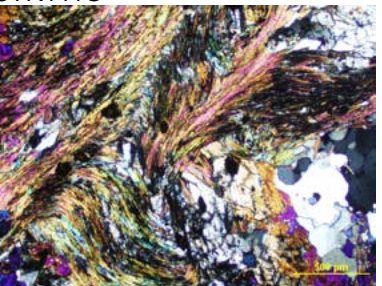
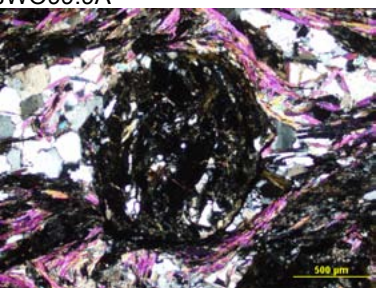
- Schumacher, J.C., Brady, J.B., Cheney, J.T., Tonnensen, R.R. (2008) Glaucophane-bearing marbles on Syros, Greece. *Journal of Petrology*, 49, 1667-1686.
- Schulte, B., and Sindern, S. (2002) K-rich fluid metasomatism at high-pressure metamorphic conditions: Lawsonite decomposition in rodingitized ultramafite of the Maksyutovo Complex, Southern Urals (Russia). *Journal of Metamorphic Geology*, 20, 529-541.
- Spear, F.S., and Kohn, J.M., GTB: <http://ees2.geo.rpi.edu/MetaPetaRen/Software/software.html>
- Tomaschek, F., Kennedy, A.K., Villa, I.M., Lagos, M., Ballhaus, C. (2003) Zircons from Syros, Cyclades, Greece – Recrystallization and Mobilization of Zircon During High-Pressure Metamorphism. *Journal of Petrology*, 44, 1977-2002.
- Trotet, F., Jolivet, L., and Vidal, O. (2000) Tectono-metamorphic evolution of Syros and Sifnos islands (Cyclades, Greece). *Tectonophysics*, 338, 179-206.
- Trotet, F., Vidal, O., and Jolivet, L. (2001) Exhumation of Syros and Sifnos metamorphic rocks (Cyclades, Greece). New constraints on P-T paths. *European Journal of Mineralogy*, 13, 901-920.

Sample ID	Matrix Modes (%) (+graphite)	PS Description	PS Modes	Textures
LFL02	 <p>White mica 20 Quartz 15 Calcite 25 Albite 25 Garnet 8 Epidote 0 Sphene 2 Glaucophane 0 Chlorite 4 Opauques <1</p>	There are diamond shaped PS up to 5mm in diameter and chlorite replaced garnets.	-The PS make up 15% of the whole rock. -Comp: Ab, Mica, Chl, Qtz, Sph	The mica folds around the PS indicating metamorphism after the clumps grew. The albite in the rock has a "flowery" texture.
LFL06	 <p>White mica 25 Quartz 22 Calcite 50 Albite 0 Garnet 0 Epidote 0 Sphene 2 Glaucophane 0 Chlorite 0 Opauques 1</p>	Both round and angular PS, most are diamond shaped. Up to 3mm in diameter, abundant.	-The PS make up 20% of the whole rock. - Comp: Qtz, Mica, Cc, Ab	The albite in the PS is full of inclusions. Graphite is most concentrated in the PS and micaceous areas of the rock. Many small opaques.
LFL13	 <p>White mica 40 Quartz 13 Calcite 0 Albite 0 Garnet 15 Epidote 0 Sphene 2 Glaucophane 30 Chlorite 0 Opauques <1</p>	PS are potentially present, but not well defined, the texture could just be due to weathering.	-If PS, they make up 5% of the rock. -Comp: Qtz, Ab, Mica, Gar, Sph	Some skeleton garnets. Little to no calcite in the whole rock - slight variation in bulk composition. No strong mica fabric. The glaucophane is in clumps.
LFL40	 <p>White mica 30 Quartz 25 Calcite 28 Albite 0 Garnet 0 Epidote 0 Sphene 2 Glaucophane 15 Chlorite 0 Opauques <1</p>	None visible	N/A	Microfolds in the mica. Graphite is concentrated in the micaceous and glaucophane-rich parts of the rock.

Sample ID	Matrix Modes (%) (+graphite)	PS Description	PS Modes	Textures
LFL44	 <p>White mica 40 Quartz 40 Calcite 0 Albite 0 Garnet 5 Epidote 2 Sphene 2 Glaucophane 10 Chlorite 0 Opagues <1</p>	None visible	N/A	Garnets thoroughly replaced with retrograde chlorite. Microfolds in the mica throughout the rock. Weathered sample.
LFL53	 <p>White mica 45 Quartz 10 Calcite 10 Albite Garnet 10 Epidote Sphene 2 Glaucophane 15 Chlorite 7 Opagues <1</p>	None visible	N/A	Garnets are partially replaced with chlorite, inclusions in the garnet. Two horizons of mica that span the thin section. Microfolds in the mica.
LFL60	 <p>White mica 30 Quartz 30 Calcite 0 Albite 0 Garnet 25 Epidote 6 Sphene 2 Glaucophane 6 Chlorite 0 Opagues <1</p>	A few weathered pseudomorphs, up to 5mm in diameter	-The PS make up 5% of the whole rock. -Comp: fine-grained mica, Qtz, Sph	The garnet has not been replaced in this sample, there are many inclusions in the garnet. There are quartz-rich horizons, mica-rich horizons and mixed layers. The quartz in the rock is near/in the PS frequently.
LFL65	 <p>White mica 25 Quartz 25 Calcite 23 Albite 23 Garnet 0 Epidote 0 Sphene 3 Glaucophane 0 Chlorite 0 Opagues 1</p>	At least on PS, 6mm in diameter. Other possible PS are not v. well defined in TS.	-Unknown percentage of rock is being taken up by the PS due to the texture. -Comp: Qtz, Cc, Ab, Mica	Weathered sample. The mica in this rock does not occur in well-defined layers, it is jumbled up throughout the TS. Abundant opaques.

Sample ID	Matrix Modes (%) (+graphite)	PS Description	PS Modes	Textures
JB	 <p>White mica 20 Quartz 25 Calcite 40 Albite 0 Garnet 10 Epidote 3 Sphene 0 Glaucophane 0 Chlorite 2 Opauques <1</p>	None visible	N/A	Mica fabrics. Calcite in this rock is v. fine-grained, not like most of the samples that contain calcite.
JBB99-33B	 <p>White mica 40 Quartz 23 Calcite 33 Albite 0 Garnet 0 Epidote 0 Sphene 2 Glaucophane 0 Chlorite 0 Opauques 2</p>	Difficult to identify because of the matrix and PS similarities. There are PS present up to 5mm in diameter.	-The PS make up 15% of the rock. -Comp: Mica, Ep, Qtz, Ab, Chl	Graphite is very concentrated in the titanite. Well-developed mica fabric that wraps around the PS.
JBB00-33A	 <p>White mica 33 Quartz 23 Calcite 0 Albite 0 Garnet 26 Epidote 0 Sphene 2 Glaucophane 15 Chlorite 0 Opauques <1</p>	4 large PS, up to 9mm in diameter.	-The PS make up 25% of the whole rock. -Comp: Ep, Mica, Qtz, Ab, Chl	Large PS. Garnets in the PS are not rimmed with chlorite, garnets outside the PS are rimmed. The PS mineral distribution suggests zoning. Graphite shows distinct growth stages. PS has well-developed boundaries with the matrix.
JBB00-33C	 <p>White mica 45 Quartz 20 Calcite 0 Albite 0 Garnet 17 Epidote 0 Sphene 2 Glaucophane 15 Chlorite 0 Opauques <1</p>	2 PS visible, up to 10 mm in diameter.	-The PS make up 10% of the whole rock. -Comp: Ep, Mica, Chl, Ab, Qtz.	Skeleton garnets present. Quartz located preferentially in the garnets and PS. Mica fabric runs into the PS boundaries instead of curving around. Well-developed foliation preserved in the PS.

Sample ID	Matrix Modes (%) (+graphite)	PS Description	PS Modes	Textures
SYR99.8C 	White mica 8 Quartz 35 Calcite 8 Albite 40 Garnet 0 Epidote 0 Sphene 0 Glaucophane 0 Chlorite 8 Opaques <1	Small clumps that could be PS	-If PS, they would be 5% of the rock -Comp: fine-grained Ab, Chl.	The small clumps with "flowery" minerals are albite. This albite texture reoccurs throughout the rocks. Mica does not grow in an organized foliation.
SYR99.25C 	White mica 35 Quartz 22 Calcite 40 Albite 0 Garnet 0 Epidote 0 Sphene 2 Glaucophane 0 Chlorite 0 Opaques <1	1 large PS, 19mm in diameter	-PS makes up 30% of the whole rock. -Comp: Ph, Sph, Qtz, Chl, Opaques	PS preserves a well-developed foliation at 30° to the foliation in the matrix. There are two layers present in the rock, a calcite rich layer and mica-rich layers around it. The PS is situated in the calcite-rich layer. Mica bends around the PS.
SYR99.44A 	White mica 45 Quartz 25 Calcite 0 Albite 6 Garnet 20 Epidote 0 Sphene 3 Glaucophane 0 Chlorite 0 Opaques <1	None visible	N/A	Garnets with pressure shadows, some eyeball-shaped garnets. Quartz inclusions in the garnet. There is a mica-rich layer and a v. fine-grained layer in this rock.
SYR00-85B 	White mica 30 Quartz 40 Calcite 0 Albite 0 Garnet 22 Epidote 0 Sphene 0 Glaucophane 7 Chlorite 0 Opaques <1	PS present, difficult to distinguish in ppl	N/A	Very poor quality TS, difficult to detail.

Sample ID	Matrix Modes (%) (+graphite)	PS Description	PS Modes	Textures
SYR141A	 <p>White mica 30 Quartz 25 Calcite 0 Albite 0 Garnet 12 Epidote 0 Sphene 0 Glaucophane 33 Chlorite 0 Opauques <1</p>	None visible	N/A	V. graphite-rich glaucophane. Garnets that are not replaced and not rimmed.
SYR141F	 <p>White mica 25 Quartz 13 Calcite 0 Albite 0 Garnet 17 Epidote 0 Sphene 5 Glaucophane 40 Chlorite 0 Opauques <1</p>	1 small PS, 6mm in length	-The PS makes up 5% of the whole rock. -Comp: Ep, Mica, Chl, Qtz, Ab	Garnets intergrown, angular to rounded. Foliation in the PS is at a 20° angle to the mica foliation in the matrix. Glaucophane is chunky in habit.
SYR141G	 <p>White mica 28 Quartz 20 Calcite 0 Albite 0 Garnet 25 Epidote 0 Sphene 1 Glaucophane 25 Chlorite 0 Opauques <1</p>	1 PS, 4mm in diameter	-The PS makes up 3% of the whole rock. -Comp: v. fine-grained, but likely Ep, Mica, Chl, Ab	Mica is in books with many microfolds. Glaucophane also spread about the rock in clumps
JWO99.9A	 <p>White mica 35 Quartz 30 Calcite 20 Albite 0 Garnet 5 Epidote 0 Sphene 3 Glaucophane 0 Chlorite 6 Opauques <1</p>	None visible	N/A	V. fine-grained rock, not much variation throughout the rock. Not a very graphite-rich rock.

Paragonite Continued

Sample ID	JBB00-33A	SYR99.8C	SYR99.25C	SYR141F
SiO2	48.28963	49.16	47.99	49.09
TiO2	0.3196621	0.13	0.18	0.00
Al2O3	38.77725	39.80	37.27	40.64
FeO	0.00	0.46	0.58	0.00
MnO	0.00	0.03	0.04	0.00
MgO	0.00	0.18	0.47	0.00
Ca2O	0.6162496	0.04	0.02	0.00
Na2O	3.982624	7.62	6.26	8.49
K2O	5.339694	0.33	1.77	0.49
Total	97.32512	97.69	94.60	98.70

Ions Si	6.12	6.10	6.19	6.05
Ions Ti	0.03	0.01	0.02	0.00
Ions Al	5.79	5.82	5.66	5.90
Ions Fe	0.00	0.05	0.06	0.00
Ions Mn	0.00	0.00	0.00	0.00
Ions Mg	0.00	0.03	0.09	0.00
Ions Ca	0.08	0.01	0.00	0.00
Ions Na	0.98	1.83	1.57	2.03
Ions K	0.86	0.05	0.29	0.08
Ions O	22.00	22.00	22.00	22.00

Albite

Sample ID	JBB99-33B	JBB99-33B	JBB99-33B	JBB00-33C	SYR99.8C
SiO2	70.41	67.08	67.31	69.76	68.88
TiO2	-0.01	0.00	-0.02	0.00	0.03
Al2O3	19.56	18.53	19.00	20.05	19.09
FeO	0.19	0.07	0.04	0.00	0.29
MnO	-0.01	0.06	-0.01	0.00	-0.04
MgO	-0.12	-0.11	-0.08	0.00	-0.09
Ca2O	-0.01	0.09	0.08	0.67	0.02
Na2O	11.91	11.66	11.91	11.38	11.59
K2O	-0.03	-0.01	-0.08	0.00	-0.05
Total	101.89	97.38	98.14	101.87	99.64

Ions Si	3.01	3.01	3.00	2.99	3.01
Ions Ti	0.00	0.00	0.00	0.00	0.00
Ions Al	0.99	0.98	1.00	1.01	0.98
Ions Fe	0.01	0.00	0.00	0.00	0.01
Ions Mn	0.00	0.00	0.00	0.00	0.00
Ions Mg	-0.01	-0.01	-0.01	0.00	-0.01
Ions Ca	0.00	0.00	0.00	0.03	0.00
Ions Na	0.99	1.01	1.03	0.95	0.98
Ions K	0.00	0.00	0.00	0.00	0.00
Ions O	8.00	8.00	8.00	8.00	8.00

Epidote Continued

Sample ID	LFL60	JBB00-33A	JBB00-33A	JBB00-33A	JBB00-33C	JBB00-33C
SiO2	39.71	39.65	39.89	38.48	38.79	39.14
TiO2	0.64	0.65	0.74	0.00	0.00	0.00
Al2O3	31.63	31.91	31.68	26.86	27.35	27.76
FeO	1.47	1.02	0.58	7.05	6.78	6.63
MnO	0.08	0.00	0.00	0.32	0.00	0.00
MgO	-0.05	0.00	0.00	0.00	0.00	0.00
Ca2O	24.81	24.03	24.56	23.28	23.52	23.58
Na2O	-0.02	0.00	0.00	0.00	0.00	0.00
K2O	0.00	0.00	0.00	0.00	0.00	0.00
Total	98.27	97.26	97.96	95.99	96.44	97.10

Ions Si	3.03	3.04	3.03	3.09	3.09	3.09
Ions Na	0.04	0.04	0.04	0.00	0.00	0.00
Ions Ti	2.84	2.88	2.84	2.54	2.57	2.59
Ions Al	0.09	0.07	0.04	0.47	0.45	0.44
Ions Fe	0.01	0.00	0.00	0.02	0.00	0.00
Ions Mn	-0.01	0.00	0.00	0.00	0.00	0.00
Ions Mg	2.03	1.97	2.00	2.00	2.01	2.00
Ions Ca	0.00	0.00	0.00	0.00	0.00	0.00
Ions K	0.00	0.00	0.00	0.00	0.00	0.00
Ions O	12.50	12.50	12.50	12.50	12.50	12.50

Sample ID	JBB00-33C	JBB00-33C	SYR141F	SYR141F
------------------	------------------	------------------	----------------	----------------

SiO2	39.96	39.88	38.91	39.79
TiO2	0.65	0.00	0.00	0.00
Al2O3	30.78	30.54	26.74	28.77
FeO	2.29	3.31	7.06	6.48
MnO	0.00	0.00	0.00	0.00
MgO	0.00	0.00	0.00	0.00
Ca2O	24.63	23.85	22.74	24.32
Na2O	0.00	0.00	0.00	0.00
K2O	0.00	0.00	0.00	0.00
Total	98.31	97.59	95.45	99.35

Ions Si	3.05	3.08	3.13	3.07
Ions Na	0.04	0.00	0.00	0.00
Ions Ti	2.77	2.78	2.54	2.62
Ions Al	0.15	0.21	0.48	0.42
Ions Fe	0.00	0.00	0.00	0.00
Ions Mn	0.00	0.00	0.00	0.00
Ions Mg	2.02	1.97	1.96	2.01
Ions Ca	0.00	0.00	0.00	0.00
Ions K	0.00	0.00	0.00	0.00
Ions O	12.50	12.50	12.50	12.50

Chlorite Continued

Sample ID	SYR99.8C	SYR99.25C
SiO2	28.52	27.74
TiO2	0.10	0.14
Al2O3	21.06	20.55
FeO	0.03	0.04
MnO	24.81	21.83
MgO	0.34	0.09
Ca2O	16.57	18.71
Na2O	0.19	0.04
K2O	0.21	0.11
Total	91.78	89.26

Ions Si	5.68	5.61
Ions Na	0.08	0.04
Ions Ti	0.02	0.02
Ions Al	4.94	4.90
Ions Fe	4.13	3.69
Ions Mn	0.06	0.02
Ions Mg	4.92	5.64
Ions Ca	0.04	0.01
Ions K	0.01	0.01
Ions O	28.00	28.00